TECHNISCHE UNIVERSITÄT WIEN

MEDIZINISCHE UNIVERSITÄT WIEN

DIPLOMARBEIT

Regional distribution of lung ventilation during high-frequency jet ventilation in anesthetized patients

Thema

Universitätsklinik für
Anästhesie, Allgemeine Intensivmedizin und Schmerztherapie
der Medizinischen Universität Wien / AKH Wien

E350 - Fakultät für Elektrotechnik und Informationstechnik
Institut für Biomedizinische Elektronik
der Technischen Universität Wien

Ausgeführt am

Dr. Marita Windpassinger, MBA
Univ.Prof. Dipl.-Ing. Dr. techn. Eugenijus Kaniusas

unter der Anleitung von

durch

BSc. Ahmed Kamal Mohamed Hussein Khattab

Name

18. March. 2022

Datum

Unterschrift (Student)

Master Thesis

Regional distribution of lung ventilation during high-frequency jet ventilation in anesthetized patients

Author

BSc. Ahmed Kamal Mohamed Hussein Khattab

Supervisor

Dr. Marita Windpassinger, MBA
Univ.Prof. Dipl.-Ing. Dr. techn. Eugenijus Kaniusas

March 2022 Vienna

Medical University of Vienna / Vienna General Hospital
Clinical Department for General Anesthesia and Intensive Care Medicine

Vienna University of Technology
Faculty of Electrical Engineering and Information Technology
Institute of Biomedical Electronics

In memory of my mother and brother.

Acknowledgments

From the bottom of my heart, I would like to say a big thank you to my supervisor Dr. Marita Windpassinger, MBA for her energy, guidance, co-operation, and invaluable effort throughout our collaboration. I enjoyed the time spent in the operation room and our discussion on how to do the analysis and the many times of trial and error until we reached our awesome results.

I would like to express my gratitude and appreciation for my supervisor Univ. Prof. Dipl.-Ing. Dr. techn. Eugenijus Kaniusas whose guidance, support, and encouragement have been invaluable throughout my project. I am extremely fortunate to have conducted my master thesis work under his supervision.

Last but not least, I would like to thank my father, brother, sisters, and fiancée for their continuous encouragement and support during my master's journey.

Ahmed Kamal Khattab

Contents

List of abbreviations

ANOVA	Analysis Of Variance
ASA	American Society Of Anaesthesiologists
BMI	Body Mass Index
BPF	Band-Pass Filter
BSF	Band-Stop Filter
Cath	Catheter
CO2	Carbon-Dioxide
CoV	Center Of Ventilation
CoVvd	Center Of Ventilation In Ventro-Dorsal Direction
CT	Computer Tomography
df	Degree Of Freedom
DP	Driving Pressure
DSS	Gravity-Dependent Silent Spaces
ECG	Electrocardiogram
EELI	End Expiration Lung Impedance
EFPG	Electric Field Plethysmogram Signal
EILI	End Inspiration Lung Impedance
EIT	Electrical Impedance Tomography
F	Test Statistic In The One-Way ANOVA Test
F crit	Critical Value Of F
FFT	Fast Fourier Transform
FiO2	Fraction Of Inspired Oxygen
FIR	Finite Impulse Response Filter
GUI	Graphical User Interface
HF	High Frequency
HFJV	High-Frequency Jet Ventilation
HoV	Horizon Of Ventilation
HPF	High-Pass Filter
I/E	Inspiration To Expiration Rate
ICU	Intensive Care Unit
IIR	Infinite Impulse Response Filter
JV	Jet Ventilation
Lary	Laryngoscope
LF	Low Frequency
LPF	Low-Pass Filter
MRI	Magnetic Resonance Imaging
MS	Mean Square
NIRS	Near-Infrared Spectroscopy
NSS	Non-Gravity-Dependent Silent Spaces
PaCO2	Arterial Carbon Dioxide Partial Pressure
PaO2	Arterial Oxygen Partial Pressure

pb	Pass Band
PEEP	Positive End Expiratory Pressure
PET	Positron Emission Tomography
PH	Potential Of Hydrogen
ROI	Region Of Interest
RR	Respiration Rate
sb	Stop Band
SBG	Subglottic
SD	Standard Deviation
SIHFJV	Superimposed High-Frequency Jet Ventilation
Single HFJV	Single High-Frequency Jet Ventilation
sMRG	Bio-Signal Mechanorespirogram
sMSG	Bio-Signal Mechanospirogram
SoS	Sum Of Squares
sPCG	Bio-Signal Phonocardiogram
SPG	Supraglottic
SpO2	Oxygen Saturation
TCM	Transcutaneous Monitor
tcPCO2	Transcutaneous Carbon-Dioxide Partial Pressure
tcPO2	Transcutaneous Oxygen Partial Pressure
TIV	Tidal Impedance Variation
TV	Tidal Volume

List of Variables

Variable	Description
$u_{\sim}$	Alternating component of the body measured output voltage
u, U	Body measured output voltage
α	Bonferroni correction
γ	Conductivity
U_0	Constant component of the body measured output voltage
I	Electrical current intensity
Z, z	Electrical impedance
f	Frequency
f_C	Heart rate
N	Number of tests
U_E	Output voltage due to expiration
U_I	Output voltage due to inspiration
ε	Permeability
P	Pressure
f_R	Respiratory rate
P-value	Statistical significance
T	Time

Abstrakt

Die elektrische Impedanztomographie (EIT), ist ein Bildgebungsverfahren, das strahlungsfrei und nicht-invasiv ist. Die EIT ermöglicht eine bettseitige kontinuierliche Überwachung, um die regionalen Ventilationsverhältnisse der Lungen zu verteilen. Die EIT ist ein neuartiges bildgebendes Verfahren, das billig, tragbar und leicht zugänglich ist. Diese kann in einer Intensivstation oder einem Operationssaal verwendet werden. Die Hochfrequenz-Jet-Ventilation (HFJV) ist eine der gebräuchlichen mechanischen Beatmungsformen bei den operativen Eingriffen an den Atemwegen unter Anästhesie.

Das Hauptziel dieser Masterarbeit ist es, die regionale Ventilationsverteilung der Lunge mit zwei verschiedenen HFJV-Methoden durch das EIT-Gerät bei Patienten unter Anästhesie zu evaluieren. Die erste Methode ist die Single Hochfrequenz Jet-Ventilation (Single HFJV), wo eine Portion der Single Hochfrequenz-Gasströme für das Ventilation-Verfahren verwendet wird. Die Zweite ist die Superponierte Hochfrequenz Jet-Ventilation (SIHFJV), bei der zwei verschiedene Beatmungsfrequenzen kombiniert und in die Lunge gleichzeitig appliziert werden.

Die Patienten, die sich der Operation an den Atemwegen unterzogen haben, wurden durch eine Maske mit einem Tidalvolumen (TV) von 6 ml/kg für 2 Minuten und einer Atemfrequenz (RR) von 12/min beatmet, gefolgt von den 2 Methoden der HFJV nach dem Zufallsprinzip aufeinanderfolgend. Die SIHFJV-Methode wird supraglottisch über ein Jet-Laryngoskop für 5 Minuten mit einer niederfrequenten RR von 12/min kombiniert mit einer hochfrequenten RR von 600/min bereitgestellt. Die Single-HFJV-Methode wird subglottisch über einen dünnen Katheter für 5 Minuten mit einer Hochfrequenz RR von 120/min bereitgestellt. Die Jet-Ventilation-Beatmungsdruck (DP) war eine Funktion des Körpergewichts.

Siebenundzwanzig Patienten, die sich verschiedenen elektiven endotrachealen Operationen unterzogen wurden, die die HFJV erfordern, sind in dieser klinischen Studie eingetragen. Dreiundzwanzig Patienten sind in der endgültigen Analyse enthalten, da 4 Patienten ausgeschlossen wurden. Die regionale Ventilationsverteilung der Lunge bzw. Region of Interest (ROI) wurde während des gesamten Prozesses von der EIT aufgezeichnet und offline analysiert.

Es gab keinen signifikanten Unterschied zwischen den HFJV-Methoden bei der Ventilationsverteilung der Lungen-ROIs und der Silent Spaces (SS). Die Tidal-Impedance-Variation verringerte sich signifikant (P-Wert < 0.05) von durchschnittlich 1566 AU auf durchschnittlich 300 AU während der Single-HFJV im Vergleich zur SIHFJV, was mehr TV in der SIHFJV-Methode im Vergleich zur Single HFJV-Methode reflektiert.

Darüber hinaus wird eine Erhöhung des DP um 0.5 bar während der SIHFJV als wirksam angesehen. Eine Erhöhung des DP führt durch der Überblähung der bereits ventilierten Lungenregionen zur Erhöhung des TV ohne Änderung bei der Ventilationsverteilung.

Während der Single HFJV ändern die Position und die Spitzenrichtung des Jet-Katheters innerhalb der Trachea die Ventilationsverteilung in der Lungen-ROI und zwischen rechter und linker Lunge. In einigen Fällen könnte die Spitzenrichtung zu mehr als 90% des TV in nur einer Lunge oder in bestimmten Regionen der Lunge führen.

In der Rückenlage entwickeln die dorsalen Regionen (abhängige Regionen) die SS mehr als die ventralen Regionen (unabhängige Regionen), die während der Masken- und SIHFJV-Methode signifikant sind. Die SIHFJV-Methode entwickelt sich zu durchschnittlich 8 % als abhängige SS, während sie nur zu durchschnittlich 3 % als unabhängige SS entwickelt wird. Es gab keinen signifikanten Unterschied bei den entwickelten SS zwischen den dorsalen und ventralen Regionen während der Single HFJV-Methode.

In dieser Studie war die EIT eine effektive Bildgebungstechnik, um die Ventilationsinhomogenität in der Lunge zu erkennen. Es hat widergespiegelt, dass es zwischen den HFJV-Methoden keine signifikante Verbesserung in der Ventilationsverteilung oder in den entwickelten SS gab. Die Erhöhung des DP von HFJV wird klinisch angewendet, um das TV zu erhöhen. Diese Studie beweist, dass das TV durch die erhöhte Ventilation der bereits ventilierten Lungen-ROI zunimmt, ohne die Ventilation auf die weniger ventilierten Bereiche zu verteilen.

Abstract

Electrical Impedance Tomography (EIT) is a radiation-free non-invasive imaging technique that allows a bedside continuous monitoring of lung regional ventilation distribution. It is a novel imaging tool that is cheap, portable, easily accessible, and can be a part of the intensive care unit or the operation rooms. The High-Frequency Jet Ventilation (HFJV) is one of the common mechanical ventilation techniques used in patients under anesthesia during airways surgeries.

The main objective of this thesis is to evaluate the regional ventilation distribution of the lung during the application of two different HFJV modes by the usage of the EIT tool in patients under anesthesia. First, Single High-Frequency Jet Ventilation mode (Single HFJV), where a single high-frequency portion of the gas is used for the ventilation process. The second mode is the Superimposed High-Frequency Jet Ventilation mode (SIHFJV), where two different ventilation frequencies are combined together and delivered simultaneously to the lung.

Patients undergoing surgeries in the airways were ventilated through a mask with a Tidal Volume (TV) of 6 mL/kg for 2 minutes and Respiration Rate (RR) of 12/min, followed randomly by the 2 modes of the HFJV sequentially. The SIHFJV mode was provided supraglotticaly via a Jet Laryngoscope for 5 minutes with a low-frequency RR of 12/min combined with a high-frequency RR of 600/min. The Single HFJV mode was provided subglotticaly via a thin Catheter for 5 minutes with a high-frequency RR of 120/min. The jet ventilation Driving Pressure (DP) was a function of the body weight.

Twenty-Seven patients undergoing different elective endotracheal surgeries requiring HFJV were enrolled for This clinical study. Four patients were excluded and the final analysis included 23 patients. The regional ventilation distribution of the lung Region of Interest (ROI) was recorded by the EIT during the whole process and analyzed offline.

There was no significant difference in the ventilation distribution of the lung ROIs and the Silent Spaces (SS) between the HFJV modes. The Tidal Impedance Variation significantly decreased (P-value < 0.05) from an average of 1566AU during the SIHFJV to an average of 300AU during the Single HFJV, which reflects more TV during the SIHFJV mode compared to Single HFJV mode.

Furthermore, during the SIHFJV, increasing the DP by .5 bar is considered to be effective. Increasing the DP increases the TV by over-inflation of the already ventilated lung regions without change in the lung ventilation distribution.

During the Single HFJV, the Jet Catheter's position and tip direction inside the trachea change the ventilation distribution in the lung ROIs and in between the right and the left lung. In some cases, the tip direction could lead to more than 90% of the TV in only one lung or in a specific lung ROI.

In the supine position, the dorsal regions (dependent regions) develop more SS than the ventral

regions (non-dependent regions) which is significant during mask and SIHFJV modes. SIHFJV mode develops an average of 8% as dependent SS, while develops only average of 3% as Non-dependent SS. There was no significant difference in the developed SS between the dorsal and ventral regions during the Single HFJV mode.

In this study, EIT was an effective imaging technique to detect the ventilation inhomogeneity in the lung. It reflected that there was no significant improvement in the ventilation distribution or in the developed SS between the HFJV modes. Increasing the DP of HFJV is applied clinically to increase the TV. This study proves that the TV increases due to increased ventilation of the already ventilated lung ROIs without distributing the ventilation to the less ventilated areas. The anesthesiologists should be careful while handling the DP during HFJV modes to avoid ventilator-induced lung injury.

Keywords: Electrical Impedance Tomography, High-Frequency Jet Ventilation, Region of Interest.

1 Introduction

Patients under anesthesia are at risk for a number of complications related to the regional ventilation distribution across the lung. Intensive monitoring is required to identify early signs of clinical issues. Pulse oximetry and capnography are used to ensure that appropriate oxygenation and carbon dioxide elimination are achieved and maintained. Such monitoring is not sufficient and the need for real time monitoring of the lung is needed to assess the lung ventilation closely. Medical imaging is considered to be an optimum solution to monitor the lung functionality.

Current imaging techniques like Magnetic Resonance Imaging (MRI), Computer Tomography (CT), and Positron Emission Tomography (PET) are bulky, expensive, accessed only at a specific place in the hospitals, and cannot be a part of the operation rooms or Intensive Care Unit (ICU). Due to their nature, these traditional imaging techniques are mostly harmful and usually invasive and radiative procedures. These challenges opened the way for a new imaging technique that is cheap, portable, easily accessible, and can be a part of ICU or operation rooms. This novel tool is the Electrical Impedance Tomography (EIT). Before we go into details of the EIT, some basics about the anatomy of the lung, the bio-signals, registration of the human body impedance and how it can be recorded are illustrated.

1.1 Lung Anatomy

The lung is a body organ located inside the thoracic cavity, responsible for breathing. Its base sits on the diaphragm, and its apexes extend into the root of the neck. the lung performs the breathing in air sacs called alveoli through two repeating phases, inspiration and expiration phase. The alveoli extract the oxygen from the air and pass it into the bloodstream during the inspiration phase while releasing the carbon dioxide outside of the body during the expiration phase.

The lung consists of two cone-shaped organs in the chest, the right and left lung. The right lung is slightly large and consists of three lobes, while the left lung consists of only two lobes, Fig 1.1. Anatomically, the respiratory system can be divided into the upper and lower respiratory tracts. The upper respiratory tract consists of the nose, pharynx, and larynx. The lower respiratory tract is located in the chest and consists of the trachea, Two tubes called bronchi lead from the trachea to the right and left lungs, bronchioles, alveolar ducts, and alveoli, Fig 1.2.

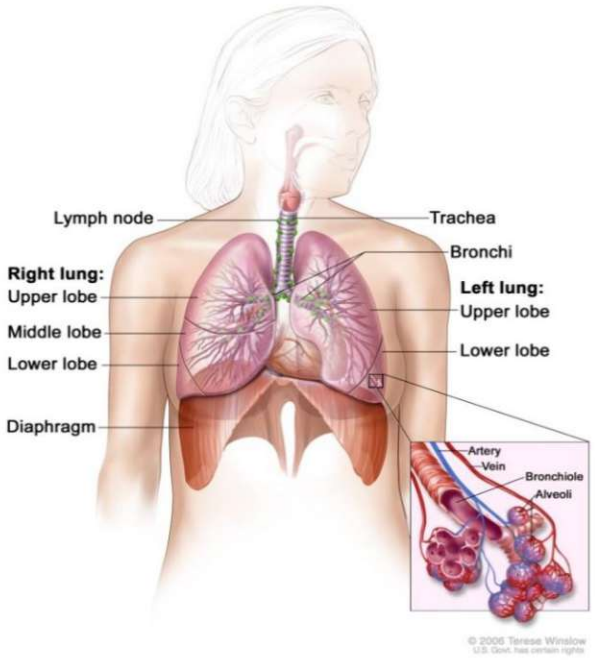

Fig 1.1 Lung structure [1].

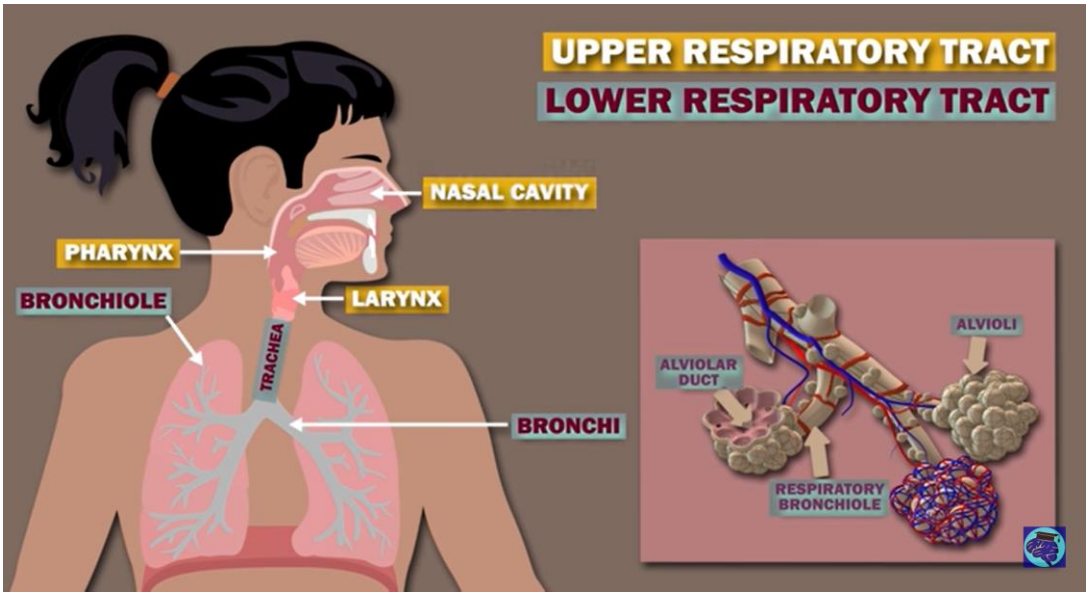

Fig 1.2 anatomical structure of the respiration system [1].

There are two membranes surrounding the lung, the first membrane lining the inner wall of the rib cage and called the costal pleura and the other is resting on the surface of the lung and called the visceral pleura, between these two membranes is the pleural cavity. The movement of the lung counters a little fraction due to the pleural fluid inside the pleural cavity which acts as a lubricator, Fig 1.3.

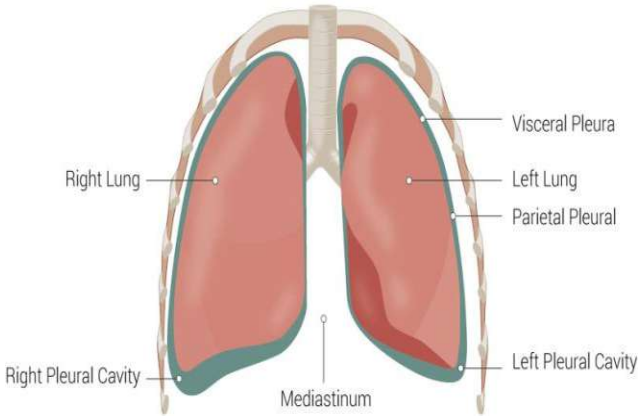

Fig 1.3 pleural fluid inside the pleural cavity acts as a lubricator [2].

To perform the respiration process, the lung expands and relaxes through the expansion and relaxation of the thoracic cavity. This happens through the activity of the diaphragm and the muscle of respiration. To perform the inhalation phase, the diaphragm contracted, developing a negative pressure inside the thoracic cavity and the air moved toward the lung. During the exhalation phase, the diaphragm relaxes, developing a pressure inside the body higher than the atmospheric pressure and the air moves outside the body through the airways. The lung has two forms of blood supply, pulmonary circulation and bronchial circulation. The pulmonary circulation brings the deoxygenated blood from the body to the lung through the pulmonary artery and returns the oxygenated blood through the pulmonary veins. The bronchial circulation supplies the lung tissues with blood.

1.1.1 Regions of Interest

During the respiration process, the lung volume changes due to the change of the air amount inside the lung. The amount of air increases inside the lung during the inspiration, while decreasing during the expiration. This amount of air moved into or out of the lung, called the Tidal Volume (TV), usually 7 mL/kg of body weight. The impedance changes due to the change of the amount of air inside the lung.

In this project, the ventilation analysis was performed offline through a special software from swisstom©, Switzerland called ibeX. The tidal EIT image provided by ibeX for the right and the left lung is divided into four equally Region of Interest (ROI), each representing 25% of the lung through the ventrodorsal diameter. ROI1 represents the ventral region, ROI2 represents the central-ventral region, ROI3 represents the Central-dorsal region and finally and ROI4 represents the dorsal region, Fig 1.4A. The regional ventilation distribution for each ROI represented in percent of the total TV is shown in Fig 1.4B. The impedance change waveform for each ROI during the ventilation process is shown in Fig 1.4C [3].

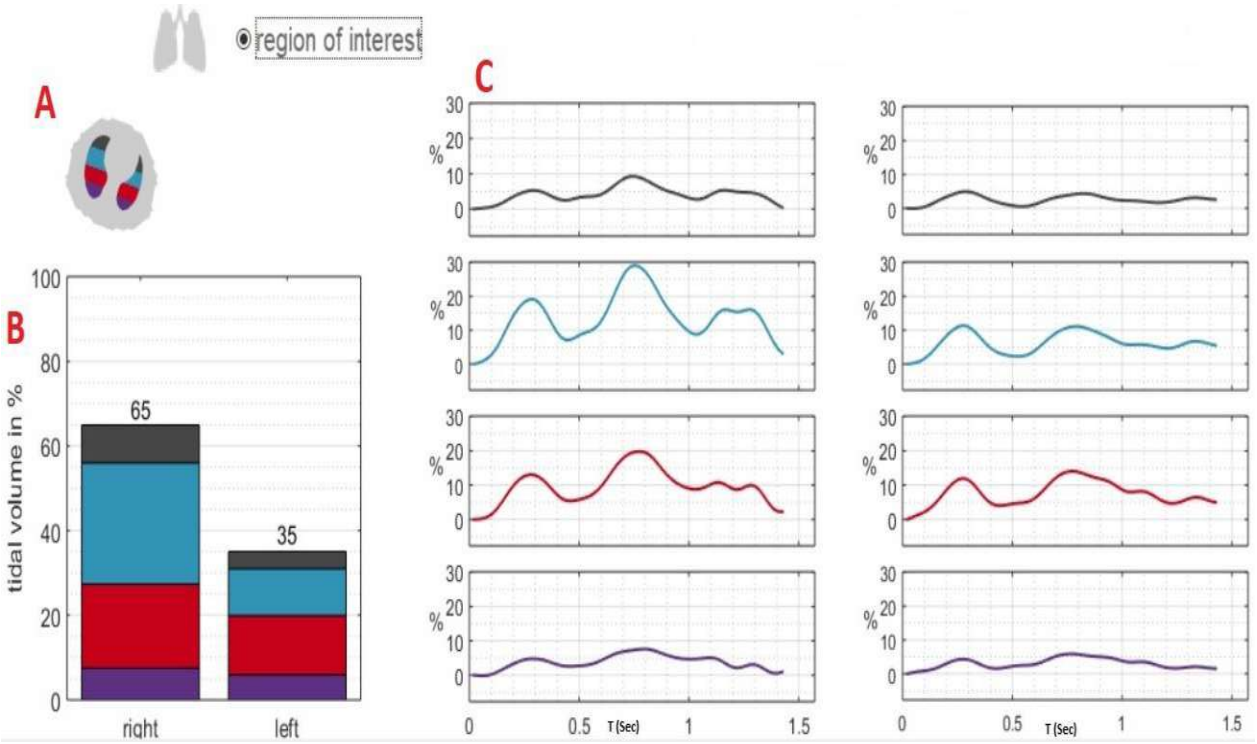

Fig 1.4(A): ROI representation, ROI1-ROI4 from top (Ventral) to bottom (Dorsal), (B) Ventilation distribution of the tidal EIT image in (%), (C) Impedance change waveform during the ventilation process in each ROI [4].

1.1.2 Silent Spaces

The Silent Spaces(SS) represent the areas in the lung that doesn't ventilate or even with poor ventilation. The lung is divided into two SS, the Non-gravity-dependent Silent Spaces(NSS) and the Gravity-Dependent Silent Spaces (DSS). ROI1 and ROI2 are usually called NSS. ROI3 and ROI4 are usually called DSS. These two regions are separated by a line that is perpendicular to the gravity and passes through the Center of Ventilation (CoV). This line is called Horizon of Ventilation (HoV). In supine position, DSS are located below the HoV, while the NSS are located above the HoV, Fig 1.5 [3].

It is worth knowing that ventilation in the lung is non-homogeneous, the main reason is the gravity. The effect of gravity depends on the patient's position during the ventilation and hence, the orientation of the lung [5].

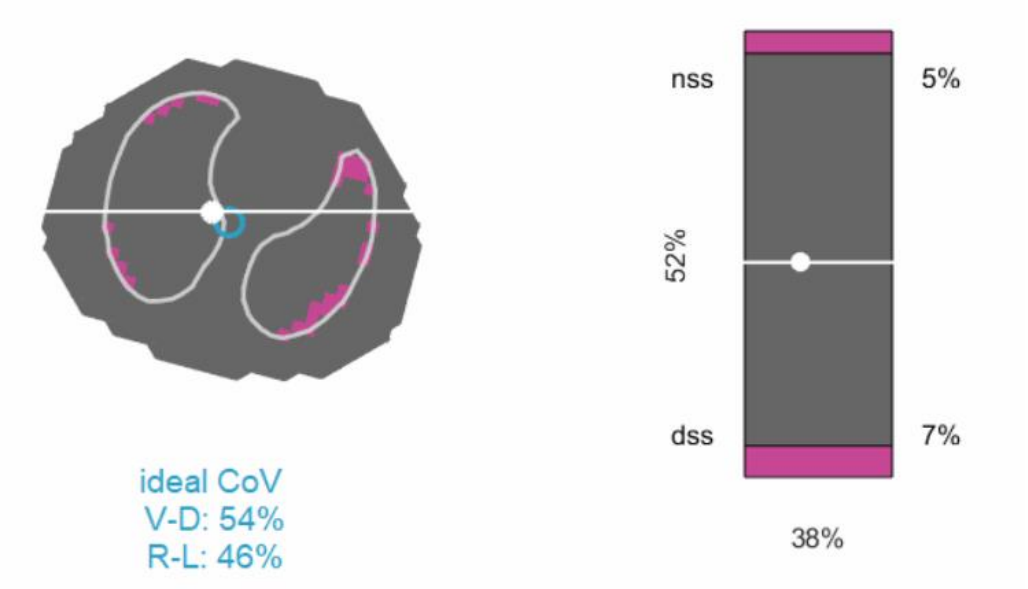

Fig 1.5 The lung regions that receive normal ventilation are displayed in dark grey color, the SS displayed in pink. spatial distribution displayed on left and numerical representation of the DSS and NSS silent displayed on right [4].

During the study, all patients were tested in the supine position. In this position, the gravity exerts on the DSS more than the NSS. Another factor that plays a role in the development of the SS, is the accumulation of fluids around the lung, which also affects the DSS in the supine position.

1.2 Bio-signals

Bio-signals can be classified based on their existence, dynamics and origin. The existence of bio-signal can be classified as permanent or induced bio-signal. Permanent bio-signals can exist without any stimulus or excitation from the outside of the body and can be investigated or measured at any time. Electrocardiogram (ECG) and heart beating sounds are clear examples of permanent bio-signal. On the other hand, induced bio-signals require external stimulus or excitation to be measured, it is always available as the external stimulus is applied. After the removal of the external stimulus, the induced signal will be decayed at a specific time constant based on the body properties.

Electrical Plethysmogram is an example of the induced bio-signal. The external alternating current is applied through a couple of electrodes on the tissue under investigation. The resulting voltage along with the current path representing the tissue impedance can be registered. Fig 1.6 shows examples of the permanent and induced bio-signals [6].

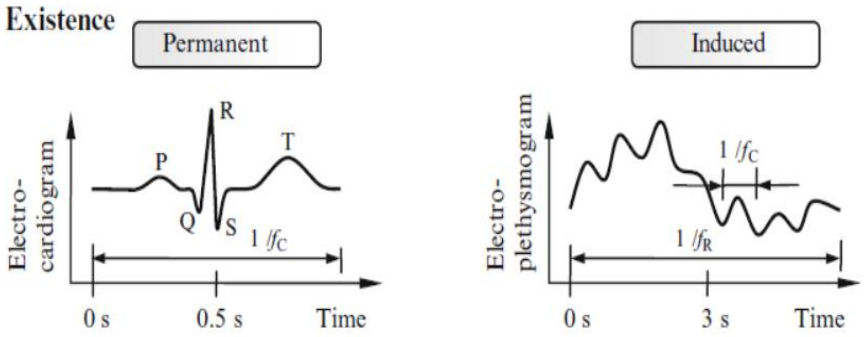

Fig 1.6 Classification of bio-signals based on their existence into permanent and induced bio-signals (f_C: Heart rate, f_R: Respiratory rate) [6].

This clinical study is based on registering the respiration activity. There are many methods of recording respiration activity. Three types of the respiration recording methodologies are described in Fig 1.7 [7].

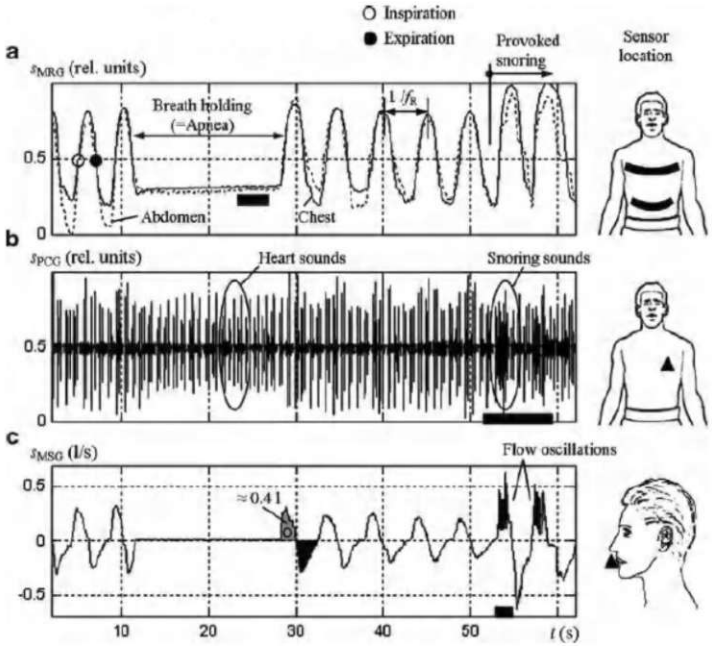

Fig 1.7
(a) mechanic bio-signal mechanorespirogram sMRG (from the chest and abdominal circumference changes)
(b) acoustic bio-signal phonocardiogram sPCG (from the heart region on the chest)
(c) mechanic bio-signal mechanospirogram sMSG (from mouth airflow) [7].

In analogy to mechanic bio-signal mechanorespirogram, instead of registering the change of chest circumference due to respiration process, there is another method to register the respiration activity based on the change of chest electrical impedance due to the inhalation and exhalation of the lung. Here a belt of wires is placed around the chest, the electrical inductance of wires is measured which is increased during the inspiration phase and reduced during the expiration phase [7].

1.2.1 Registration of impedance of the human body

The electrical impedance of the human body can be measured through the application of the alternating electric field. Four electrodes are used to build up a device that measures the human body impedance. The alternating current is applied through the two outer electrodes and the resulting voltage is measured between the two inner electrodes. Fig 1.8 describes the arrangement of the electrodes and the measuring setup components. Amplifier is used to amplify the difference and Band-Pass Filter (BPF) to pass only the applied current frequency. The demodulator is used to obtain the absolute values and a kind of average and deliver the Electric Field Plethysmogram Signal (EFPG) [8].

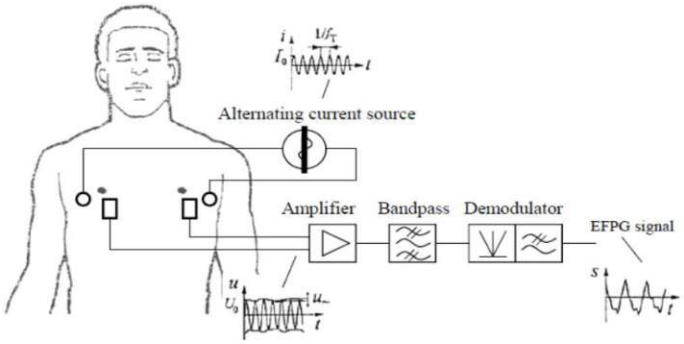

Fig 1.8 arrangement of human body impedance measurement [8].

The output signal contains two components. The first component is the constant component U_0, where U_0> 90% of u (body measured output voltage) due to the initial state of medium impedance. The second component is the alternating component $U_{\sim}$ <10% of u due to the respiration and cardiac activity, displacement of organs and liquids or blood volume change.

As mentioned, the current is applied through the outer electrodes and the resulting voltage is measured between the two inner electrodes. The resulting output voltage is the summation of the equipotential lines through the chest. The distribution of the equipotential lines through the chest is described in Fig 1.9. With more equipotential lines, the electrical conductivity (γ) decreases, and the electrical impedance (z) increases. Hence, the inspiration phase releases more equipotential lines than the expiration phase providing higher impedance. this increases output voltage during inspiration while decreasing during the expiration phase [8].

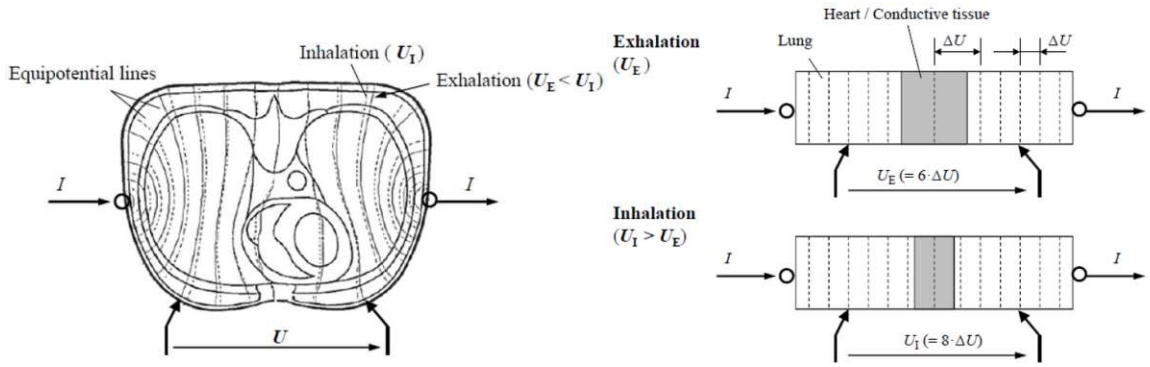

Fig 1.9 The distribution of the equipotential lines through the chest, (output voltage due to inspiration) $U_I > U_E$ (output voltage due to expiration). $U_E=6\Delta U$ during the exhalation phase, while $U_I=8\Delta U$ during the inhalation phase [8].

1.2.2 Recording system

There are two major techniques to detect the electrical impedance of the human body. The first technique is the previously mentioned technique which called four electrodes technique, where the current is applied between 2 electrodes and the resulting voltage is measured between the other two electrodes. The second technique is called two electrode technique, where the same two electrodes are used for current application and resulting voltage measurements, Fig 1.10.

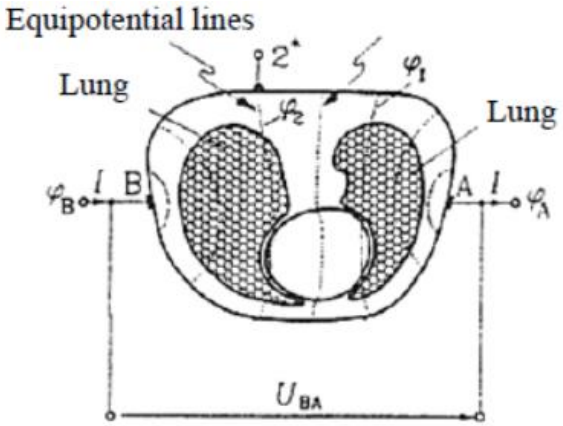

Fig 1.10 Body impedance recording system, 2 electrodes technique [8].

The two electrodes technique is not preferable as the contact and electrode impedances are directly affecting the measured voltage. The movement artifacts are the main player in varying the contact impedance.

$$Z_{BA}=U_{BA}/I=Z_{Bcontact} + Z_{BAtissue} + Z_{Acontact} \quad \text{(Eq. 1)}$$

To get rid of the contact impedances, four electrodes technique is used. Fig 1.11 illustrates the

equivalent circuit of the four electrodes technique, where no influence of $Z_{Acontact}$, $Z_{Bcontact}$. Furthermore, there is no current passes through $Z_{1contact}$, $Z_{2contact}$ and hence no influence of both impedances. The resulting voltage will be only across the tissue impedance $Z_{BAtissue}$ [8].

The two main parameters of the four electrode technique are the frequency and amplitude of the applied alternating current. The applied frequency lies between 20-100kHz. It is higher than 20kHz to avoid the neural stimulation and lower than 100kHz to avoid dispersion. With higher frequencies, the permeability ε and the conductivity of the heart, lung and blood will become identical and the separate activity of each cannot be registered. The applied current amplitude is in the range of ~1mA. It should not be too high to avoid neural stimulation and the thermal effect [8].

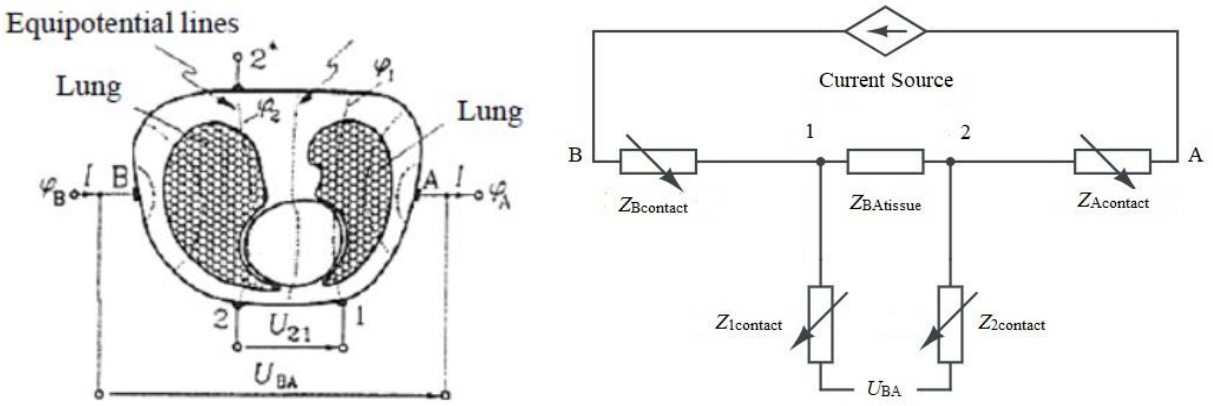

(A) (B)

Fig 1.11 (A) Body impedance recording system, four electrodes technique [8].
(B) The electrical equivalent circuit of the four electrodes technique to register the body impedance.

1.2.3 Voltage and Current Application

Fig 1.12 illustrates the reasons that current application is more favorable than voltage application to register the body impedance. The first reason is that current application provides a local assessment of the conductivity changes. If a voltage is applied instead of the current, U will be a function of the fixed impedance. While if the current is applied, U will not be a function of the fixed impedance [8]

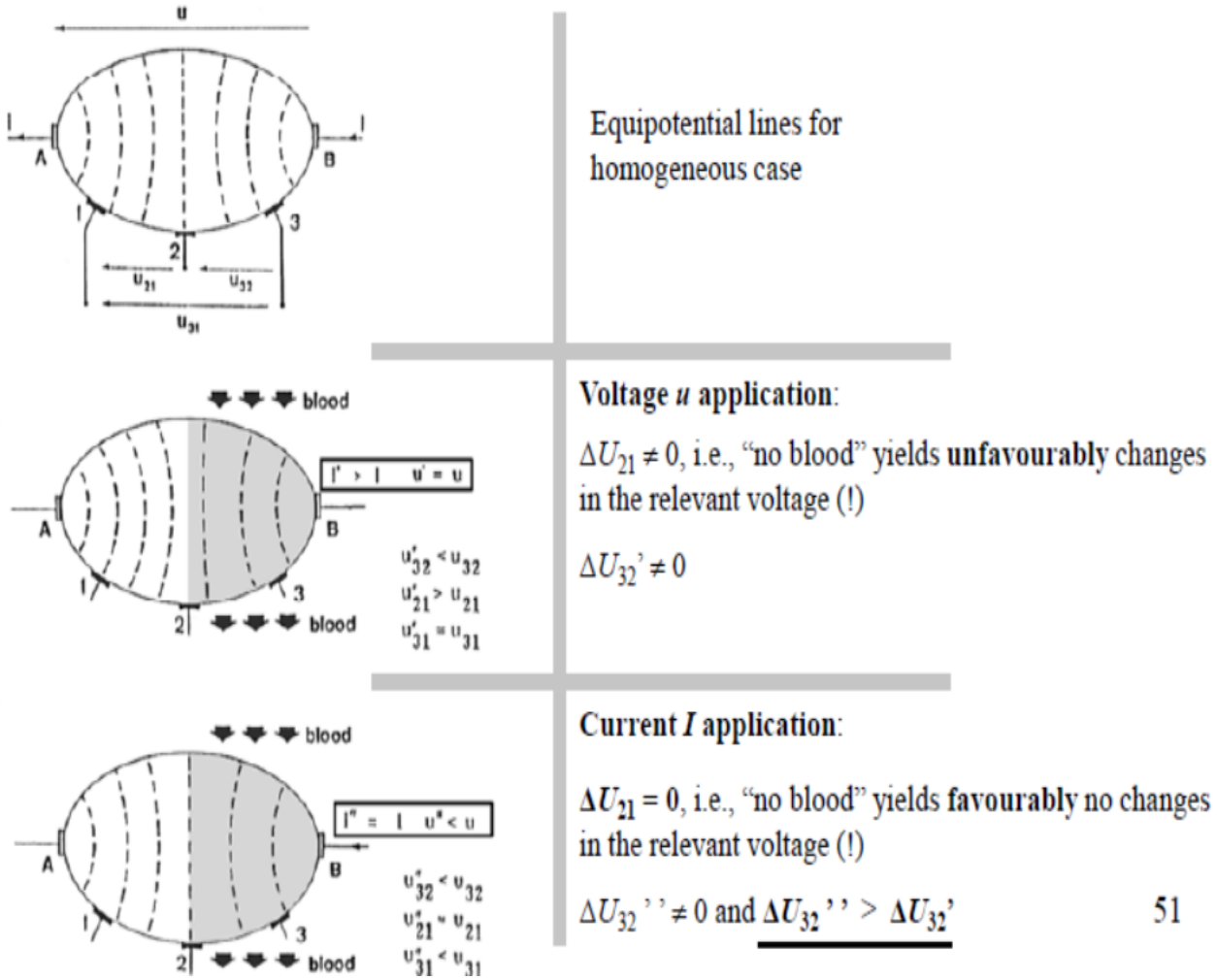

Fig 1.12 the current application provides a local assessment of the conductivity changes. $\Delta U_{21} = 0$ in case of the current application, means no changes in the voltage across no-blood regions. While, in voltage application, $\Delta U_{21} \neq 0$, changes in the voltage across no-blood regions are developed [8].

The second reason is that the current application provides higher sensitivity than the voltage application, Fig 1.13. In the homogeneous case and no blood flows, the output voltage U_0 measured between electrode pair 2,3 is $U/2$, half of voltage across the body circumference due to the voltage divider effect. In case of voltage U application and blood flows across the half of the region, the change in the voltage across the blood flow region is $U/6$. While, in the case of current application, the change in the voltage across the blood flow region is $U/4$.

Since $U/4 > U/6$, it ends up with higher sensitivity during current application compared to voltage application [8].

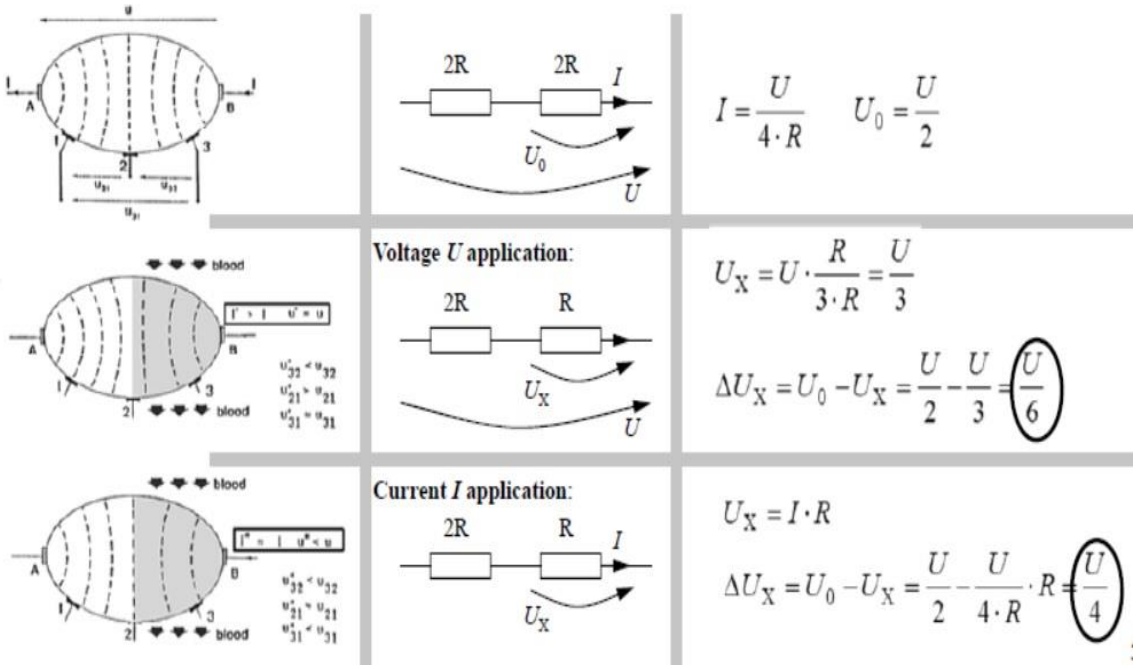

Fig 1.13 The current application provides higher sensitivity than the voltage application [8].

1.3 Electrical Impedance Tomography

EIT has been introduced in 1985 by (Brown et al) [9]. A Few years later, it was realized that mechanical ventilation has an impact on lung injury [10]. The need for EIT becomes more and more to have a continuous lung monitoring tool to avoid such lung injuries.

The main advantage of EIT is that it is a radiation-free non-invasive imaging technique that allows a bedside continuous monitoring of lung regional ventilation. It yields a functional tomogram based on the change of the chest impedance due to the changes in the volume. EIT allows a fast response, which means that the therapy can be modified based on the physiological response of the patient where we need to make a fast clinical decision.

as previously illustrated, to register the bio-impedance, an electric current is applied to the tissue and the resulting voltage is measured. In EIT, not only 4 electrodes but a belt of 16 or 32 electrodes surrounding the chest is used. The image generated by the EIT reflects the impedance of the chest. There are many reasons for the chest impedance to be changed. the main reason is the inspiration and expiration phases of the lung ventilation. Also, it can be changed due to the heart filling in and out phases with blood, as well as the perfusion.

The impedance change of the lung is directly proportional to the lung volume, which representing the amount of air inside the lung. This amount of air can be measured noninvasively with the textile belt fixed around the chest. For example, 16 electrodes surrounding the chest, each electrode will have a

specific contribution to the image generation. A pair of electrodes will induce a few current (~1mA) amplitude through pair of electrodes, whereas the other passive electrodes measure the resulting potential in different areas of the lung. Once the first recording is done, the next two electrodes will induce the current and all the other passive electrodes will record the image. This sequence happens in turns, which means there are 16 pairs of electrodes where the current is applied in turn and the remaining electrodes measure the voltage which is proportional to the lung impedance, Fig 1.14.

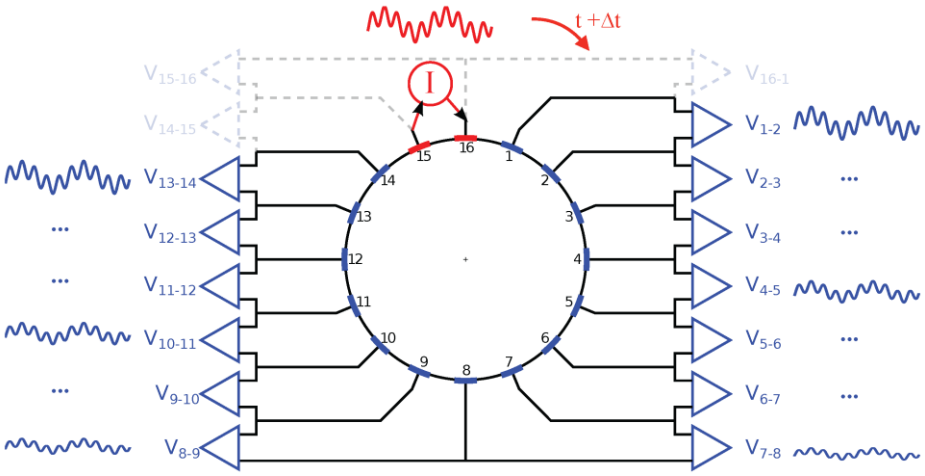

Fig 1.14 electrodes positions, the current applied between two electrodes in red and the voltage is measured passively between the rest in blue [11].

Once the whole measurements are there, the resulting voltages are used to build a frame with a resolution of about 50 frames per second [12]. the EIT system will build a pixel matrix out of the produced frames. Each pixel will have a value of resistivity which will correspond to the volume of the region in that particular area in the lung. Through a mathematical software, the EIT will generate an image. This image is a color-scaled image to indicate a change in resistivity from no change to maximum change, Fig 1.15.

Fig 1.15 color scaled image produced by EIT to indicate a change in lung. Regions with large changes, reflecting better ventilation, are shown in white colors. Regions with small changes are graded from white to blue, regions with no changes displayed in black [4].

One of the main advantages of EIT is illustrated in Fig 1.16, it can provide a large slice which depends on the size of the patient, but it can be 7-10 cm across the belt. The main limitation of EIT is that despite the very high temporal resolution, it yields a very poor spatial resolution depends on the total number of electrodes and the chest volume. This is not too important; it is not an anatomical imaging technique like CT.

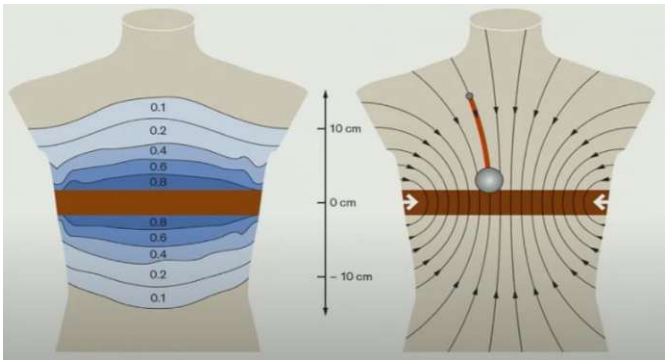

Fig 1.16 EIT can provide a large slice that can be 7-10 cm across the belt [13].

1.4 Jet Ventilation

Conventional mechanical ventilation techniques induce a generous number of issues to both anesthesiologists and surgeons. For example, the anesthesiologist needs an uninterrupted airway in micro-laryngeal surgery, while surgeons need to access the larynx and have good visibility. Such challenges opened the way for Jet Ventilation (JV) to replace the conventional ventilation techniques, especially in thoracic surgeries.

JV or Venturi jet injector has been introduced by Sander in 1967. He used a high flow of oxygen for ventilation through a bronchoscope at a pressure of (50 PSI) under full Anesthesia. [14] Giunta F, et al used high-frequency jet ventilation (HFJV) between 1981 and 1989 in 300 patients during general anesthesia for endoscopy and surgery of the airways. They used it for different types of surgeries like laryngoscopy, bronchoscopy, laryngeal microsurgery and laser surgeries [15]. Now, it is used as a ventilation procedure in both ICU and airway surgeries.

In this clinical study, two main modes of JV are used. The first mode is the Single High-Frequency Jet Ventilation (Single HFJV), where a single high-frequency portion of the gas is used for the ventilation process. The second mode is Superimposed High-Frequency Jet Ventilation (SIHFJV) where two different ventilation frequencies are combined together and delivered simultaneously to the lung.

1.4.1 Single High-Frequency Jet Ventilation

Klain and Smith in 1976 described HFJV as it is a procedure that consists of a source that delivers a high-pressure gas through a thin cannula placed in the airway and the expiration happens passively [16]. Another definition from Fritzsche K et al, that HFJV involves facilitating gas exchange with a small TV of 2 to 5 ml/Kg and rate of (110–400/min) followed by passive expiration [17] [18].

Subglottic JV involves placing a (~2 to 3 mm diameter) thin catheter through the glottis and down into the trachea, allowing delivery of a jet of gas directly into the trachea, Fig 1.17. Subglottic JV results in reduced driving pressure, minimal vocal cord movements and a good surgical field.

In the Single HFJV a shot of gas with specific pressure is applied, followed by passive expiration for a very short time before the arrival of the second shot. This fast sequence builds up auto Positive End Expiratory Pressure(PEEP). The risk for barotrauma and pneumothorax is maintained but it is less likely to happen. The main advantage of HFJV over auto-PEEP is that it supplies enough ventilation to the lung with a low motion of the patient airway, so it can be useful for thoracic surgeries. Also, it is beneficial to reduce ventilation-related movement during radiofrequency ablation of small tumors from the liver [21].

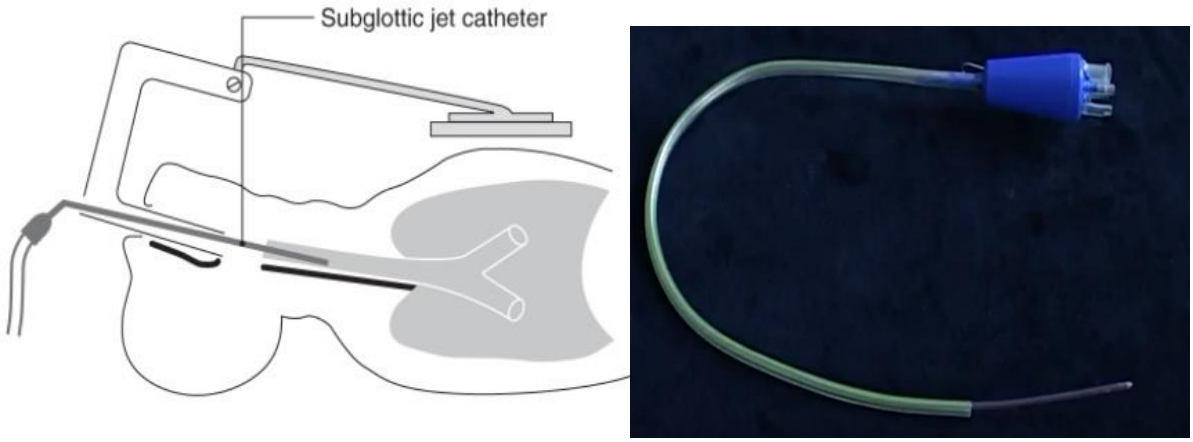

Fig 1.17 subglottic jet catheter [19] [20]

The main complication with HFJV is that when only one jet flow is used in patients with stenosis or airway obstructions, a hypercapnia -build-up of Carbon-dioxide (CO2)- might occur. The CO2 can be eliminated by increasing the driving pressure (DP) [22]. However, increasing the DP might develop air trapping and may lead to lung injury. To overcome the issue of CO2 accumulation inside the body, SIHFJV is developed.

1.4.2 Superimposed High-Frequency Jet Ventilation

SIHFJV was firstly introduced in 1990 by Dr. Alexander Aloy and his colleagues from the department of anesthesia, University of Vienna (later is the Medical University of Vienna). They developed a tubeless ventilation system supplies the patient with a low frequency superimposed with high-frequency JV. They tested this novel technique in 60 patients and the results were awesome. All the patients were ventilated optimally without hypercapnia or other complications [23].

Supraglottic JV is a true Venturi type of ventilation. Venturi Effect means gas flow at a constriction speeds up causing a pressure drop and entrainment. TV in that case is the sum of injected and entrained air.

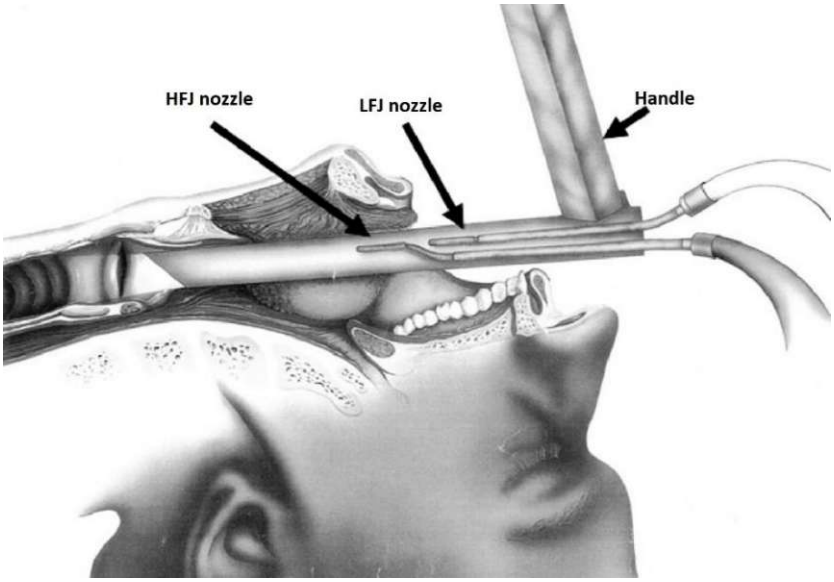

Fig 1.18 Supraglottic JV via a Jet Laryngoscope [24].

SIHFJV is suitable for use with endolaryngeal and tracheal surgeries, it doesn't require a tracheal tube or catheter, especially in patients with stenosis in the airways. It is the ideal form of JV where only one respirator supplies the supraglottic area via a jet laryngoscope with 2 jet components, Fig 1.18. The first component is the Low Frequency (LF) component, usually in the range of (12–20/min). the second component is the High Frequency (HF) component with a frequency starting with 50/min and up to 1200/min and DP between 1-3 bar.

Fig 1.19 displays the pressure waveform of the SIHFJV technique that consists of continuous high-frequency components and two low-frequency component cycles. The peak airway pressure represents the TV and the Positive End Expiratory Pressure (PEEP) represents the remaining air pressure in the lung at the end of expiration [24].

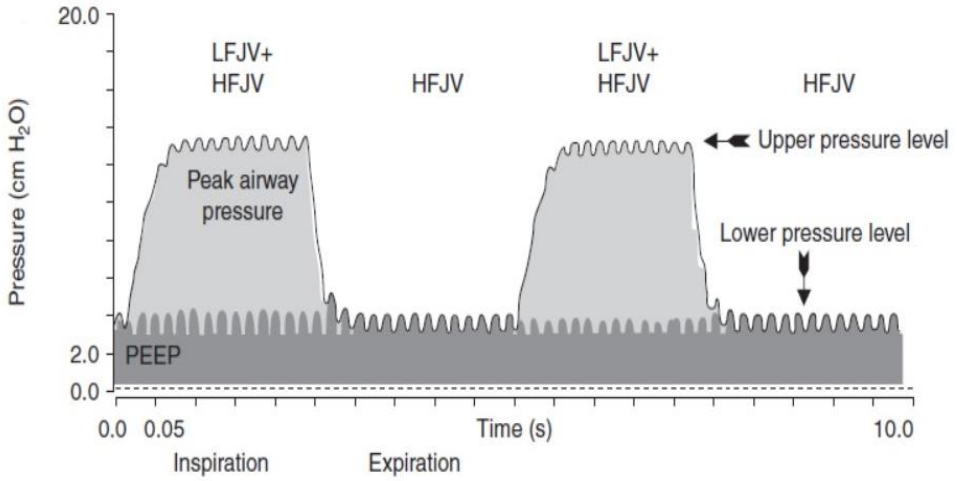

Fig 1.19 SIHFJV pressure waveform via jet laryngoscope during SIHFJV with continuous HFJV and two cycles of LFJV using an adult test. The peak airway pressure provides the TV and the PEEP correlates with the volume of gas remaining in the lung at the end of expiration [24] [25].

In the medical university of Vienna, the SIHFJV technique was tested in more than 1500 patients for nearly 14 years. The results show that SIHFJV reduces the risk of barotrauma, it is considered to be low. Also, it was reported that SIHFJV allows continuous PEEP and suitable gas exchange even for patients with high Body Mass Index (BMI) [24].

2 Materials and Method

Twenty-Seven patients undergoing different elective endotracheal surgeries (Laser microsurgery, panendoscopy, local cord surgery, supraglottic surgery, subglottic surgery, carcinoma, etc…) requiring HFJV were enrolled for This clinical study. The patients were enrolled at the Medical University of Vienna between June 2019 and February 2022 with ethical approval number 1298/2019. The study was registered in clinicaltrials.gov on (Identifier: NCT03973294; posted on clinical trials in June 2019). Inclusion criteria were age between 18 and 99 years, elective laryngotracheal surgeries with JV under general anesthesia, American Society of Anesthesiologists (ASA) classification I-III and BMI <30 kg/m2. Patients with acute laryngeal/Tracheal bleeding, infectious lung disease, thoracic wall deformity and implantable electronic devices were excluded.

2.1 Study Description

The study aimed to assess the regional ventilation distribution of the lung by the application of Single HFJV and SIHFJV using EIT in patients under anesthesia. During the SIHFJV, the gas is supplied supraglotticaly via a surgical instrument called a jet laryngoscope from (TwinStream™, Fa. Reiner, Vienna, Austria), specially developed for this system. The gas jet is supplied with 2 frequency components, the HF component is 600 min-1 and the LF component is 12min-1. the Inspiration to Expiration rate (I/E) was 1:1. During the Single HFJV, the gas was supplied subglotticaly via a thin laser jet catheter with only a single HF component of 120 min-1 and 1:1.5 I/E. The DP for both JV modes was a function of the body weight. Table 2.1 contains the DP values for different body weights.

Body Weight (kg)	DP (bar)
1-50	1
51-80	1.2
81-100	1.5
101-125	1.9
126-142	2.1

Table 2.1 HFJV DP values against patient body weight

The sequence of the JV was randomized, in some cases, the ventilation starts with SIHFJV followed by Single HFJV and vice versa. During the study, the values of SpO2 and tcPCO2 were continuously checked.

2.2 Study Protocol

Patients who are supposed to be ventilated via JV during laryngeal surgery, arrived at the operating room. The EIT device (Swisstom BB2-SenTec, Landquart, Switzerland) is installed and loaded with patient's data such as age, gender, weight, length, etc. An appropriate sensor belt with the appropriate size is placed around the patient chest. the connectivity of the belt electrodes is enhanced by application of a specific gel on the belt before being placed around the patient chest, Fig 2.1(A, B). The belt is tightened and then connected to the EIT device via the special connector. The quality of the connection is checked on the EIT monitor to adjust the belt and avoid any failing electrodes during the measurements, Fig 2.1(C). The EIT device starts to measure the impedance change due to the lung ventilation. these measurements are saved on a portable USB stick and used later for the lung ventilation analysis offline. An example for one breath cycle is shown in Fig 2.1(D), where a sequence of Global Dynamic Images is put in relation to the total impedance changes over time.

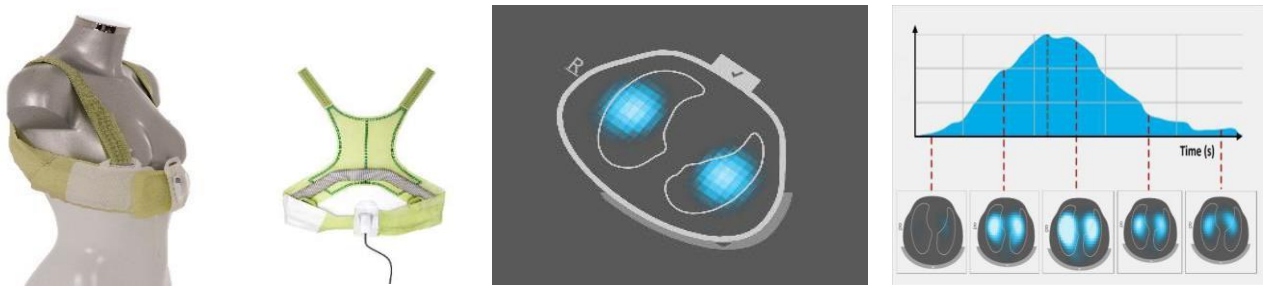

(A) (B) (C) (D)

Fig 2.1 EIT installation (A), (B) the electrode belt placed around the chest at the 5th intercostal space. (C) the quality of the electrodes connection to the body is checked by the surrounding grey line, in case of failing electrodes, the failed area turns into red, the connection can be enhanced by adding extra gel or retightening the belt. (D) a sequence of Global Dynamic Images (at bottom) is put in relation to the total impedance changes over time (at top) for one breath cycle [12].

For real-time monitoring, a pulse oximeter was used for the measurement of the Oxygen Saturation (SpO2). The Carbon-dioxide Partial Pressure (PaCO2) was monitored transcutaneously with (SDM-PO2, SenTec AG, Landquart, Switzerland). The heart rate and blood pressure were also monitored as a clinical routine. After preparations and devices installation, the general anesthesia was inducted and monitored by brain oxygen saturation via Near-Infrared Spectroscopy (NIRS) from (CAS Medical Systems Inc, Branford, Connecticut).

Once the patient's muscles are reported at complete relaxation, the mask ventilation mode starts and remains for 2 minutes as a reference ventilation mode. After that, the surgeon positioned a rigid bronchoscope through the patient throat. The JV starts with one of the previously mentioned two modes, SIHFJV or Single HFJV (TwinStream™, Fa. Reiner, Vienna, Austria).

In the case of the SIHFJV, the JV is applied through a jet laryngoscope supraglotticaly, Fig 2.2. The HF and LF jet ventilation are applied through the two separate nozzles integrated into the jet laryngoscope. The HF was set at 600/min, the LF was set at 12/min, I/E was set at 1:1 and Fraction of Inspired Oxygen (FiO2) at .8. The DP of each frequency component is a function in the weight (Table 2.1). This mode was applied for 5 min under stable conditions of the patient, i.e. SpO2 is higher than 95% and the transcutaneous Carbon-dioxide Partial Pressure (tcPCO2) is lower than 45 mmHg. In case of different values, intervention occurred as indicated in the intervention flow chart in sub-chapters 2.2.1, 2.2.2.

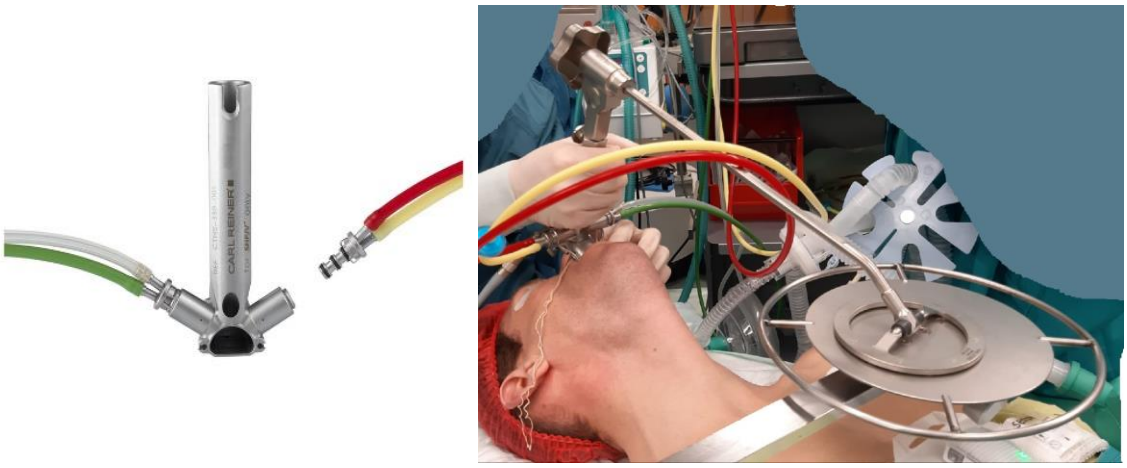

(A) (B)

Fig 2.2 (A) Jet laryngoscope used for SIHFJV, has two openings for the LF and HF jet streams [20].
(B) Jet laryngoscope installation through the patient larynx

In case of the Single HFJV, a thin jet catheter was inserted – in some cases through the rigid bronchoscope- and ventilation happens subglotticaly, Fig 2.3. The high frequency was supplied through this thin catheter with 120/min and I/E of 1:1.5 and FiO2 of .8. the DP was also a function of the body weight as in table 2.1. This mode was applied for 5 min under stable conditions of the patient, i.e. SpO2 is higher than 95% and the tcPCO2 is lower than 45 mmHg. In case of different values, intervention occurred as indicated in the intervention flow chart in sub-chapters 2.2.1, 2.2.2.

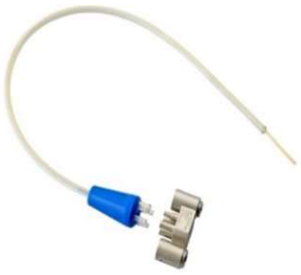

Fig 2.3 Jet catheter used for the Single HFJV mode [20].

After the end of the surgery, the EIT device was uninstalled, and the recorded measurements were excluded for further offline analysis for each of the JV modes.

The flow of the study from the recruitment to the end of the study is illustrated in Fig 2.4. It's important to notice that during the study, especially the JV modes, the SpO2 value might be decreased and tcPCO2 value might be increased in the blood stream, which require fast intervention. The intervention consists of a series of steps of base line parameters change depending on the applied ventilation mode. The next 2 sub-chapters are discussing these issues and how it can be solved.

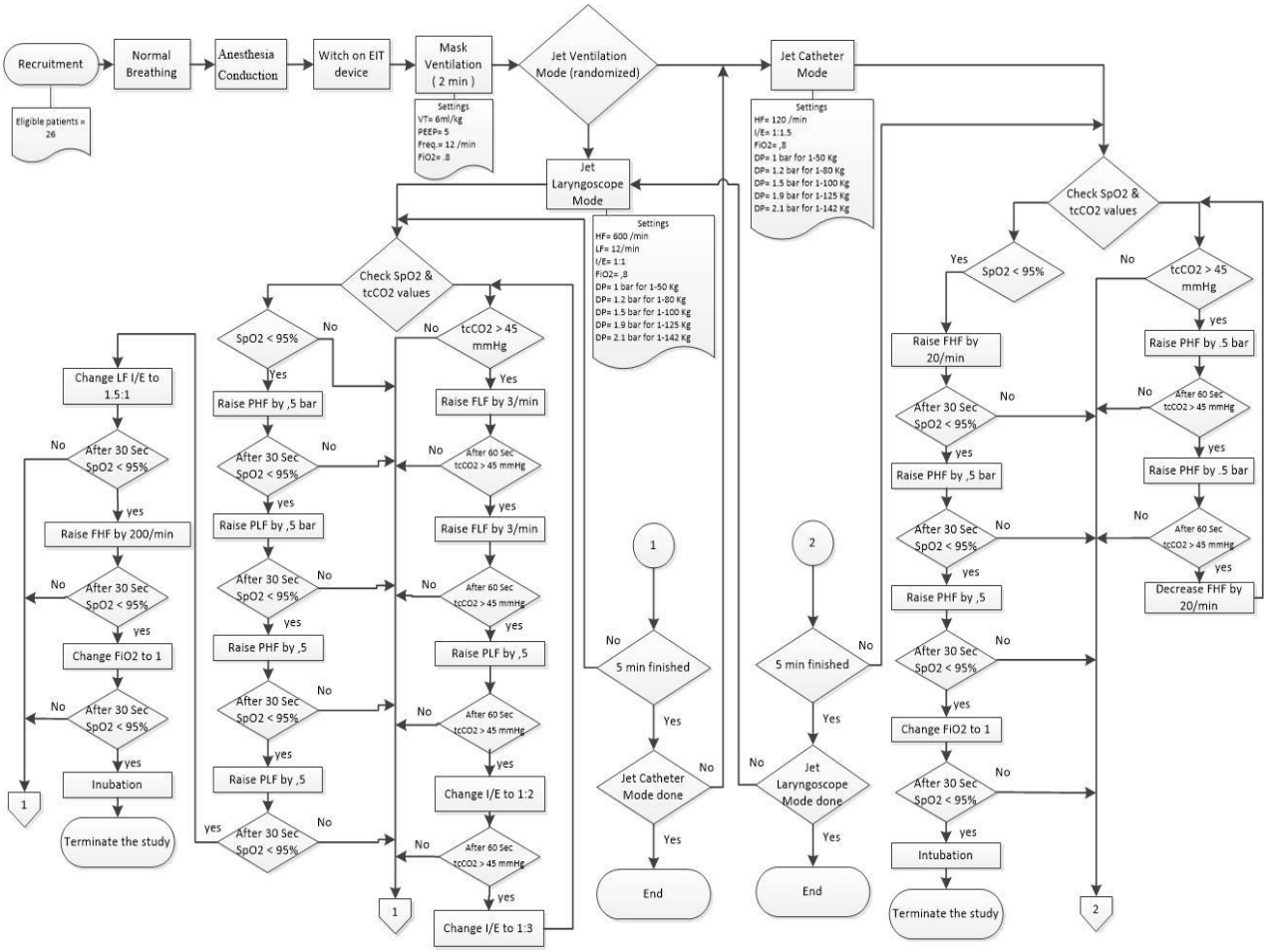

Fig 2.4 Flow chart of the jet study

2.2.1 Intervention in case of Oxygen Saturation below 95%

After the application of any of the two JV modes, the oxygen saturation might be reduced (hypoxemia). Oxygen Partial Pressure (tcPO2) lower than 80 mmHg or SpO2 values lower than 95% is considered low. The more the reduction is, the more severe is the hypoxemia, the faster intervention is required.

During the SIHFJV mode, the DP of both HF and LF components is increased wisely and the SpO2

value is monitored for 30 seconds before applying the next intervention. If the increase of the DP is not enough to get SpO2 > 95%, the I/E rate is increased to 1.5:1 before increasing the HF component by 200/min then FiO2 to 1 instead of ,8. These series steps are applied one after the other as per the flow chart in Fig 2.5, Fig 2.6 until SpO2 higher than 95% is achieved and the intervention is terminated. the JV is then last for 5 minutes as mentioned in the study protocol. During the Single HFJV, the frequency has to be raised by 20/min while monitoring the SpO2 value for 30 seconds before applying the next intervention as per the flow chart in Fig 2.5, Fig 2.6.

2.2.2 Intervention in case of Carbon-dioxide Partial Pressure higher than 45 mmHg

Hypercapnia or carbon dioxide accumulation inside the blood might be developed during the HFJV, especially for the semi-open systems like thin jet catheters. Ventilation with a jet laryngoscope is considered an open system, where the Venturi effect plays a role in the elimination of expired air from the body, but still CO2 accumulation in the body might be developed. CO2 build-up inside the blood-stream usually happens in patients who have higher BMI and stenosis within the airway.

As previously mentioned, during jet catheter ventilation, the CO2 can be eliminated by increasing the DP by .5 bar for two steps before decreasing the ventilation frequency by 20/min. these intervention steps are separated by 1 min to assess the CO2 values and can be terminated when it reached a value lower than 45 mmHg Fig 2.5, Fig 2.6. During the jet laryngoscope, hypercapnia can be counteracted by increasing the LF component before increasing the LF pressure. If the CO2 value is still higher than 45 mmHg, the I/E has to be reduced to 1:2 before 1:3, Fig 2.5, Fig 2.6.

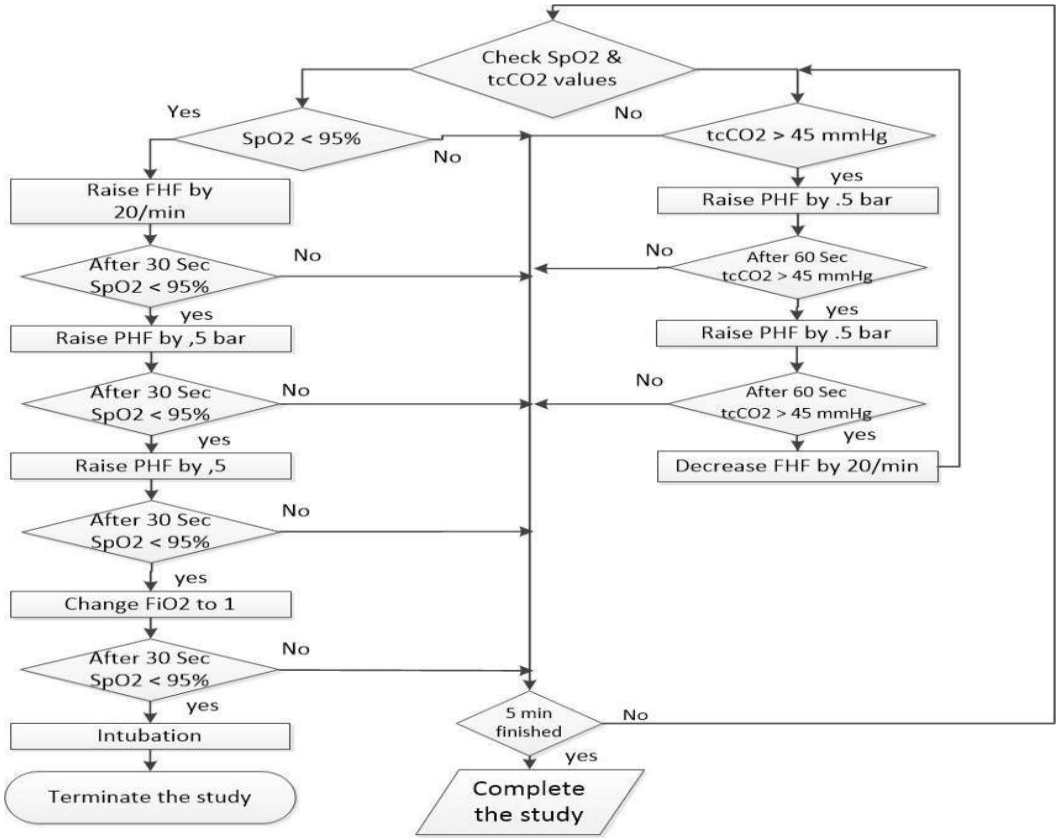

Fig 2.5 Intervention steps during Single HFJV

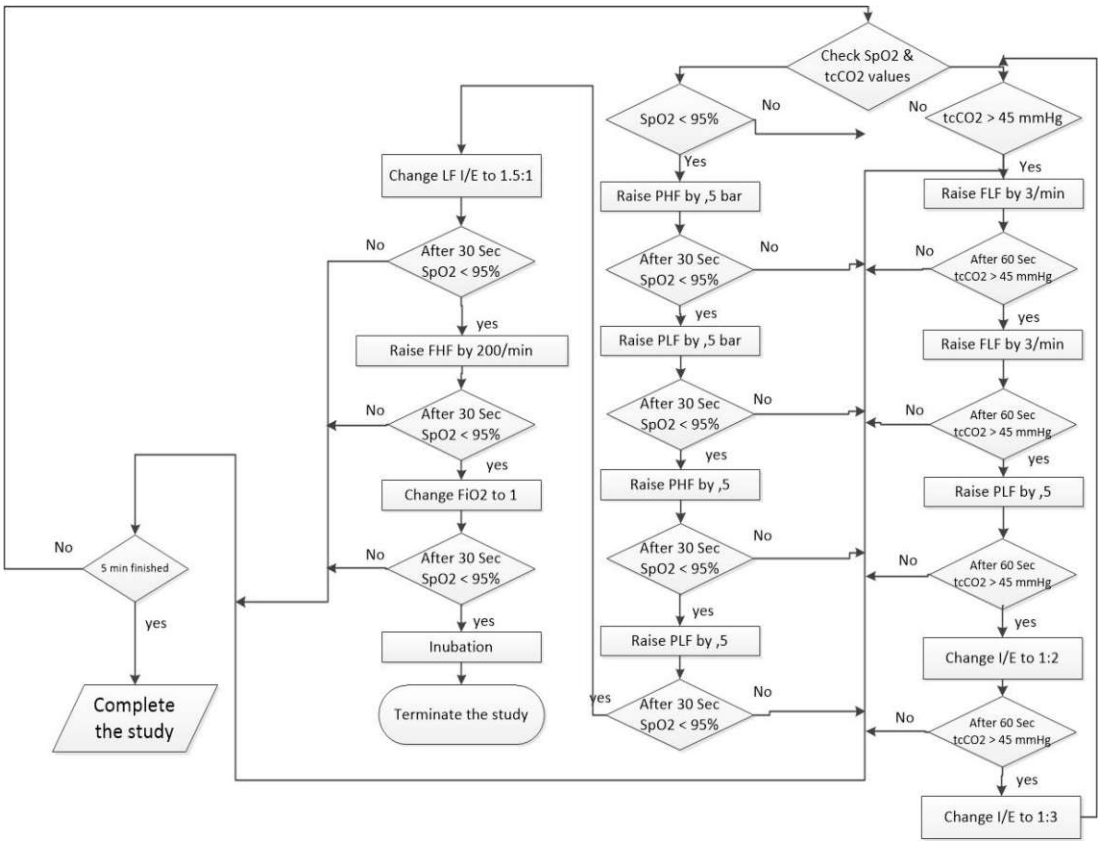

Fig 2.6 Intervention steps during SIHFJV

2.3 Measurements and Devices

In this chapter, the devices used during the study are discussed. The main concept and principle of operation of each device are summarized.

2.3.1 Transcutaneous Monitor of Blood Oxygen and Carbon-dioxide

As mentioned before, the carbon dioxide and oxygen saturation inside the bloodstream are required to be monitored during the whole study. A transcutaneous monitor (TCM) from (SenTec AG, Ringstrasse 39, CH-4106 Therwil, Switzerland, www.sentec.ch) is used to monitor the CO2 and oxygen levels transcutaneously, Fig 2.7. TCM measurement is an accepted and effective procedure. Although there would be a delay of approximately 1 min in the measurements of CO2 values, the results correlate well with changes in CO2 over time [22] [26].

Fig 2.7 Transcutaneous monitor and sensor [27].

TCM uses a continuous and non-invasive procedure to measure the tcPCO2 as well as tcPO2 at the skin surface to provide an estimate of the Arterial Carbon Dioxide Partial pressure (PaCO2) and Arterial Oxygen Partial pressure (PaO2). So it's not a substitution to the arterial values, as it is measured at the skin tissue and not inside the vessels. The preferred location to obtain transcutaneous measurements in adults are the highly vascularized areas such as the upper chest, biceps, forearm, the zygomatic bone, the ear lobe, cheek, or the forehead may be used as recording sites, Fig 2.8 [27]. The sensor is fixed to the skin through a specially designed ring and contact gel is added to improve the efficiency of CO2 diffusion as well as the sensor accuracy.

The main advantage of TCM is that it is non-invasive, means less pain associated with arterial blood gases analysis which needs access to the vessels. Also due to continuous mode of ventilation, it is required to have a trend of the changes in alveolar ventilation.

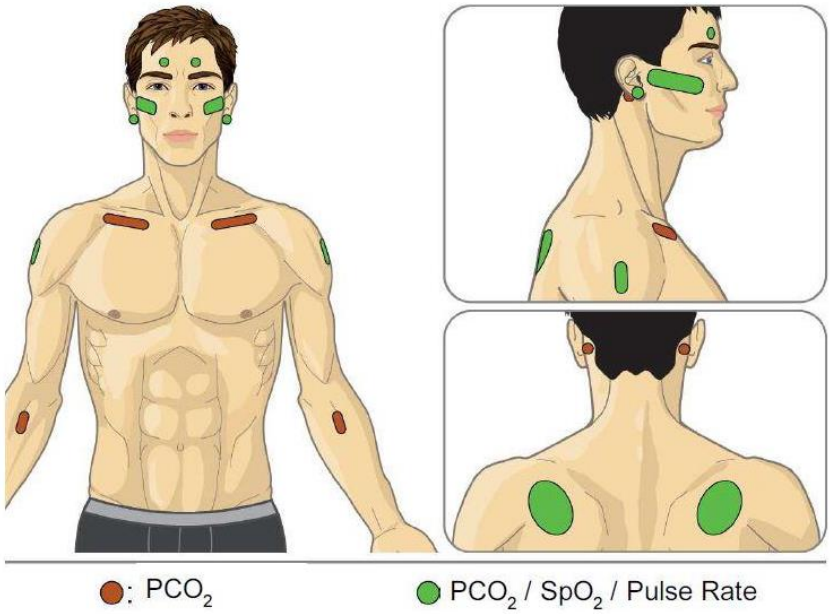

Fig 2.8 Manufacturer's recommendation for TCM sensor placement. Highly vascularized areas in green and red for the transcutaneous measurements [27].

The principle of operation of the TCM device is very simple. Inside the skin capillaries, the blood flows at a few millimeters below the skin surface. The transcutaneous sensor is placed on the skin where it elevates the temperature of the underlying tissues slightly above the body temperature, usually between 41 - 44 C°. the CO2 becomes more soluble and the metabolic rate of the skin increases by 4-5% for each extra 1 C°. This heating elevation also induces hyper-perfusion of the skin capillaries and the body reacts by letting the skin breathe, allowing for gas diffusion through the skin, Fig 2.9.

The sensor contains a thin electrolyte layer with a CO2 permeable membrane, where the CO2 diffuses and alters the Potential of Hydrogen (PH) value of the electrolyte. This PH change is correlated to the PaCO2 across the body, which can be recorded and continuously monitored.

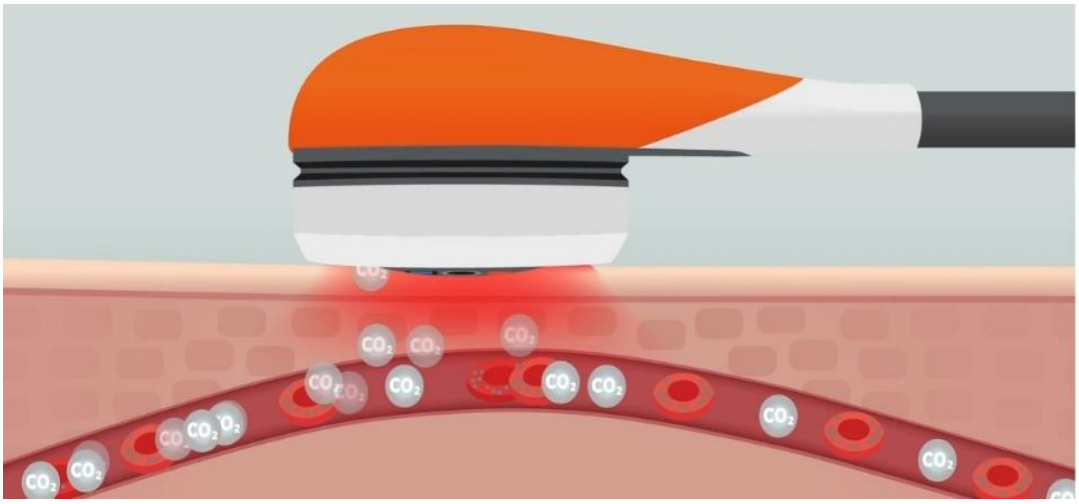

Fig 2.9 gases diffusion through the skin toward the transcutaneous Sensor [27].

2.3.2 Multi-Mode Respirator

One of the main parts of the study is the JV. TwinStream™, A device from (Fa. Reiner, Vienna, Austria) is used for the delivery of the JV components during each of the two previously investigated JV modes. TwinStream™ delivers simultaneously the LF and HF components for the SIHFJV mode via a specially designed jet laryngoscope (TwinStream™, Fa. Reiner, Vienna, Austria), Fig 2.10. during the Single HFJV, it delivers the single frequency component through a thin jet catheter (TwinStream™, Fa. Reiner, Vienna, Austria), Fig 2.11.

The jet laryngoscope supplies the LF and HF components through two integrated nozzles positioned at the outer part of the laryngoscope, so the primary jet pressure changes to a low ventilation pressure inside the tube and not in the surgical field. this preventing pressure change on the mucosa, at the same time the Venturi effect is shifted to the outer third of the laryngoscope. The jet laryngoscope has an opening for moisturizing and warming the ventilation gas in order to prevent serious injuries to the tracheal mucosa, Fig 2.12. The LFJV produces a variable inspiratory plateau but not an expiratory plateau, the expiration happens passively. Depending on the frequency, The HF component produces a length of inspiration and intrinsic PEEP, Fig 2.13 [20].

Fig. 2.10 JV [20].

Fig. 2.11 Jet Catheter [20].

Fig 2.12 Gas moisturizing [20].

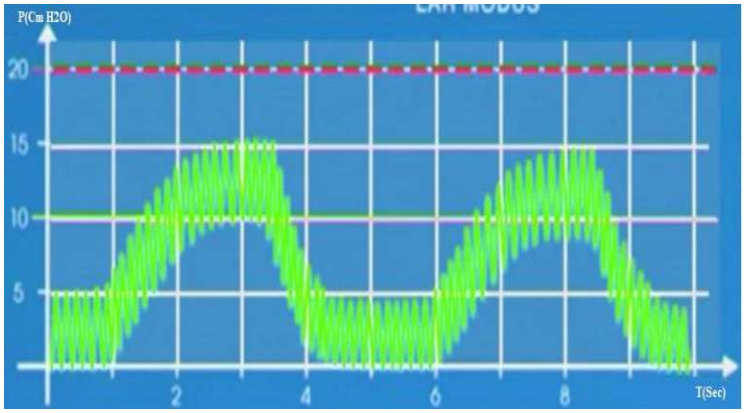

Fig 2.13 SIHFJV Plateau pressure [20].

The ventilation parameters are set through the control monitor of the TwinStream, Fig 2.14. Both high and low frequency JV units are switched on during the SIHFJV, while only the HFJV unit is switched on during the Single HFJV. The JV parameters for both HF and LF JV are the Frequency, I/E rate and the DV. The base line settings were discussed in sub-chapter 2.2.

Fig 2.14 Control monitor (TwinStream™, Carl Reiner, Jet Ventilator)

2.3.3 Electrical Impedance Tomography

As previously mentioned, the EIT is a non-invasive imaging technique that allows monitoring the ventilation distribution and lung functionality. In this study, an EIT device BB2 (LuMon™) from (SenTec AG (formerly Swisstom AG) Location Landquart Schulstrasse 1 CH-7302 Landquart Switzerland) is used to register the regional ventilation distribution and SS of the lung. EIT BB2 device consists of a sensor belt, pre-amplification unit, a belt connector device, measurement electronics, and a data acquisition system, Fig 2.15. The textile belt includes a striped electrically conductive textile cover and consists of 32 electrodes connected to the EIT monitor via a specially designed connector. The belt has to be positioned circumferentially around the chest at the 5th intercostal space. Each electrode contains electronic buffers to pre-process the measured voltages as close as possible to the patient [12].

Fig 2.15 From left, EIT monitor of LuMon^{TM} – Belt Connector – Electrodes Belt [12].

BB2 can generate 48 EIT images per second. This high temporal resolution allows the visualization of regional ventilation distribution even at higher respiratory rates like in JV. As described in Fig 2.16, the electrodes are controlled by a pre-amplification unit, which switches between the current injection and difference voltage measurement functions. The device consists mainly of:

1- voltage measurement unit.
2- current source
3- contact impedance measurement circuit.

The amplitude of the injected alternating current is 0.7 – 3.7 mA rms with a frequency of 200 kHz ± 10%. The electrode-skin contact impedances, which include the junction between the electrode and the skin, skin impedance and the body tissue between the two electrodes, are measured at the current injecting electrode pair. The compliance voltage of the system is 6 Volt. This is defined as the maximal voltage that the current source can supply to a load.

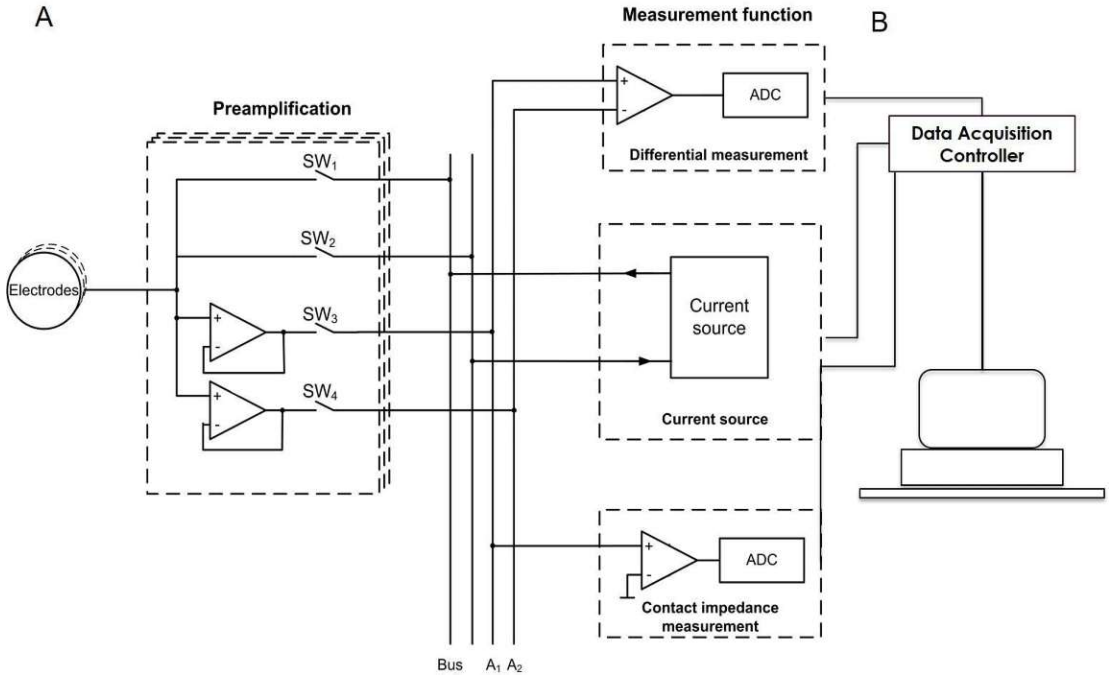

Fig 2.16 Architecture of the EIT device [27].

The current is injected through an electrode pair, and the resulting boundary voltages are measured from all electrode pairs, including the injection pair, resulting in 32 voltage measurements. Subsequently, the current injection moves to the next pair and this process is repeated until the current has been injected between all 32 pairs of electrodes, Fig 2.17. This process produces 32 ×32=1024 measurements. EIT BB2 device collects ~48 frames per second (20ms per frame). EIT systems should be run at a frame rate of at least twice larger than the frequency of the dominant physiological signals to avoid aliasing, which is still in the scope of the maximum JV frequency of this study. A threshold of 700 Ω skin contact impedance is defined according to the manufacturer's specifications.

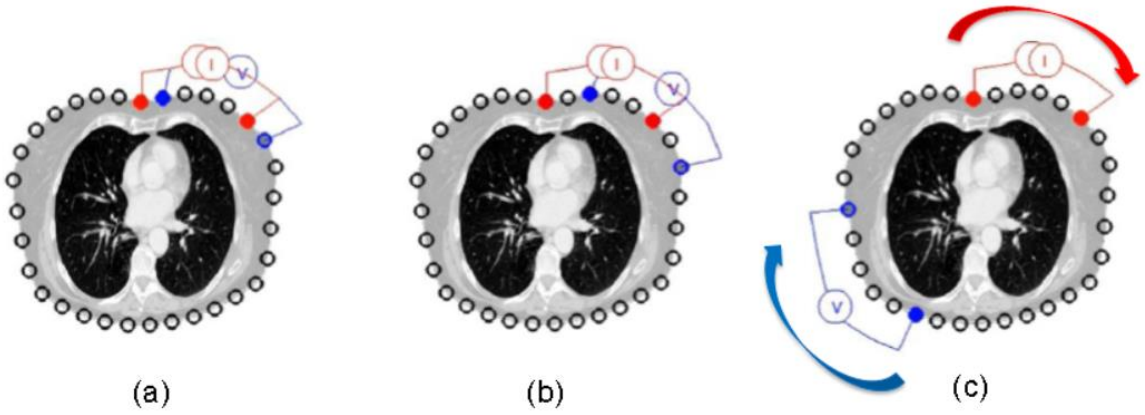

Fig 2.17 Electrodes belt applied around the chest. (a) The 1st impedance measurement. The current is applied between electrode pair (1, 6), and the resulting voltage is measured between pair (2, 7). (b) The 2nd impedance measurement. The current is applied between electrode pair (1, 6), and the resulting voltage is measured between pair (3, 8). (c) a snapshot of a measurement where the current is applied between pair (1, 6) and the resulting voltage is measured between pair (20, 25) [12].

The LuMonTM system is controlled via a Graphical User Interface (GUI) touch screen that is divided into 3 sub-sections as described in Fig 2.18, ScoutView, LuFuView and VentView sections.

(A) ScoutView (B) LuFuView (C) VentView

Fig 2.18 LuMonTM System monitor sub-sections [12].

Under ScoutView section, the global dynamic image can be monitored. Also, patient and belt settings can be defined through this screen. LuFuView consists of two different areas, the stretch area and the SS area. The stretch area displays the regional distribution of relative tidal stretch within the Lung ROI, called Stretch Image. It also displays a ten-part bar chart, called the weighted relative tidal stretch histogram Fig 2.19.

Fig 2.19. LuFuView sub-section A) Stretch image, B) Weighted relative tidal stretch histogram [12].

The silent spaces area displays the Silent Spaces Image, the CoV and the HoV. It provides as well, the functional lung spaces bar and the SS bar, Fig 2.20.

Fig 2.20 LuFuView, Silent spaces area [5].

VentView displays the Global Dynamic Image, the Plethysmogram and the calculated (RR), Fig 2.21.

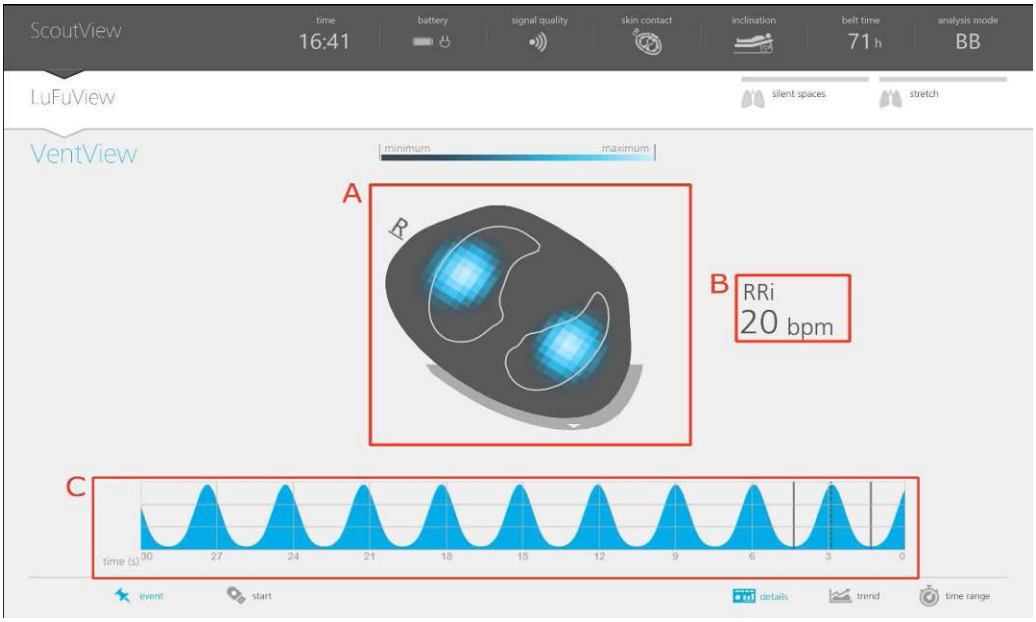

Fig 2.21 VentView, A) Global Dynamic Image, B) Respiration Rate, C) Plethysmogram [12].

2.3.4 IbeX Software

The EIT device provides a raw data representing the lung status, which is required to be processed and converted into graphical designs allowing easy identification and analysis of the lung function. The IbeX, is a Matlab based software from (SenTec AG, Landquart, Switzerland), developed to facilitate the analysis of the lung function parameters from the EIT data [3].

Fig 2.22 shows a global impedance signal (Plethysmogram) of 10 breaths and standard deviation image -based on the whole 10 breaths- of the lung ventilation driven from the raw data of the EIT by the IbeX software. The Plethysmogram is a waveform representing the lung impedance changes ΔZ over time, i.e. the sum of the impedance values of all lung pixels, thereby reflecting lung volume variations with breathing.

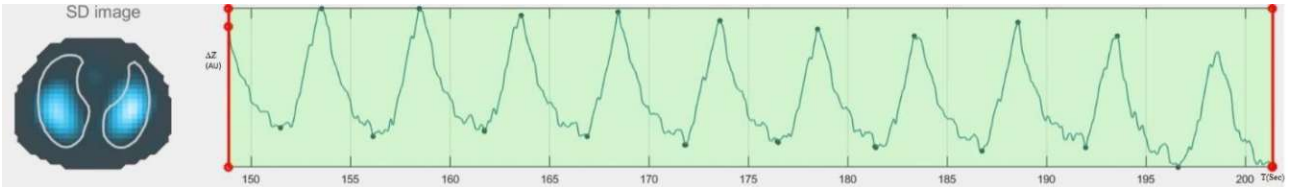

Fig 2.22 standard deviation at left and Plethysmogram at right between the two red lines [4].

This signal can be analyzed to deliver further information about the lung regional ventilation distribution in all ROIs and the developed SS. the software can provide breath by breath data analysis, and provide a tidal image, ventilation distribution for every ROI and the SS for each breath separately Fig 2.23, Fig 2.24.

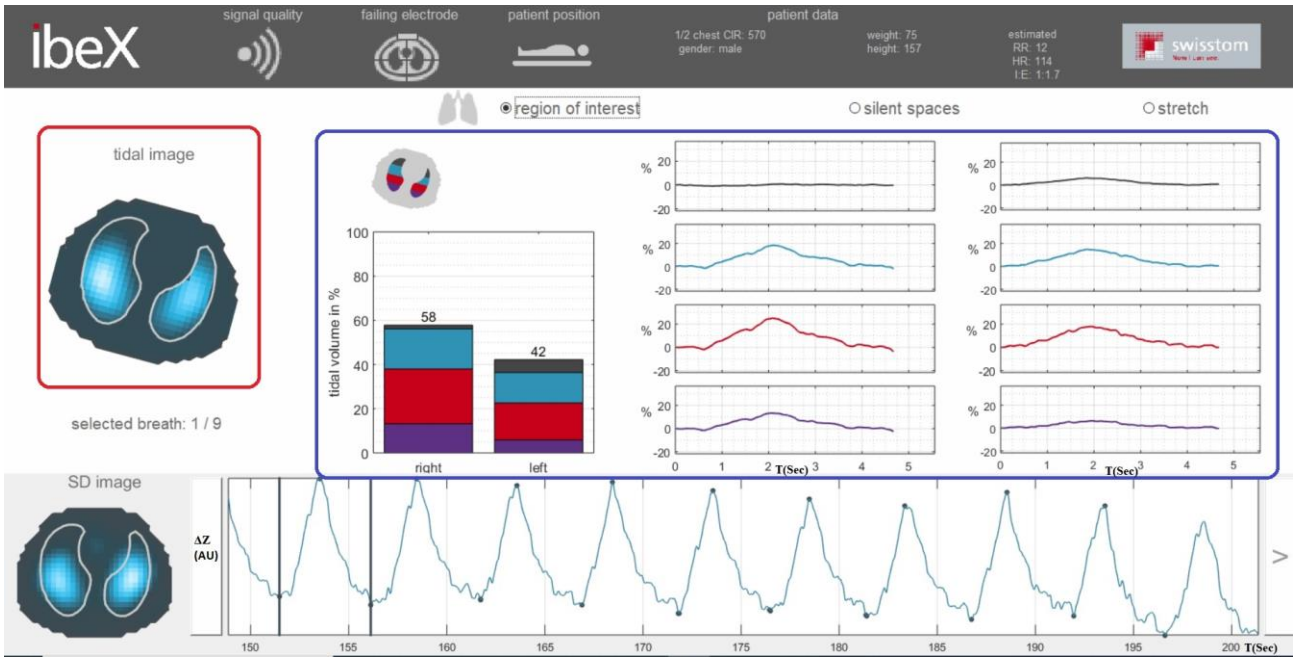

Fig 2.23 Analysis of the first breath from left, the tidal image surrounded with red, ROI analysis surrounded with blue [4].

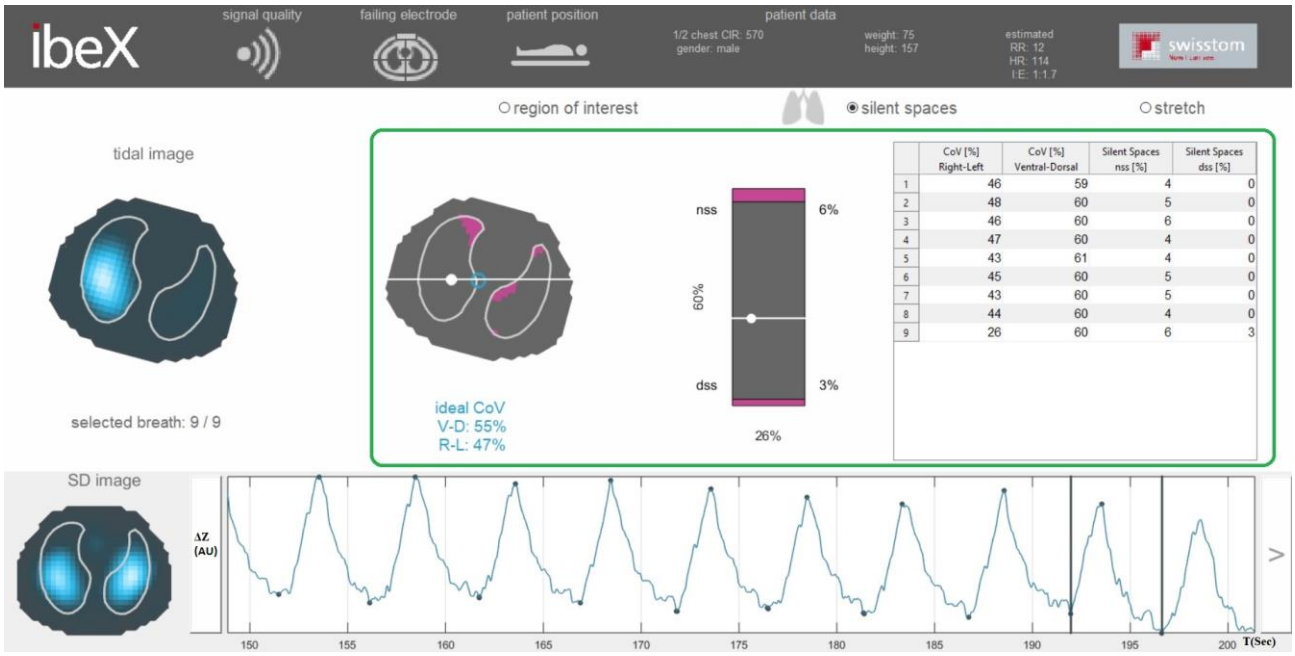

Fig 2.24 analysis of the last breath, the SS analysis surrounded with green [4].

It is worth knowing that small impedance changes caused by cardiac-related impedance changes can also be detected in the global impedance signal by the EIT. So it is preferable to filter the global impedance signal to remove the components of the heart activity (cardiac related impedance) and obtain only the impedance change due to the respiration activity.

2.4 Statistical Analysis

Statistical analysis was performed using Excel (Microsoft, US, Washington). Statistical Significance (*P*-value) was set below 0.05. For comparison of data, a one-way ANOVA analysis was performed to determine if there is a significant difference between the average of ROI, SS and Tidal Impedance Variation (TIV) of the three ventilation modes. Null hypothesis means that there is no significant difference, while alternative hypothesis means that there is a significant difference between the mean of the three ventilation modes. Hence, if (P-value ≤0.05), I will reject the null hypothesis and accept the alternative hypothesis. If (*P*-value >0.05), I will accept the null hypothesis and reject the alternative hypothesis.

The one-way ANOVA test can only tell that there is a significant difference between the ventilation modes, but will not tell where these differences lie. In other words, we will not determine which specific mode is different from the rest. A post-hoc test is performed to determine where the difference between the modes lies in case of significant difference presence. To do this, a separate two tailed two sample T-Tests analysis was performed and controlled the multiple comparisons between the three ventilation modes with the Bonferroni correction method. This means, comparing the mask to the SIHFJV (laryngoscope), laryngoscope to Single HFJV (catheter) and finally catheter to mask ventilation. For post-hoc test, the α level was adjusted via the Bonferroni method.

$$\alpha = P\text{-}value / N \qquad \text{(Eq. 2.1)}$$

Where, α is the Bonferroni correction, N is the number of tests and *P-value* is the probability or statistical significance value. In our case Bonferroni correction α = 0.05/3 = 0.0167.

3 Results

The BB LuMon™ EIT system calculates 47.68 frames/second to provide a raw data that can be represented in a form of a Plethysmogram or what is called the global impedance signal. The global signal represents the Change of Impedance ΔZ through the chest along with the time. ΔZ, is derived from the sum of all pixels within a given ROI of a relative image and plotted against time to obtain the global impedance signal. Hence, it reflects the impedance change across the chest due to the ventilation components, perfusion and cardiac-related changes, Fig 3.1.

It is worth keeping in mind that what matters in the current EIT paradigm is how the impedance values change over time rather than the absolute values of the measurements. It should also be remarked that, although we talk about impedance, the values obtained through the reconstruction algorithms are expressed in arbitrary units, as they are not units of a physical variable [12].

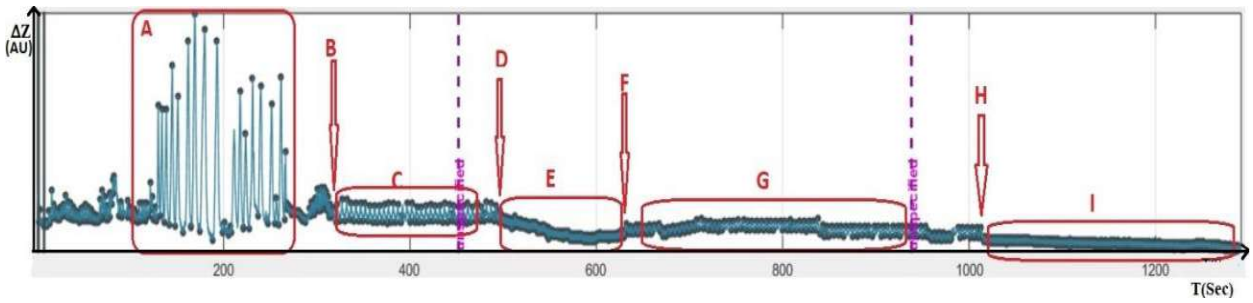

Fig 3.1 EIT Plethysmogram/ Global Signal of Patient Nr.13, represents ΔZ over time [4].

An example of a mask ventilation Plethysmogram is visualized in Fig 3.2. It displays an increase plateau during the inspiratory phase between (A-C) and a decreased plateau during the expiratory phase between (C-B). The signal between (A-B) represents the breathing-related lung impedance changes due to a single ventilation cycle. (A) represents the start of new inspiration or the end of previous expiration, in other words, End Expiration Lung Impedance (EELI). (B) represents the end of current breath expiration or start of new breath inspiration. (C) represents the end of current inspiration and the start of expiration, in other words, End Inspiration Lung Impedance (EILI). The two circles represent the cardiac-related impedance change due to heart activity during the filling in and out phases.

For more clarification, patient Nr.13 is chosen to illustrate many different impedance change signals that can be detected by EIT during the study. The reason to choose patient Nr.13, is that his global impedance signal measured by the EIT, contains various types of signals representing different phenomena, Fig 3.1.

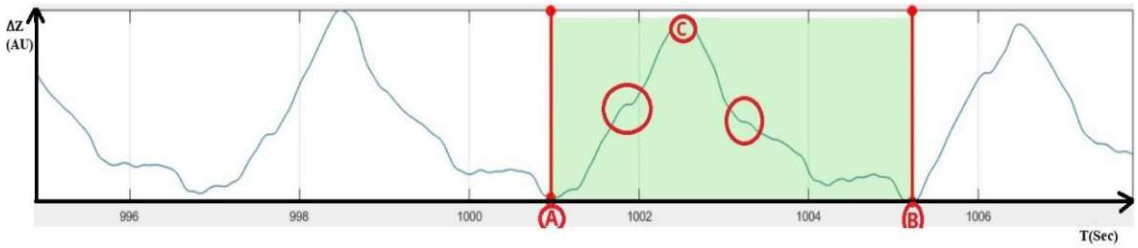

Fig 3.2 EIT Plethysmogram visualization during mask ventilation. (A-B), full breath cycle. (A), previous breath EELI. (C), current breath EILI. (B) current breath EELI. The cardiac-related impedances are in the red circles [4].

In Fig 3.1, (A) represents a deep breathing phase, where a high amplitude of ΔZ compared to the rest breathing signal can be seen. To see it clearly, (A) is zoomed-in and displayed in Fig 3.3. in this case, the patient breathed deeply before falling into a full anesthesia and being ventilated through the mask. We can see 2 full breath cycles inside the red rectangle where the RR is reduced due to the deep breathing activity. the normal RR consumes nearly 5 Seconds for a full cycle, but in this case it gets doubled to ~10 Sec per full breath cycle.

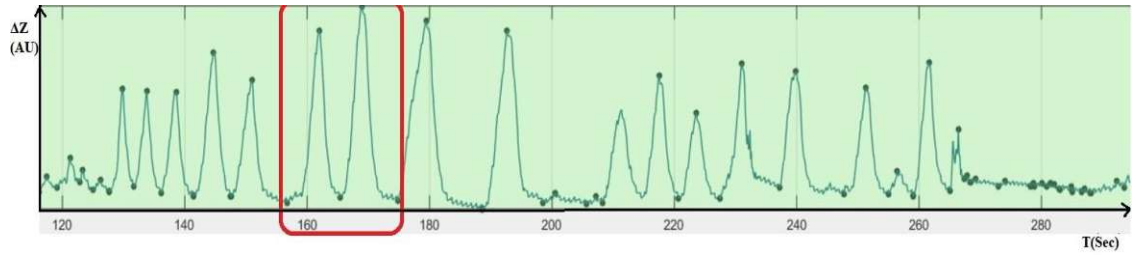

Fig 3.3 Deep breathing phase, RR is reduced [4].

In Fig 3.1, (C) represents the manually controlled mask ventilation mode with RR of nearly 12/min, starts at (B) and ends at (D). To see clearly the global impedance signal due to the mask ventilation, (C) is zoomed-in and displayed in Fig 3.4.

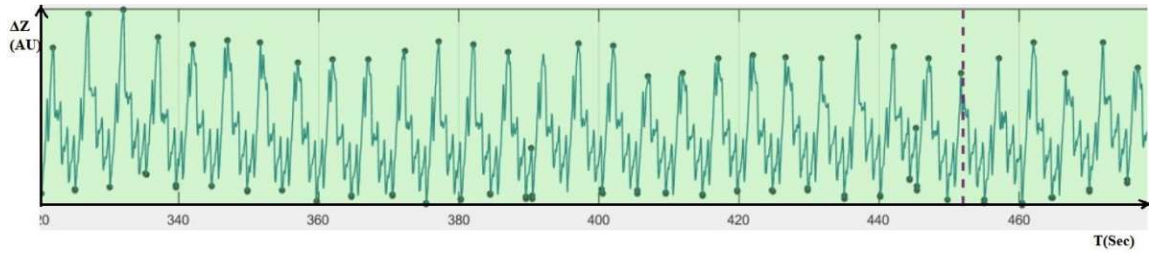

Fig 3.4 Mask Ventilation Mode (RR=12/min) [4].

The impedance variations within the thorax and particularly within areas represented by the Lung ROI, are primarily caused by lung function and to a lesser extent, perfusion and cardiac activity [28]. Therefore, the variations of impedance with the time displayed by the Plethysmogram, in the case of

normal breathing, are mainly related to lung volume/air content variations. Cardiac-related Lung Impedance changes have up to approximately 1/10 of the magnitude of Lung Impedance changes caused by normal breathing and therefore it is also visible in Plethysmogram. The cardiac-related impedance change is clearly obvious in the mask ventilation part. The heart beats appear periodically at a frequency of ~60 beats/min (~1 Hz), Fig 3.5.

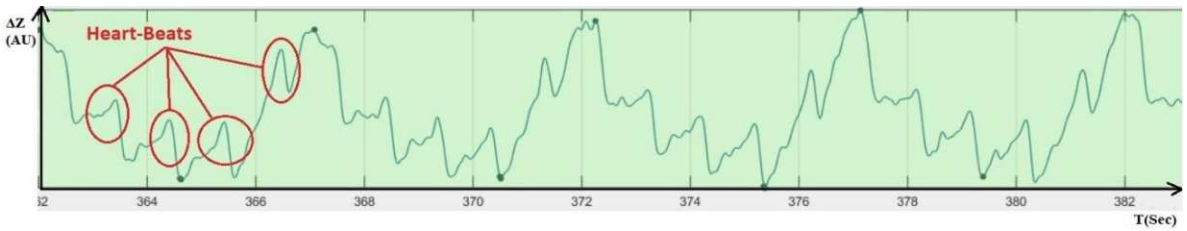

Fig 3.5 Mask Ventilation Mode, Cardiac-related impedance change in red circles [4].

As per the randomization criteria, in patient Nr.13 the mask ventilation was followed by jet laryngoscope ventilation. In Fig 3.1, (G) represents the supraglottic HFJV (Jet Laryngoscope Ventilation). The jet laryngoscope ventilation is applied with 2 frequency components of ventilation, the LF component with RR of 12/min and HF component with RR of 600/min. It starts at point (F) and ends at point (H). To see it clearly, (G) is zoomed-in and displayed in Fig 3.6. like the mask ventilation, the cardiac-related impedance changes appear very clearly in the global signal of the jet laryngoscope.

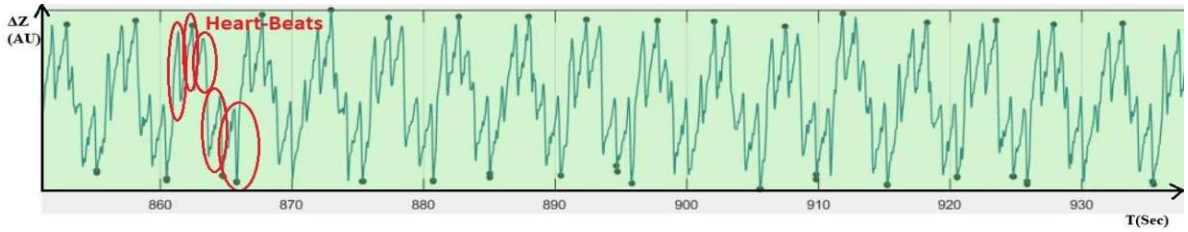

Fig 3.6 Supraglottic HFJV (Jet Laryngoscope Ventilation), red circles refer to the cardiac activity [4].

In case of very small or no TV – as this may be the case in very shallowly breathing patients, or in patients being ventilated at High Frequencies or during breath holds – the cardiac-related impedance changes will dominate the Plethysmogram [29]. The transition from any ventilation mode to another is an example of very small or no TV Fig 3.1 (E). To start the ventilation using the jet laryngoscope, it requires a few minutes to be installed through the patient larynx. During the installation time, the cardiac-related impedance changes dominate the Plethysmogram, and the EELI starts to fall. To see this clearly, part (E) of Fig. 3.1 is zoomed-in and displayed between (D) and (F) in Fig 3.7.

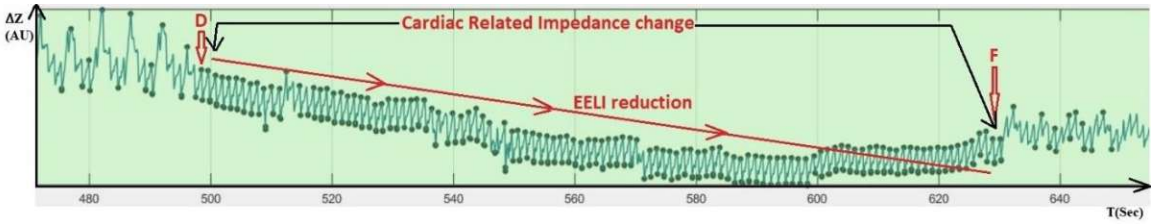

Fig 3.7 Transition from mask to laryngoscope ventilation, cardiac-related impedance change dominates the Plethysmogram, EELI decreases [4].

The last mode of ventilation that comes directly after the laryngoscope ventilation is the subglottic HFJV, or what we call Jet Catheter Ventilation, started at (H) in Fig 3.1(I). we can see no transition time due to the simplicity of catheter installation through the laryngoscope. Part (I) of Fig 3.1 is zoomed-in and displayed in Fig 3.8.

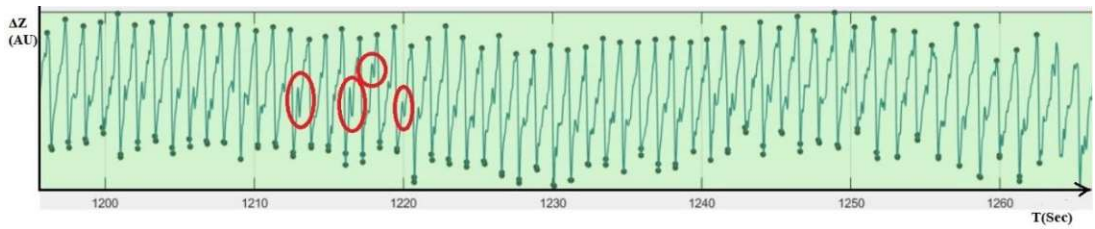

Fig 3.8 Subglottic HFJV (Jet Catheter Ventilation), Cardiac activity dominates the Plethysmogram. Some of the lung impedance changes are displayed in the red circles [4].

In spontaneous, mask, or even jet laryngoscope ventilation, the impedance changes due to ventilation are normally about 5-10 times greater than impedance changes due to cardiac activity. In jet catheter ventilation, the patient is ventilated with a Single HFJV of 120/min. This ventilation mode provides a small TV to the lung at a high rate. This means that the cardiac-related impedance changes will dominate the Plethysmogram with stable EELI.

The magnitude spectrum during the jet catheter ventilation in patient Nr.11 is plotted in Fig 3.9. The magnitude of the jet catheter lung ventilation peak is about 1/5 of the cardiac-related impedance change peak.

Another example from patient Nr.14 is shown in Fig 3.10, the mask and the jet catheter can be analyzed together in the frequency domain. We can see clearly, the peak at 2Hz, which represents the impedance change due to the catheter ventilation is very small compared to the peak at .2 Hz which represents the mask ventilation. This means that the TV change is very small during the jet catheter ventilation compared to the mask ventilation.

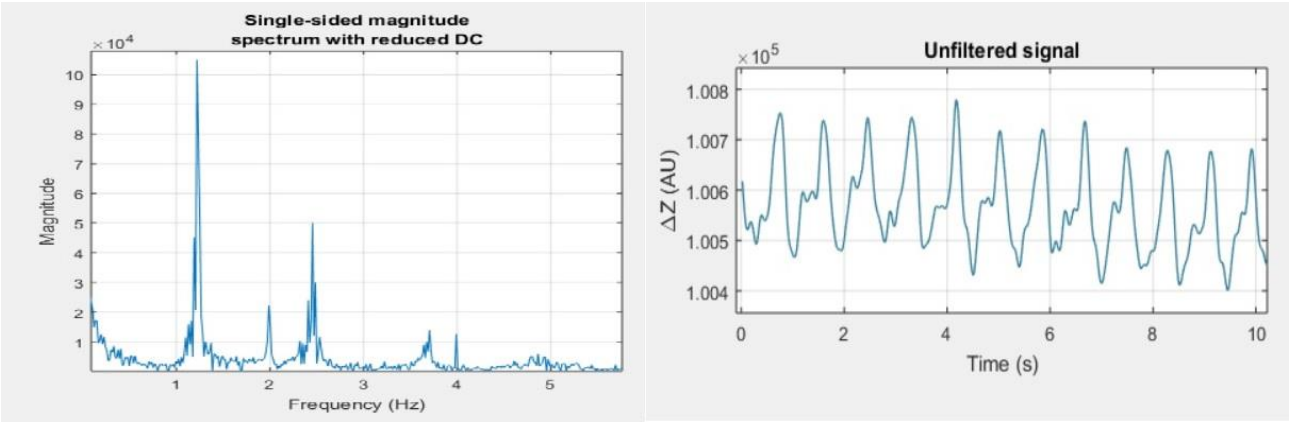

Fig 3.9 on the right, the global impedance change signal measured by the EIT during jet catheter ventilation (120/min or 2 Hz). 12 cycles within 10 seconds are measured. It actually represents the cardiac activity mainly with a frequency of 1.2 Hz. The magnitude spectrum displayed on the left, where the cardiac activity peak appears at ~1.2 Hz and the impedance change due to the lung ventilation is shown at 2 Hz with a magnitude of ~1/5 of the cardiac activity magnitude. [4].

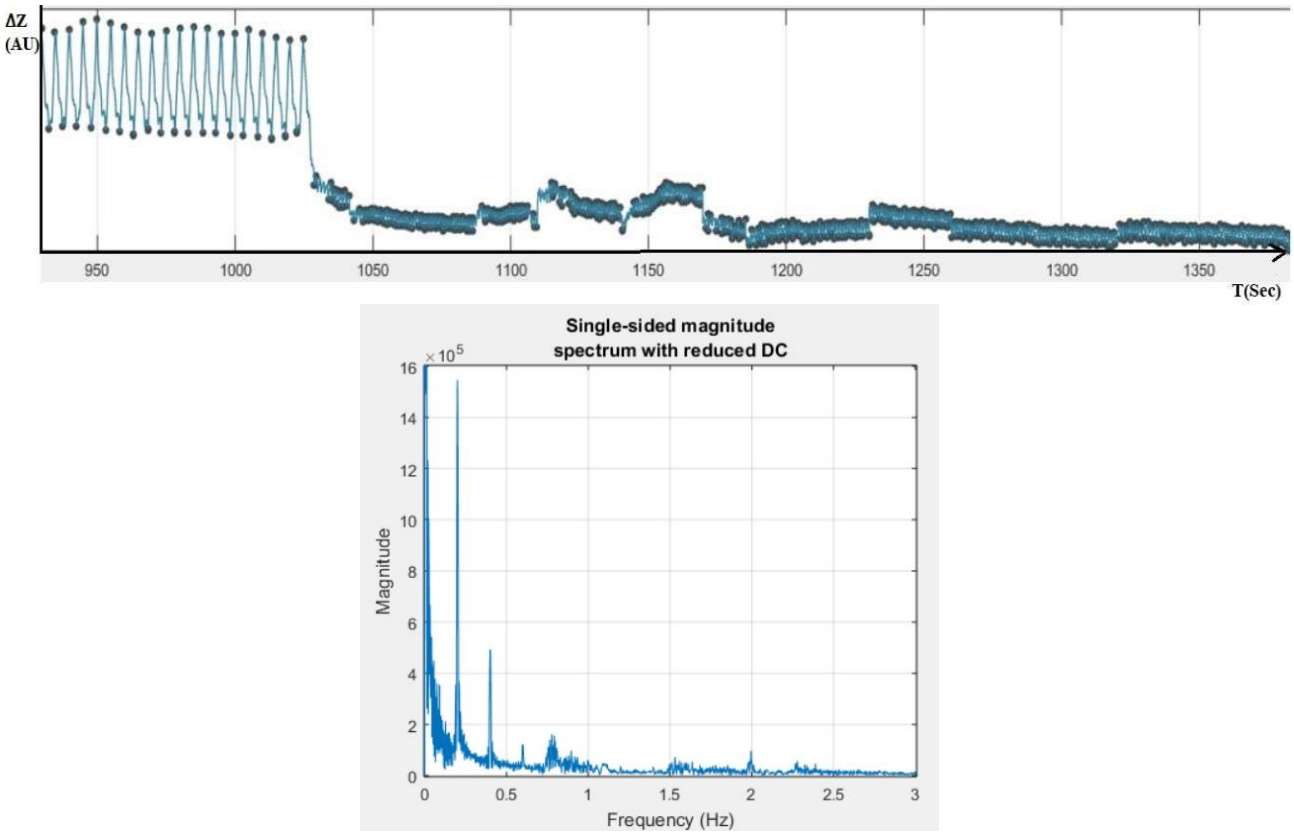

Fig 3.10 the Plethysmogram on top displays the impedance change of the Mask and jet catheter ventilation. the magnitude spectrum on the bottom displays a very small magnitude of the jet catheter ventilation signal at 2 Hz compared to the mask ventilation at .2 Hz [4].

The contact quality between skin and electrodes is enhanced by a skin-friendly contact medium applied between skin and belt. Moreover, the contact quality is continuously assessed by the EIT device, which helps to interfere when there is failing electrodes, Fig 3.11.

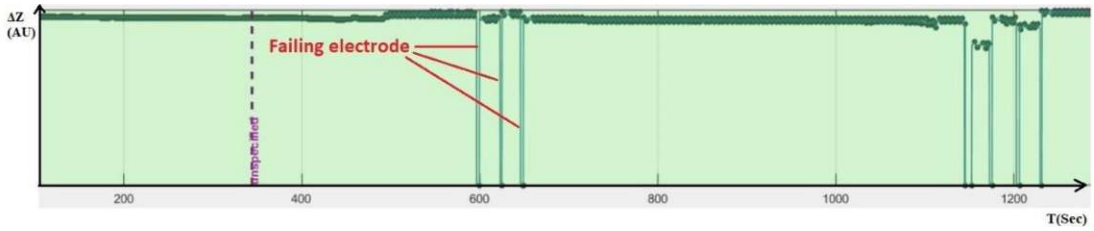

Fig 3.11 Failing electrodes [4].

Fig 3.12 displays a typical EIT original waveform without filtering. The difference between EELI and EILI, commonly referred to TIV, is used to assess regional ventilation distribution [30].

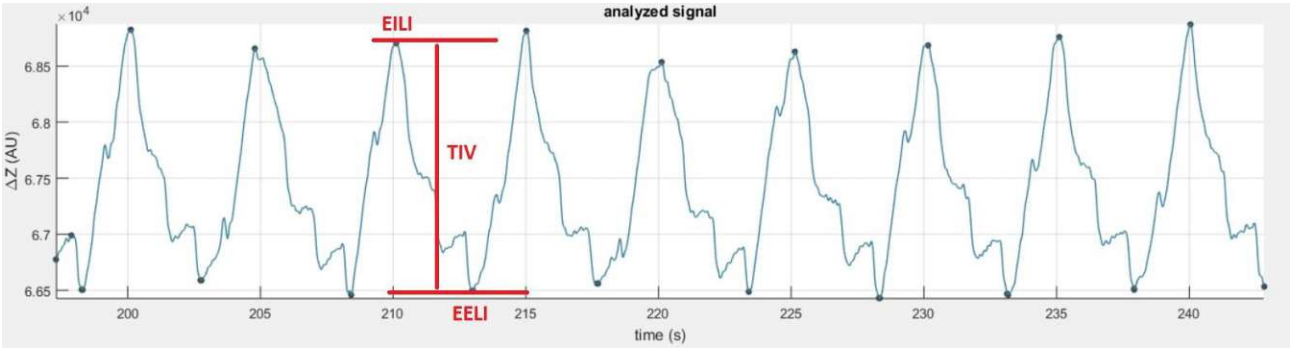

Fig 3.12 typical EIT waveform, TIV represents the difference between EELI and EILI [4].

3.1 Identification of appropriate analysis window

One of the main issues in biomedical data analysis is to define an appropriate time window to perform the analysis. The biological subjects react to stimuli differently. In other words, the response of biological organs/tissues due to external effects differs in time and magnitude from one subject to another. We have to wait such time to have a measurement that truly represents the organ status.

In this project, the organ under analysis is the lung, which is supplied with different modes of ventilation, the mask, supraglottic and subglottic JV ventilation. Each ventilation mode is applied for a certain time to give the lung a chance to adapt in response to it.

Not only the lung, but also the body has to be stable during the analysis. In our project, the stability of the body is mainly related to the oxygen and carbon dioxide in the blood stream. Their values have to be maintained at specific values to perform the analysis as mentioned in the sub-chapter (2.2.1, 2.2.2). Unless, the base line settings have to be changed and give the body enough time (60 Sec for tcPCO2 and 30 Sec for SpO2 measurements) to adapt to these new settings.

With regard to the ventilation distribution through the lung, the analysis is done for each ventilation mode for a specific time or breaths. These time windows are calculated separately for each mode to define a reasonable time frame, which represents the lung at stable conditions. The average of the measured values is calculated and recorded for further analysis and comparison between each ventilation mode.

To calculate the time window, the standard deviation (SD) is calculated from backward to forward to ensure the lung stability after each ventilation mode application. The idea is based on plotting the SD of the measured parameters along with the ascending number of breaths or time. After a specific time or breaths quantity, the SD becomes stable and doesn't change. This time or number of breaths are enough for the analysis and considered representing the values under measurement.

Depending on the ventilation mode, specific steps and number of breaths were chosen. The number of breaths increased by steps based on the application time of each ventilation mode. The ventilation

distribution and SS through the lung were calculated for each number of breaths until SD saturation is reached.

Randomly, patient Nr.22 was chosen to do the calculations. The results for each ventilation mode were calculated and shown in the next sub-chapters.

3.1.1 Mask Ventilation Analysis Window

The SD for each ROI and SS were calculated for the mask ventilation mode. The mask ventilation mode is applied for two minutes with an RR of 12/min. it ends up with around 24 breaths for the two minutes of ventilation.

Table 3.1 contains the calculations of the SD vs. ascending number of breaths from back to forward, i.e. from the end of the two minutes toward the starting point of ventilation.

Nr. Of Breaths	2	4	6	8	10	12	14	16	18	20	21
SD-ROI 1	0.13	0.08	0.34	0.31	0.28	0.25	0.23	0.24	0.22	0.24	0.29
SD-ROI 2	0.09	0.07	0.60	0.38	0.34	0.51	0.48	0.27	0.29	0.29	0.40
SD-ROI 3	0.03	0.03	0.41	0.38	0.35	0.31	0.29	0.28	0.33	0.35	0.40
SD-ROI 4	0.00	0.06	0.49	0.29	0.26	0.43	0.40	0.23	0.22	0.22	0.32
SD-NSS	0.29	0.24	0.61	0.21	0.29	0.83	0.87	0.28	0.28	0.28	0.29
SD-DSS	0.58	1.12	1.90	0.97	0.88	2.40	2.53	1.87	2.11	2.19	2.16

Table 3.1: Standard Deviation calculations for mask ventilation mode

The SD of the four ROIs of the lung as well as the SS are plotted against the ascending number of breaths in Fig 3.13. It shows that ~16 breaths (~80 Sec) from back to forward are enough to represent the lung status during the mask ventilation mode.

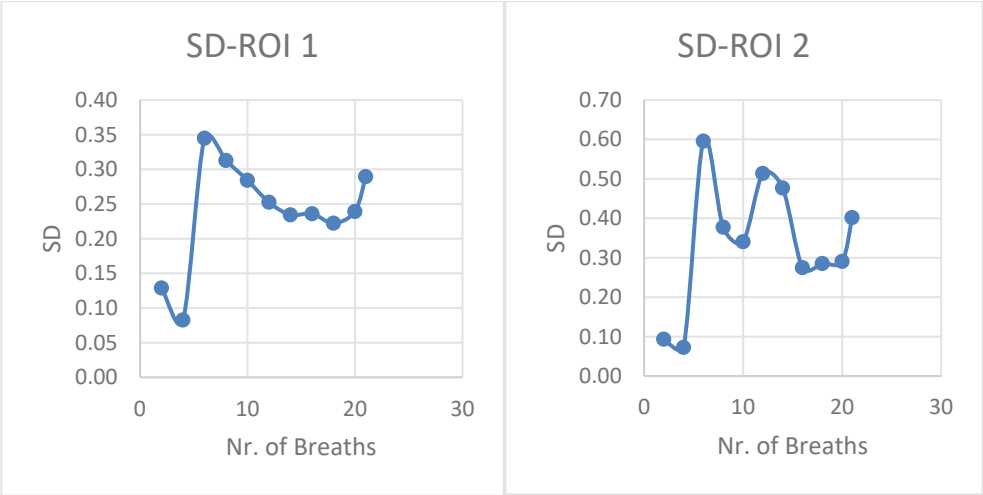

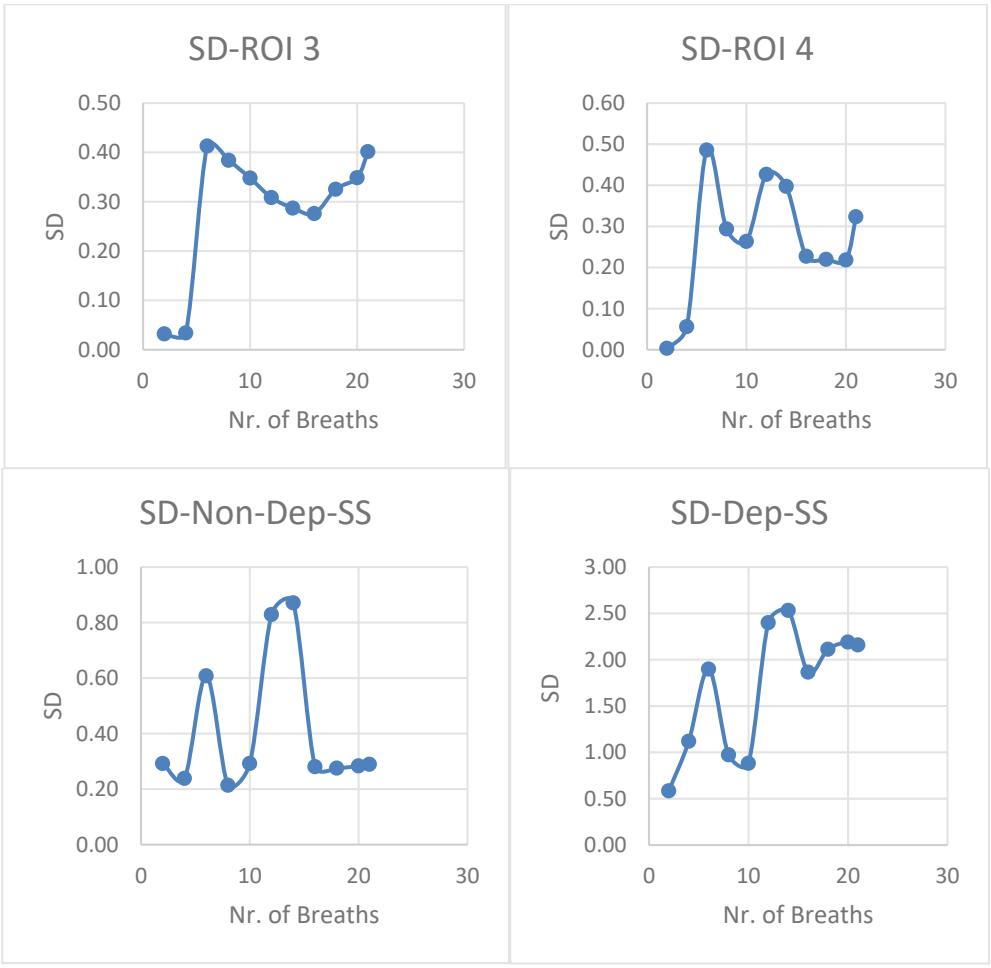

Fig 3.13 SD of ROIs and SS against the ascending number of breaths during mask ventilation mode

3.1.2 Supraglottic Jet Ventilation Analysis Window

The same procedure as of the mask ventilation was done for the supraglottic JV. The SD for each ROI and SS were calculated for the laryngoscope ventilation mode. The laryngoscope ventilation mode is applied for five minutes with a dominant low frequency RR of 12/min. it ends up with around 60 breaths for the five minutes of ventilation. Table 3.2 contains the calculation of the SD vs. ascending number of breaths from back to forward, i.e. from the end of the five minutes toward the starting point.

Nr. Of Breaths	2	3	4	5	6	7	8	9	10	12	16	20	24	28	36	40	44	48	52	56	60
SD-ROI 1	0.16	0.14	0.09	0.13	0.12	0.11	0.13	0.14	0.13	0.15	0.16	0.15	0.15	0.16	0.16	0.16	0.17	0.17	0.20	0.20	0.19
SD-ROI 2	0.10	0.02	0.05	0.27	0.25	0.14	0.22	0.21	0.21	0.28	0.21	0.19	0.18	0.19	0.19	0.19	0.20	0.21	0.31	0.32	0.31
SD-ROI 3	0.11	0.10	0.06	0.13	0.12	0.11	0.13	0.14	0.15	0.16	0.17	0.15	0.15	0.16	0.17	0.18	0.19	0.19	0.23	0.22	0.22
SD-ROI 4	0.14	0.06	0.08	0.18	0.18	0.11	0.18	0.17	0.17	0.24	0.17	0.15	0.14	0.16	0.15	0.15	0.17	0.17	0.26	0.26	0.26
SD-NSS	0.00	0.24	0.21	0.95	0.89	0.22	0.26	0.25	0.23	0.87	0.22	0.22	0.22	0.24	0.20	0.21	0.21	0.21	0.77	0.74	0.75
SD-DSS	0.58	0.24	0.92	1.26	1.13	0.81	1.22	1.15	1.08	1.56	0.93	0.86	0.79	1.09	0.80	0.83	0.87	0.89	1.47	1.43	1.44

Table 3.2: Standard Deviation calculations for supraglottic JV mode

The SD of the four ROIs of the lung as well as the SS are plotted against the ascending number of breaths in Fig 3.14. It shows that ~20 breaths (~100 Sec) from back to forward are enough to represent the lung status during the supraglottic JV mode.

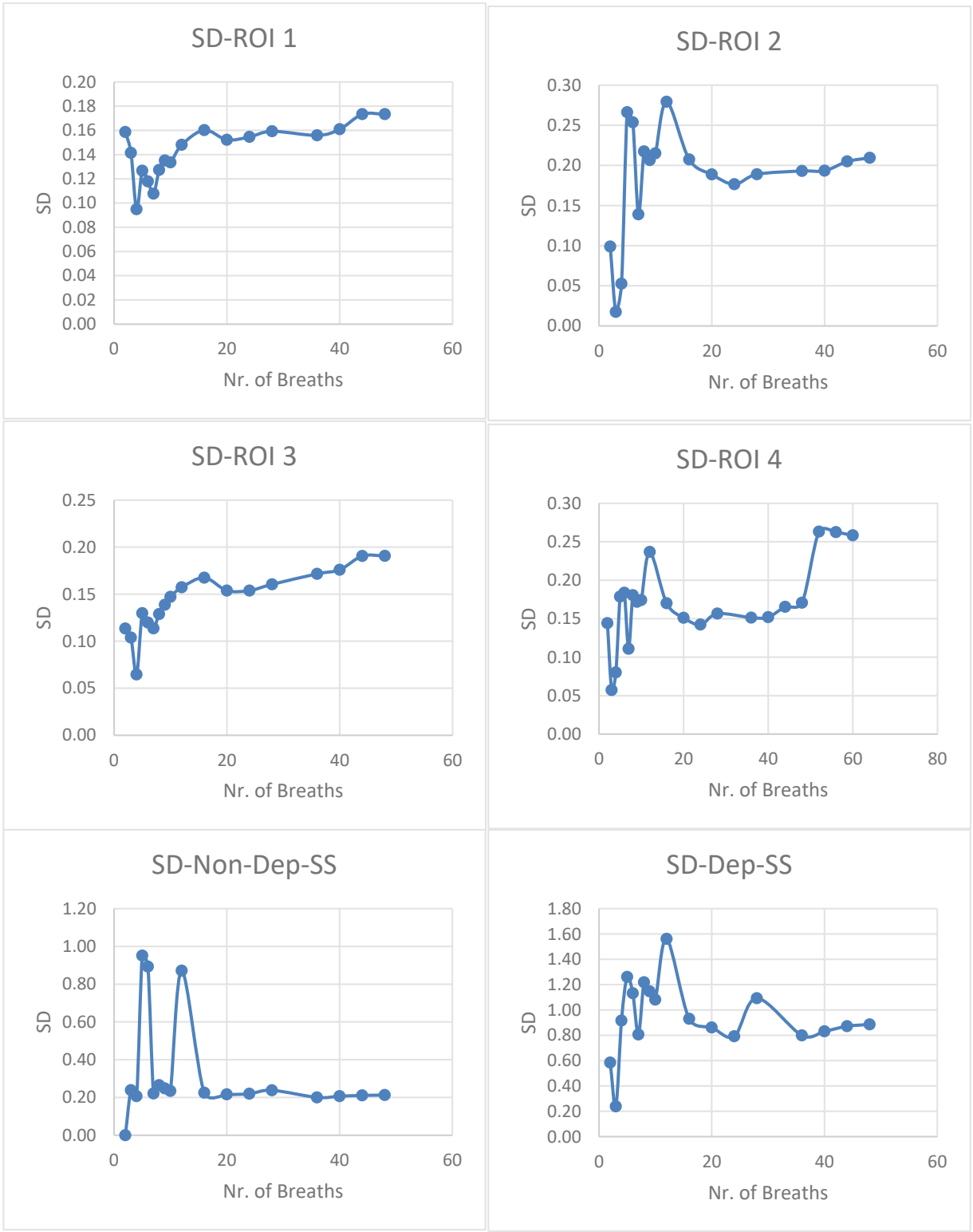

Fig 3.14 SD of ROIs and Silent Spaces against the ascending number of breaths during supraglottic JV mode

3.1.3 Subglottic Jet Ventilation Analysis Window

The same procedure as of the mask ventilation was done also for the subglottic JV. The SD for each ROI and SS were calculated for the catheter ventilation mode. The catheter ventilation mode is applied for five minutes with a single high-frequency RR of 120/min. it ends up with around 600 breaths for the five minutes of ventilation. Table 3.3 contains the calculation of the SD vs. ascending number of breaths from back to forward, i.e. from the end of the five minutes toward the starting point.

The SD of the four ROIs of the lung as well as the silent spaces were plotted against the ascending number of breaths in Fig 3.15. It shows that ~150 breaths (~75 Sec) from back to forward are enough to represent the lung status during the subglottic JV mode.

Nr. Of Breaths	10	20	30	40	50	60	70	80	90	100	110	120
SD-ROI 1	0.77	0.72	1.24	0.80	0.83	1.26	1.62	1.02	0.99	1.01	0.99	1.34
SD-ROI 2	1.02	0.88	1.56	1.02	0.94	1.28	1.65	0.97	1.02	1.03	1.06	1.46
SD-ROI 3	1.50	0.89	1.63	1.00	1.00	1.48	1.71	0.99	1.03	1.06	1.06	1.54
SD-ROI 4	1.15	1.02	1.62	1.12	1.03	1.35	1.74	1.10	1.09	1.07	1.09	1.45
SD-NSS	0.41	0.17	0.29	0.18	0.19	0.33	0.37	0.17	0.19	0.19	0.19	0.31
SD-DSS	0.23	0.17	0.34	0.17	0.15	0.32	0.34	0.14	0.16	0.15	0.15	0.33

Nr. Of Breaths	140	148	150	154	160	180	200	220	230	360	400	460
SD-ROI 1	1.39	1.37	1.73	0.94	0.97	0.99	0.97	1.01	1.01	0.97	0.96	0.99
SD-ROI 2	1.49	1.47	1.81	0.98	0.97	1.01	1.02	1.08	1.07	1.08	1.10	1.18
SD-ROI 3	1.57	1.56	1.93	0.80	0.98	1.05	1.05	1.11	1.11	1.09	1.09	1.14
SD-ROI 4	1.46	1.46	1.77	1.10	1.03	1.05	1.05	1.09	1.07	1.05	1.09	1.14
SD-NSS	0.34	0.33	0.42	0.16	0.23	0.24	0.24	0.25	0.25	0.24	0.25	0.26
SD-DSS	0.33	0.32	0.36	0.17	0.16	0.16	0.16	0.16	0.17	0.18	0.18	0.18

Table 3.3: Standard Deviation calculations for subglottic JV mode

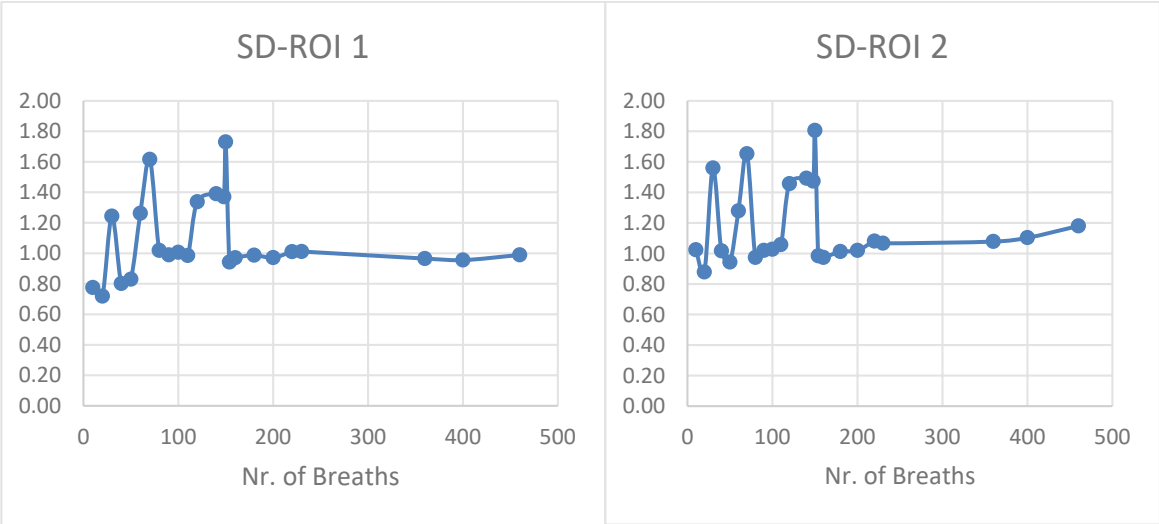

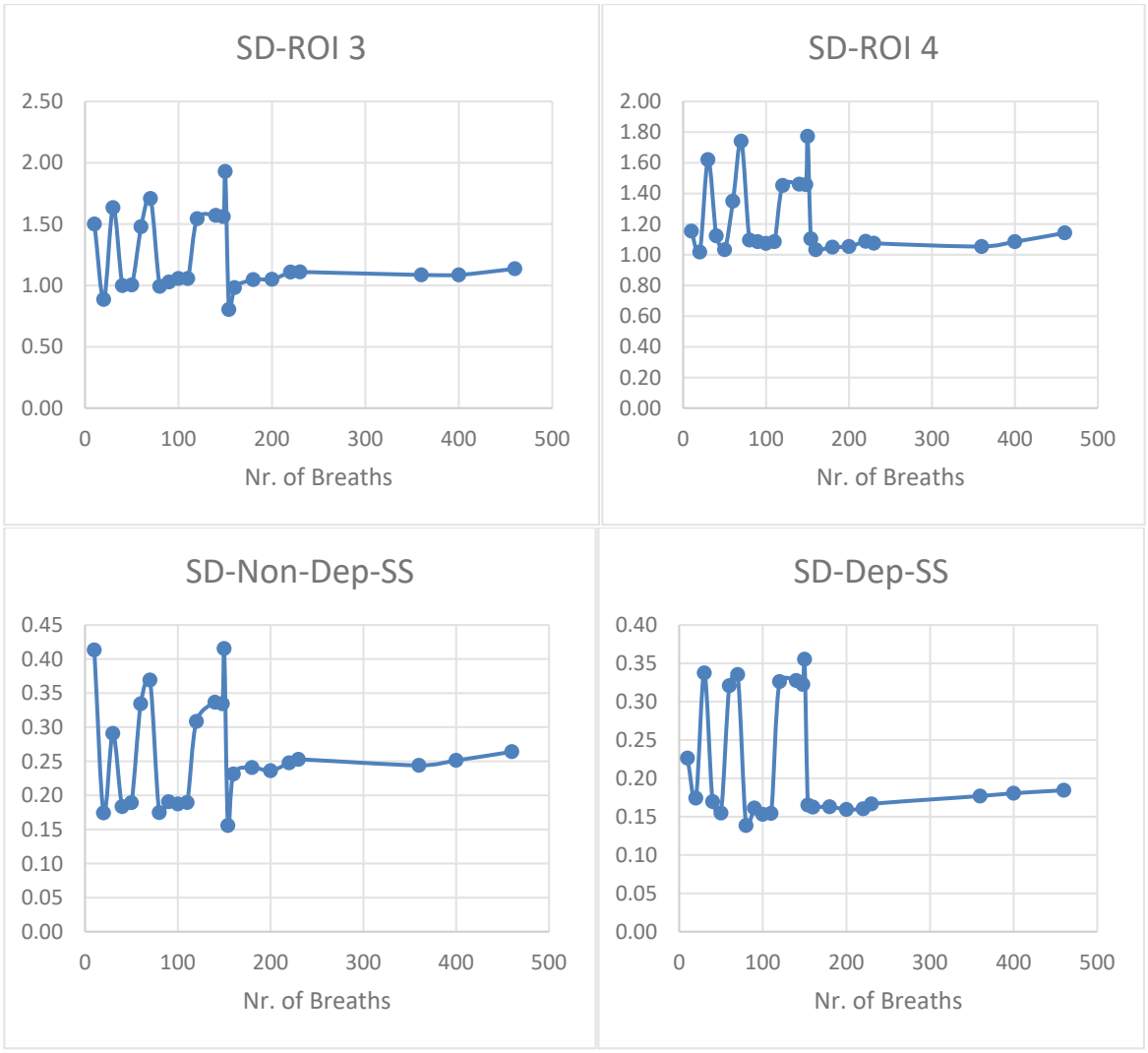

Fig 3.15 SD of ROIs and SS against the ascending number of breaths during subglottic JV mode

3.2 Filtration Technique

The Clinical data analysis and processing were performed offline using the SenTec ibeX software package. As previously mentioned, the global impedance signals contain the impedance change not only due to lung activity but also the cardiac-related activity and perfusion. As per the ibeX user guide, the built-in filter parameters are based on general assumptions that are not suitable for this project settings. *"The filter design is based on the Respiration Rate. In case of (RR>= 12 /min (i.e. >=0.2 Hz)→a band pass filter (Finite Impulse Response (FIR)) of order 10 with a range [breathrate-0.1 breath-rate*4+0.1] Hz is used. In case of (RR< 12 /min), a low pass filter FIR of order 10 with cut-off frequency [breath-rate*4+0.1] Hz is used"* [3].

Therefore, a special filter should be applied to the global impedance signal based on the actual RR of each patient for every ventilation mode. the applied filter aims to extract the impedance change due to

lung activity out of the global impedance signal. Based on the fact that the heart rate and the respiratory rate are very well separated in frequency, the Fast Fourier Transform (FFT) of the global signal can provide a good approximation of the required cut-off frequency for filtering. [31]

Fig 3.16 shows the unfiltered signal in the time domain at right and in the frequency domain using FFT at left. The frequency domain displays two frequency components of the global impedance signal. In the red circle, there are two peaks, the fundamental frequency at 0.2 Hz and the first harmonic frequency at 0.4 Hz, representing the lung impedance change. In the black circle, the cardiac-related activity peak at 1.05 Hz.

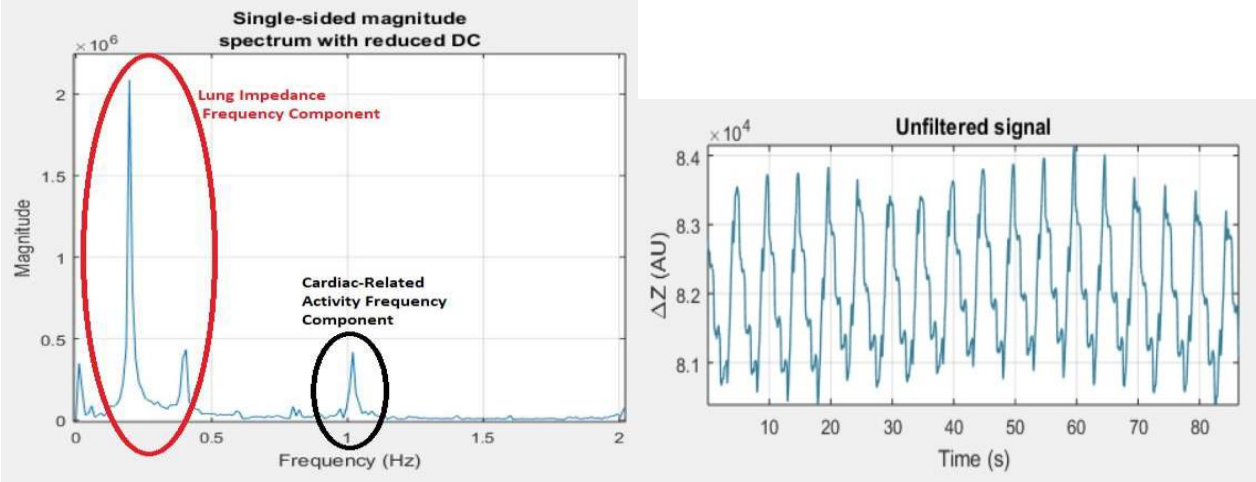

Fig 3.16 Example for unfiltered signal in time domain at right, the frequency components at left. Lung impedance frequency component surrounded by the red circle, the cardiac related activity peak surrounded by black circle [4].

A Finite Impulse Response (FIR) filter is used in all analysis. It is preferred to Infinite Impulse Response (IIR) filtering, because FIR filters are always stable and can be designed to have a linear phase. Consequently, the signal is not distorted during filtering and the time shift is predictable [32].

The analysis procedure using the ibeX software is as follows:

1- Construct the global signal in the time domain and define the analysis window.
2- Apply the FFT to the unfiltered global signal to convert it into the frequency domain.
3- Detect the ventilation frequency components.
4- Based on the frequency and mode of ventilation, a suitable cut-off frequency is assigned.
5- Design a filter function based on the pre-assigned cut-off frequency.
6- Apply the filter to the signal in the time domain.
7- To ensure that the filter parameters are correctly chosen, an FFT is applied to the filtered signal.
8- Check the frequency components of the filtered signal to ensure that the filter mission succeeded.

3.2.1 Mask Ventilation Filter

The mask ventilation is a controlled ventilation mode, where a RR of ~ 12 breath/min or (0.2 Hz) is applied manually for nearly 2 minutes. A Low-Pass Filter (LPF) with a cut-off frequency of (0.7-0.8 Hz) is sufficient to extract the lung impedance change from the global signal. Fig 3.17 shows an example of mask ventilation global signal filtered based on the previous analysis procedure.

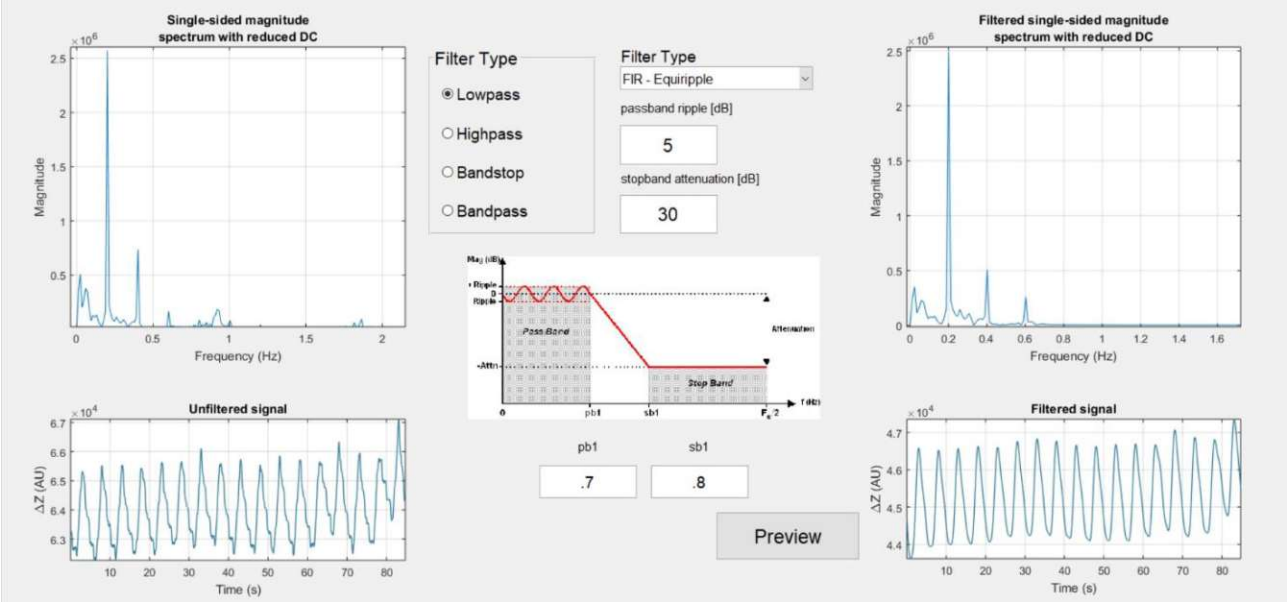

Fig 3.17 Example of the mask ventilation analysis procedure. The unfiltered global signal is at the lower left and its frequency domain using FFT is at the upper left. A low-pass filter is designed as shown in the middle with pass band frequency of 0.7 Hz and stop band frequency of 0.8 Hz. The filter is applied to the original global signal, and the result is displayed on the right. The filtered signal in time domain is at the lower right and its frequency components are at the upper right [4].

The filtered signal is then analyzed using the ibeX software to compute the ventilation distribution at each ROI as well as the silent spaces.

3.2.2 Jet Laryngoscope Ventilation Filter

The SIHFJV is a controlled JV mode that consists of 2 ventilation components:

1- Low-Frequency Component (RR=12-18 breath/min = 0.2-0.3 Hz), based on the SpO2 and the tcPCO2 values

2- High-Frequency Component (RR=600 or 800 or 1000 breath/min = 10 or 13.3 or 16.7 Hz) – most of the cases ventilates at 600/min and in a few cases, it reaches 800/min as a part interference procedure.

The change of the air content inside the lung during the SIHFJV mainly depends on the LF component and to a lesser extent on the HF component. This can be seen in the frequency domain of the global impedance signal of the jet laryngoscope ventilation, Fig 3.18. the magnitude of the LF peak is very high compared to the HF peak. In some cases, like Patient Nr.11, the HF component peak was not detected by the EIT and does not appear in the frequency domain.

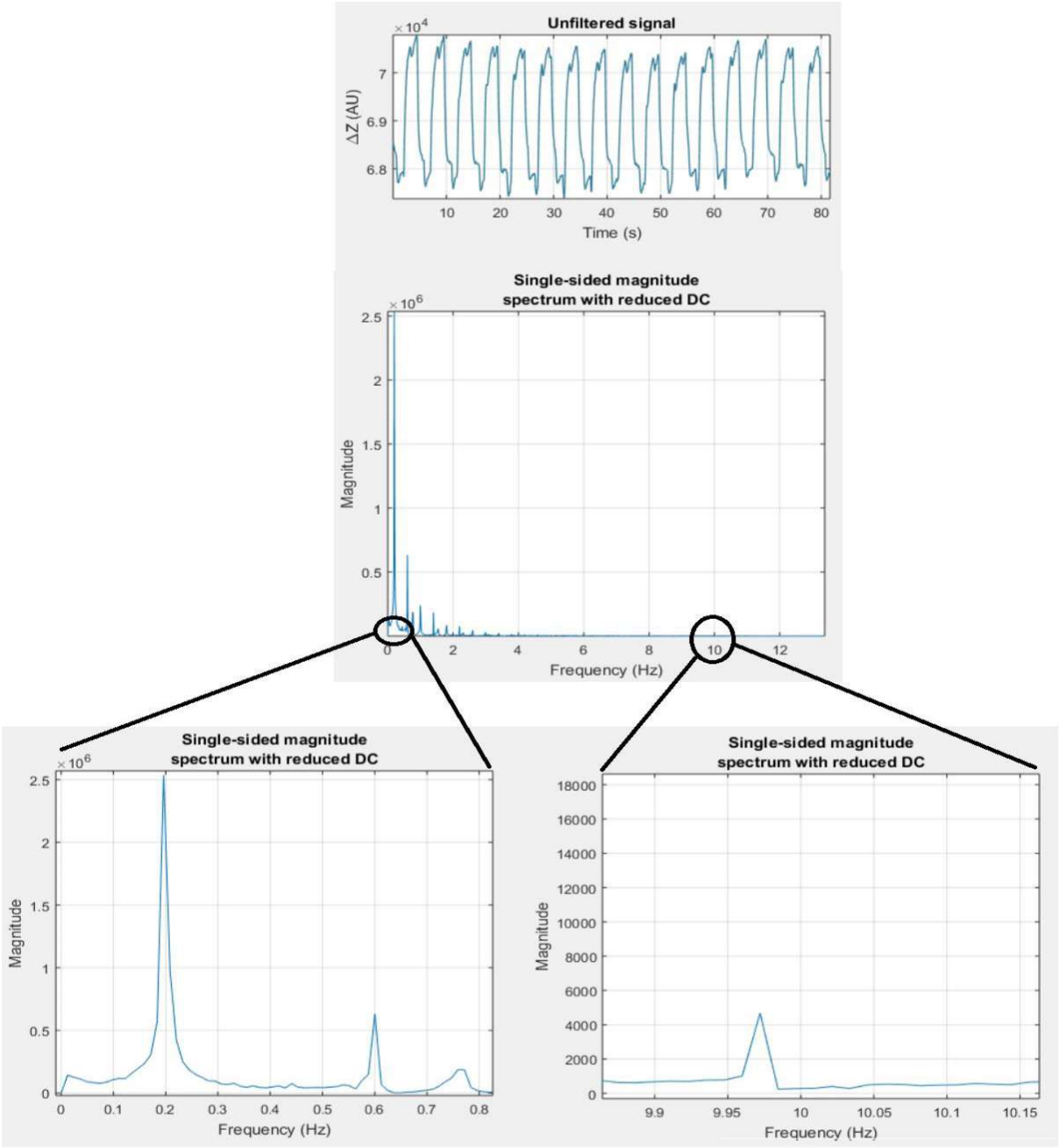

Fig 3.18 An example of the jet laryngoscope impedance change signal pre-filtering. The frequency spectrum shows two frequency components at the LF (0.2 Hz) and HF (~10Hz). The two frequency components are zoomed-in to see clearly the magnitude of each peak (LF magnitude=2,500,000, HF magnitude=4000) [4].

The most reasonable filter is a Band-Stop Filter (BSF), so as to stop all the frequencies between (0.2 Hz) and (10 Hz). The BSF is not functioning in the ibeX software. So, an LPF is enough to filter the laryngoscope signal as the HF component is very small compared to the LF component and it does not affect the signal. Fig 3.19 shows an example of jet laryngoscope ventilation global signal filtered based on the previous analysis procedure.

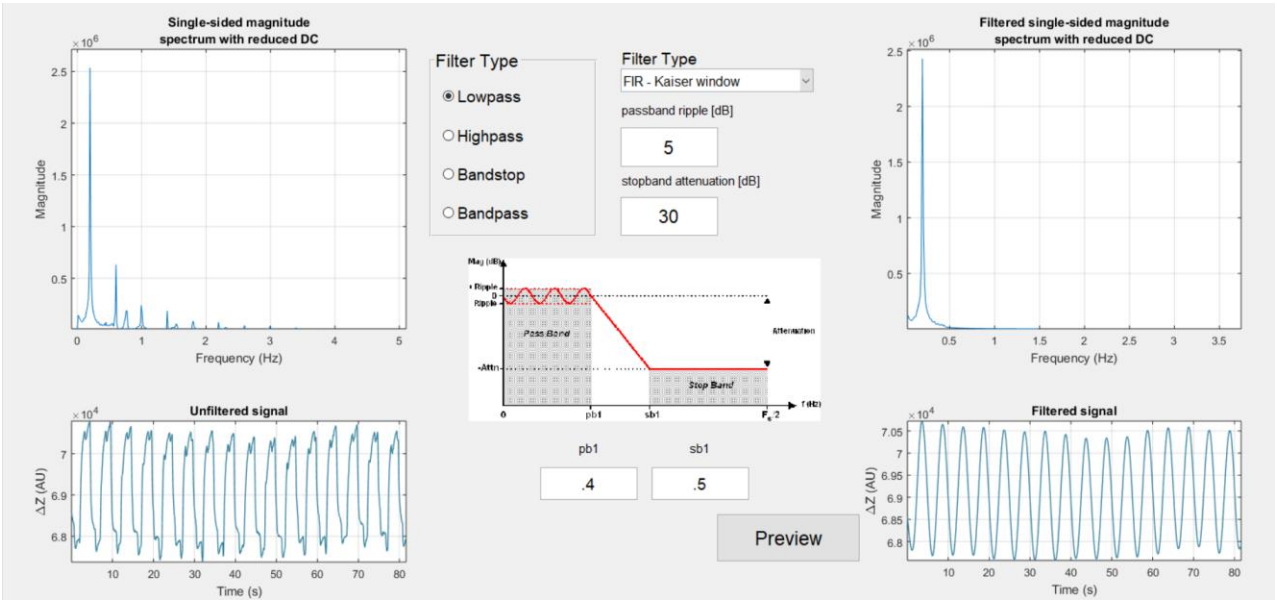

Fig 3.19 example on the jet laryngoscope ventilation analysis procedure. The unfiltered global signal is at the lower left and its frequency domain using FFT is at the upper left. An LPF is designed as shown in the middle with a pass-band frequency of 0.4 Hz and a stop-band frequency of 0.5 Hz. The filter is applied to the original global signal, and the result is displayed on the right. The filtered signal in the time domain is at the lower right and its frequency components are at the upper right [4].

To discuss more about the HF and LF components of the jet laryngoscope, an example for the analysis of the global impedance signal of patient Nr.7 is illustrated in Fig 3.20. The analysis was done separately for each frequency component. An LPF was used for the LF component filtering, and a High-Pass Filter (HPF) for the HF component. The impedance change due to the LF component was found 2000 (AU), Fig 3.20(A) and due to the HF component is only 2 (AU), Fig 3.20(B).

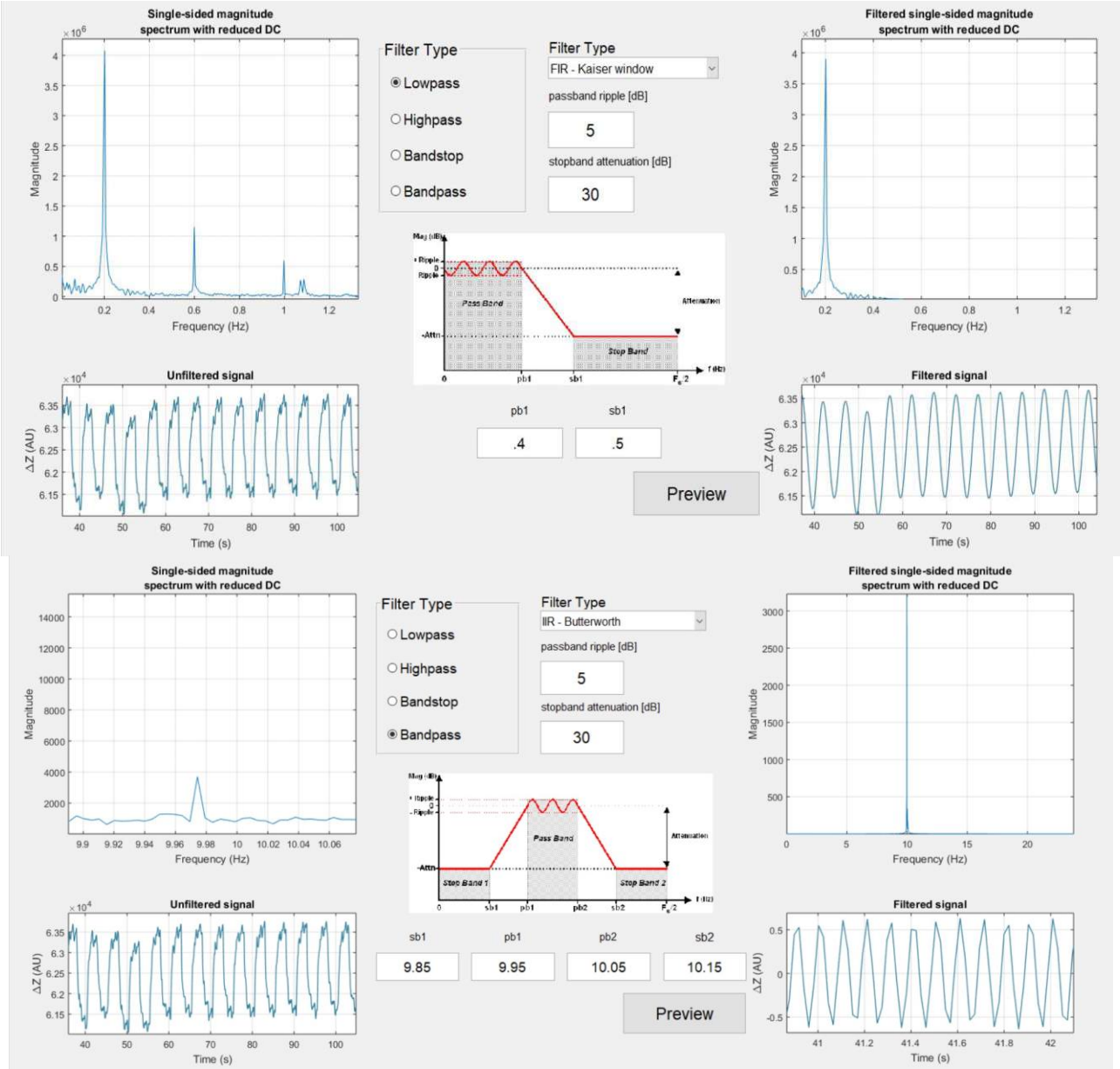

Fig 3.20 (A) on top, (B) on bottom: example on the jet laryngoscope filtering for both LF component on top and HF component on bottom separately [4].

3.2.3 Jet Catheter Ventilation Filter

The Single HFJV via thin Catheter is also a controlled JV mode with only one HF component applied through a thin catheter subglotticaly. The ventilation of (RR=~ 100-120 /min =~1.6-2.0 Hz) is applied based on the SpO2 and tcPCO2 values inside the body. In that case, the cardiac-related impedance dominates the global signal. To detect the impedance, change due to the jet catheter ventilation, a BPF is applied with cut-off frequencies surrounding the ventilation rate (1.6-2.0 Hz). Fig 3.21 shows an example of jet catheter ventilation global signal filtered based on the previous analysis procedure.

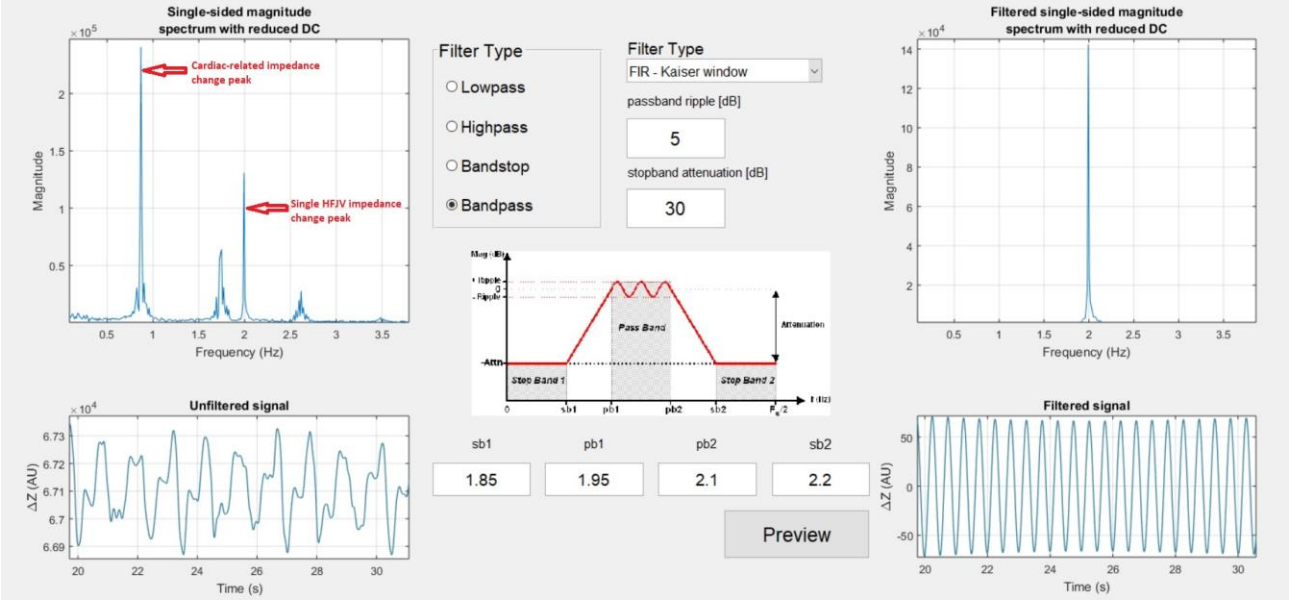

Fig 3.21 example on the jet catheter ventilation analysis procedure. The unfiltered global signal is at the lower left, its frequency domain using FFT is at the upper left (the peak of the cardiac-related impedance at (0.87 Hz) has a greater magnitude than the lung impedance change peak at (2.0 Hz). An BPF is designed as shown in the middle with pass-band frequencies of (1.95 Hz – 2.1 Hz). The filter is applied to the original global signal, and the result is displayed on the right. The filtered signal in the time domain is at the lower right (we can see 2 full breathing cycles each second (2.0 Hz)), and its frequency component is at the upper right [4].

3.3 Region of Interest data analysis

EIT can be used to assess the ventilation distribution in the lung. As previously mentioned, the lung is divided into four equally regions from ventral to dorsal direction. The regional ventilation impedance signal reflects the sum of impedance changes in a specific ROI.

Twenty-seven patients were recruited for this clinical study, four of them were excluded. The remaining 23 patients were included and underwent the mask ventilation for 2 minutes followed randomly with either Jet laryngoscope or catheter ventilation for 5 minutes. The regional ventilation distribution in all ROI of the lung under the 3 modes of ventilation for all the recruited patients are separately displayed in Fig 3.22.

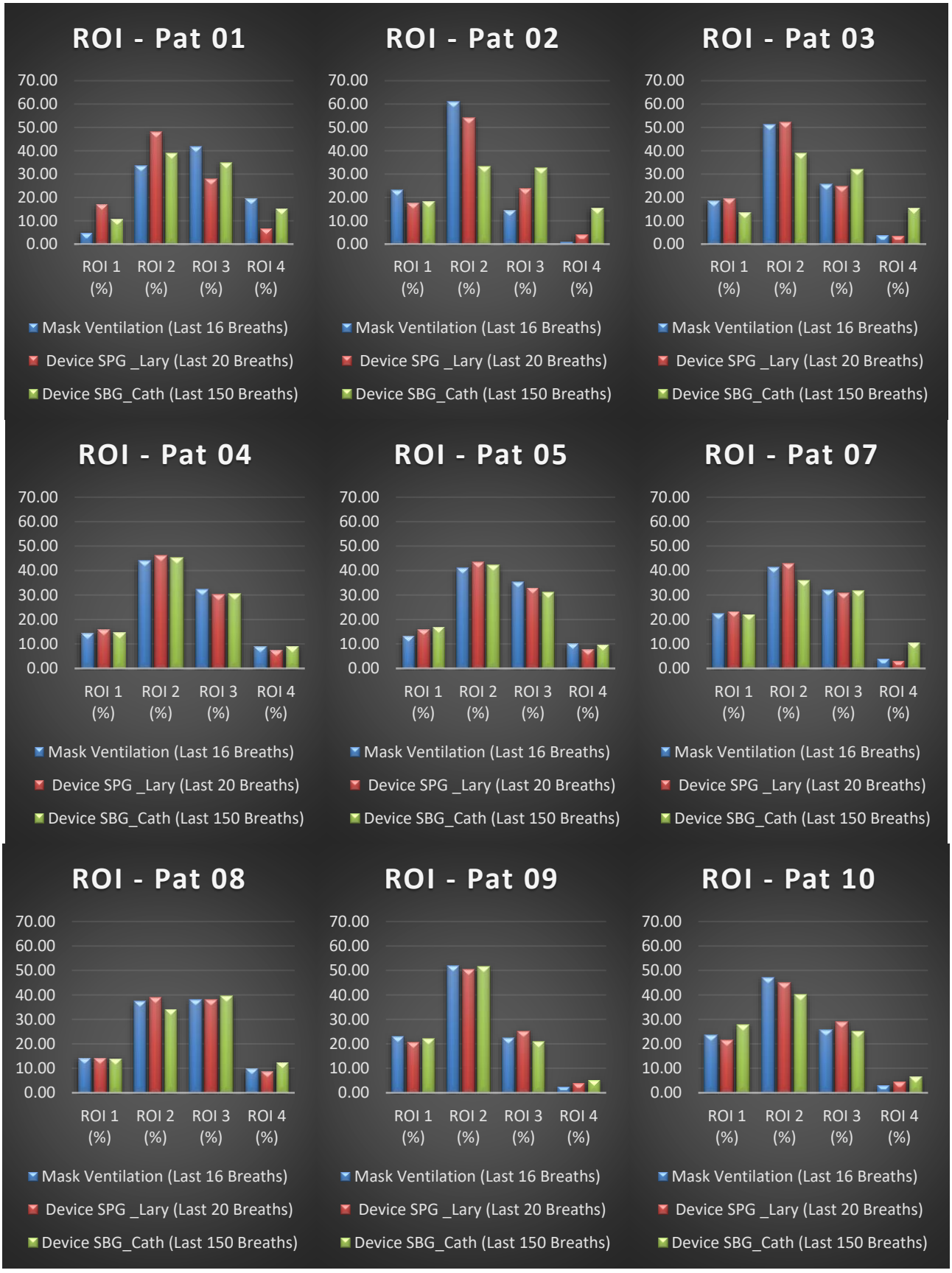

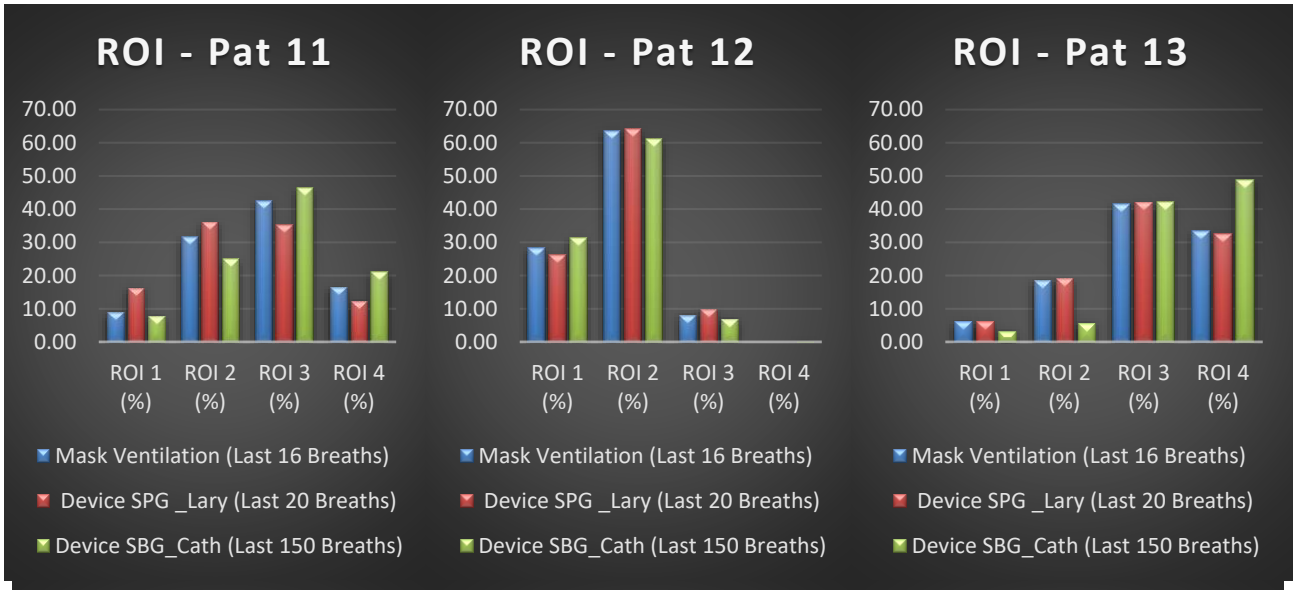

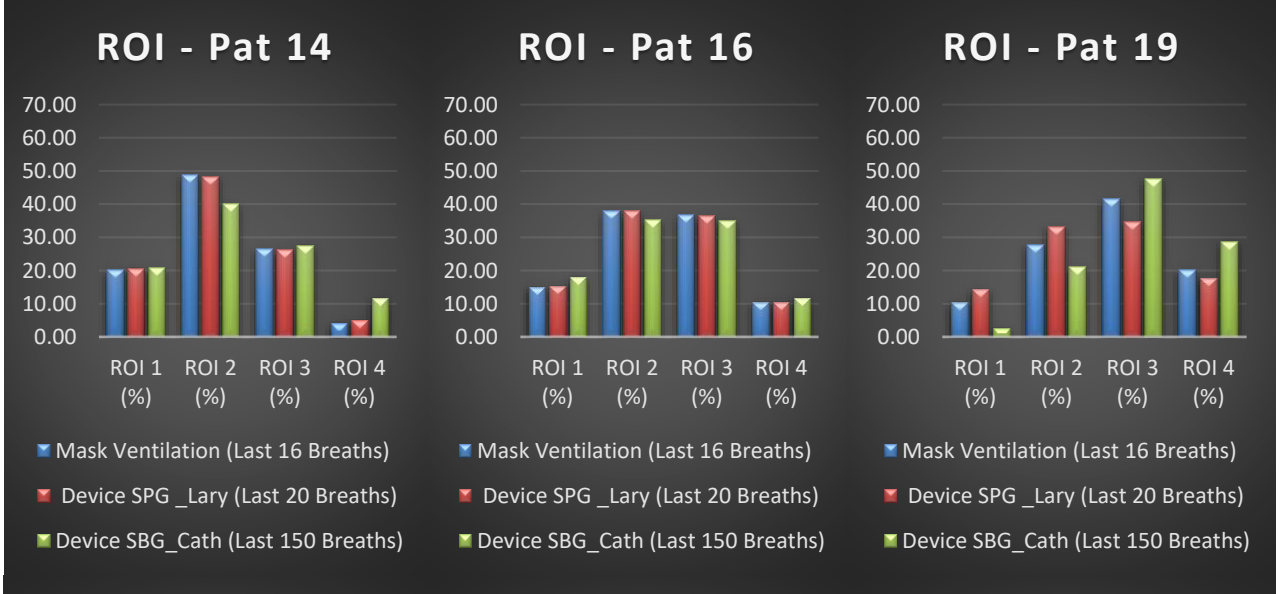

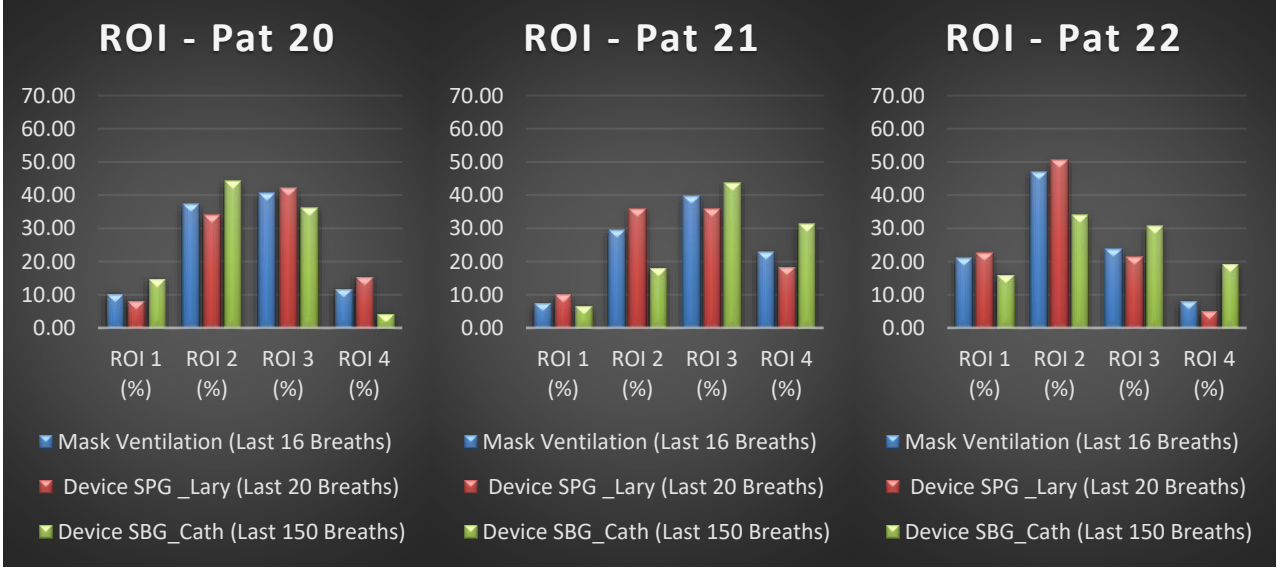

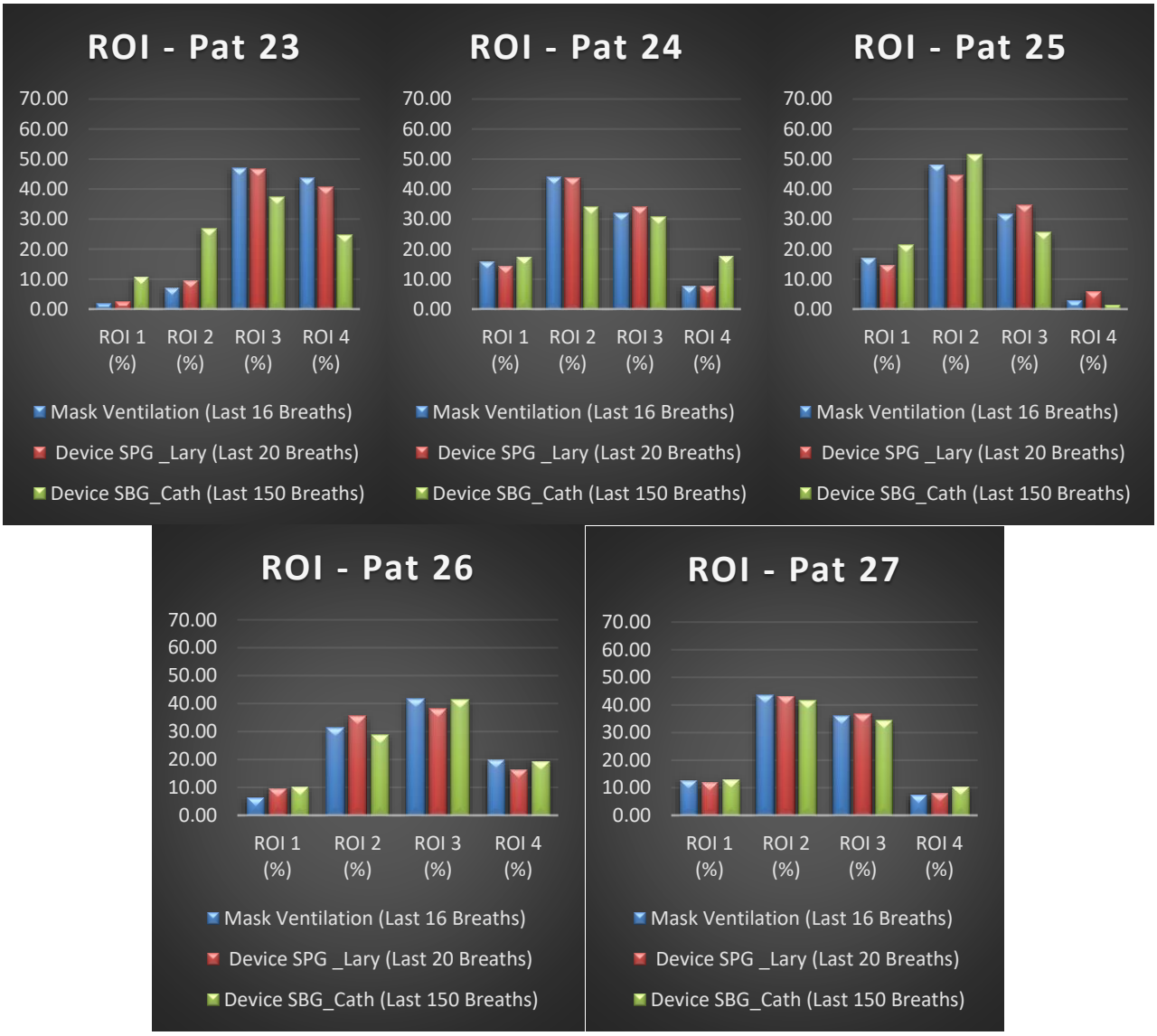

Fig 3.22 Lung ventilation distribution during the mask, jet laryngoscope and jet catheter for all patients

The ANOVA test results for each ROI are shown in Table 3.4. For all ROI, the (*P*-value > .05).

SUMMARY ROI1

Groups	*Count*	*Sum*	*Average*	*Variance*
Mask	23	341.6615	14.85485	49.2044
Lary	23	360.3705	15.66828	32.54257
Cath	23	355.6377	15.46251	50.39322

ANOVA ROI1

Source of Variation	*SoS*	*df*	*MS*	*F*	*P-value*	*F crit*
Between Groups	8.22845	2	4.114225	0.093406	0.910944	3.135918
Within Groups	2907.084	66	44.04673			
Total	2915.313	68				

SUMMARY ROI2

Groups	*Count*	*Sum*	*Average*	*Variance*
Mask	23	925.8119	40.25269	161.4776
Lary	23	956.6827	41.5949	128.5919
Cath	23	828.4128	36.01795	142.0513

ANOVA ROI2

Source of Variation	*SoS*	*df*	*MS*	*F*	*P-value*	*F crit*
Between Groups	389.7499	2	194.875	1.35292	0.265558	3.135918
Within Groups	9506.657	66	144.0403			
Total	9896.407	68				

SUMMARY ROI3

Groups	*Count*	*Sum*	*Average*	*Variance*
Mask	23	758.433	32.97535	93.2675
Lary	23	736.2669	32.0116	64.15145
Cath	23	764.392	33.23444	78.88272

ANOVA ROI3

Source of Variation	*SoS*	*df*	*MS*	*F*	*P-value*	*F crit*
Between Groups	19.09958	2	9.549792	0.121241	0.886018	3.135918
Within Groups	5198.637	66	78.76722			
Total	5217.736	68				

SUMMARY ROI4

Groups	*Count*	*Sum*	*Average*	*Variance*
Mask	23	274.0936	11.91711	116.447
Lary	23	246.6799	10.72521	92.15715
Cath	23	351.5575	15.28511	116.6746

ANOVA ROI4

Source of Variation	*SoS*	*df*	*MS*	*F*	*P-value*	*F crit*
Between Groups	257.2679	2	128.6339	1.186373	0.311753	3.135918
Within Groups	7156.132	66	108.4262			
Total	7413.4	68				

Table 3.4: ANOVA test for each ROI

There was no statistical significant difference between the average of regional ventilation of all ROIs between the three modes of ventilation. from another point of view, we can see that the central regions (ROI2, ROI3) ventilate with (~70-80%) of the TV, where the rest (~20-30%) are consumed by the ventral (ROI1) and dorsal (ROI4) regions for all 3 modes of ventilation, Fig 3.23.

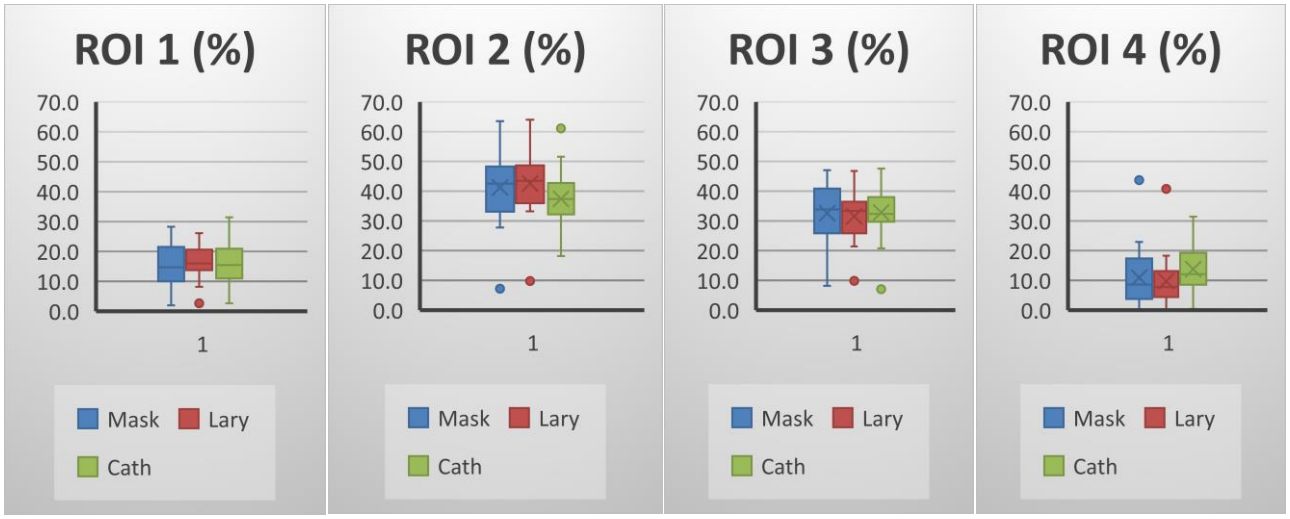

Fig 3.23 Box and whisker analysis of the regional ventilation distribution in all 23 patients during the 3 modes of ventilation

TIV is the difference between EILI and the preceding EELI. TIV is related to the TV inhaled in each breath. The results for the ANOVA test of the TIV are shown in Table 3.5, *P*-value =0.000000267 < .05. Statistically, there is a significant difference (P<0.05) in the TIV between the two modes of JV and between the mask and jet catheter ventilation. A post-hoc test with Bonferroni correction was performed to determine where the difference lies, Table 3.6. *P*-value for Lary-Cath is 0.0000004688 and for Cath-Mask 0.0000000919, are smaller than the Bonferroni correction α (0.01666667). This can be seen clearly in Fig 3.24, the TV inhaled in each breath during jet catheter ventilation is significantly lower than TV inhaled in the case of laryngoscope and the mask ventilation.

SUMMARY TIV

Groups	*Count*	*Sum*	*Average*	*Variance*
Mask	23	32592.27	1417.055	748245.27
Laryngoscope	23	36024.96	1566.302	1131905.9
Catheter	23	5284.508	229.7612	47263.479

ANOVA TIV

Source of Variation	*SoS*	*df*	*MS*	*F*	*P-value*	*F crit*
Between Groups	24673511	2	12336755	19.202026	0.000000267	3.135918
Within Groups	42403122	66	642471.6			
Total	67076633	68				

Table 3.5: ANOVA test for TIV

Post hoc test TIV

Group	*P-Value (T-Test)*	*Significance*
Mask-Lary	0.6042851042	No
Lary-Cath	0.0000004688	yes
Cath-Mask	0.0000000919	yes

ALPHA TIV

Test	*ALPHA*
ANOVA	0.05
Bonferroni Correction α	0.01666667

Table 3.6: post-hoc test with Bonferroni correction for the TIV

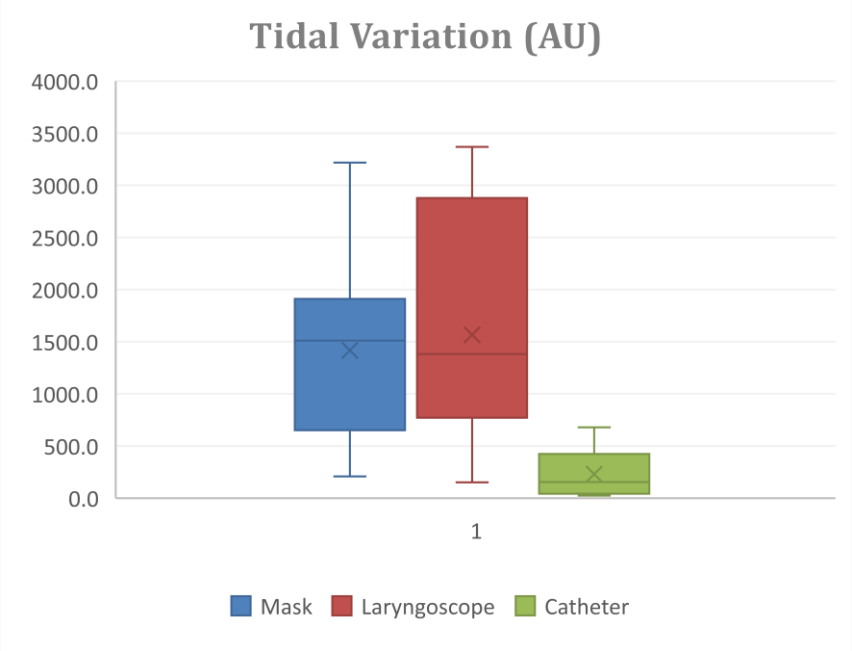

Fig 3.24 Box and whisker analysis of the tidal ventilation. there is a significant difference between the jet catheter ventilation and both mask and laryngoscope ventilation.

3.4 Silent Spaces data analysis

Areas with little or no apparent ventilation are called silent spaces (SS). SS are divided into two groups: NSS and DSS. The NSS represent the areas of the lungs above the HoV, a virtual horizontal line passing through the CoV. The DSS are the areas below the HoV, thus at the dependent part of the lungs

[33]. The NSS and DSS are calculated for each tidal image by, first, defining the HoV as a line perpendicular to the gravity vector that passes through the CoV. DSS include all pixels lying below the HoV and are expressed as a percentage of all pixels within all lung ROIs. Similarly, the NSS describe the percentage of poorly ventilated pixels that are located above the HoV. The SS developed in the lung during the 3 modes of ventilation for all the recruited patients separately displayed in Fig 3.25.

The ANOVA test results for both NSS and DSS were performed and shown in Table 3.7 where (*P*-value > .05). No statistically significant difference (p>0.05) for the NSS or the DSS between the 3 modes of ventilation.

SUMMARY NSS

Groups	*Count*	*Sum*	*Average*	*Variance*
Mask	23	75.37226	3.277055	10.98526
Laryngoscope	23	61.79869	2.686899	9.104317
Catheter	23	69.78988	3.034343	17.85989

ANOVA NSS

Source of Variation	*SoS*	*df*	*MS*	*F*	*P-value*	*F crit*
Between Groups	4.047305	2	2.023652	0.159975	0.852495	3.135918
Within Groups	834.8883	66	12.64982			
Total	838.9356	68				

SUMMARY DSS

Groups	*Count*	*Sum*	*Average*	*Variance*
Mask	23	199.3673	8.668144	52.73636
Laryngoscope	23	189.6028	8.243602	30.53297
Catheter	23	140.0162	6.087659	42.92937

ANOVA DSS

Source of Variation	*SoS*	*df*	*MS*	*F*	*P-value*	*F crit*
Between Groups	88.0687	2	44.03435	1.046786	0.356819	3.135918
Within Groups	2776.371	66	42.06623			
Total	2864.44	68				

Table 3.7: ANOVA test for NSS and DSS

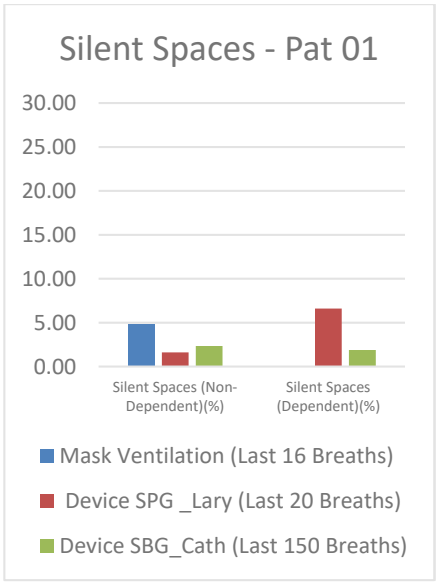

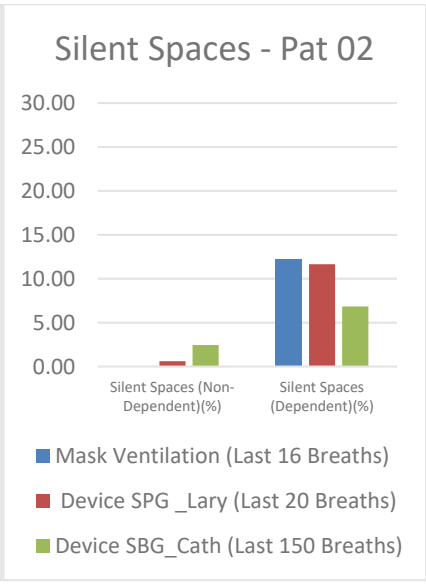

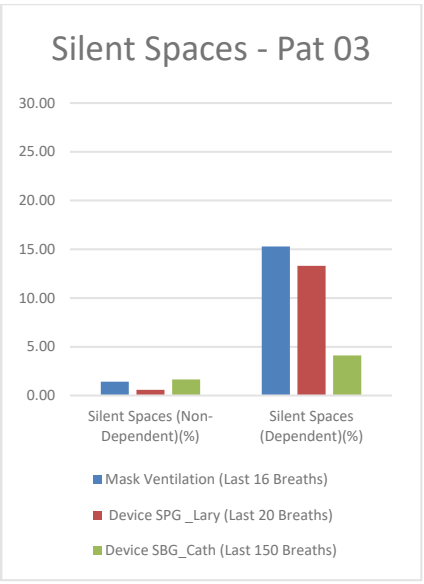

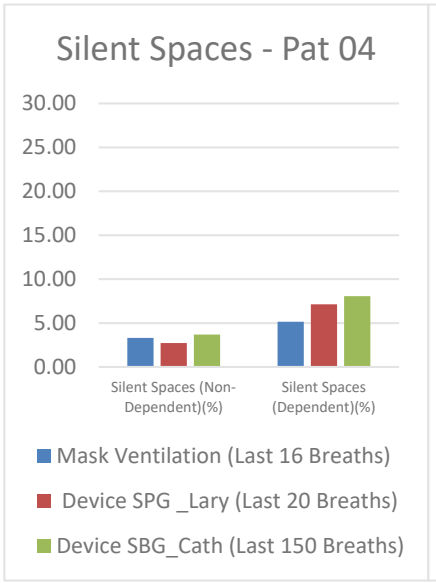

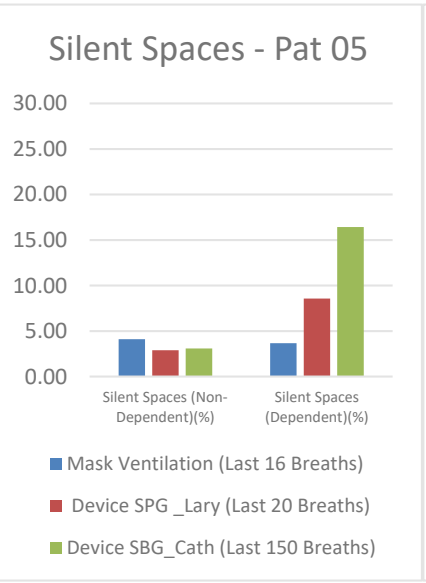

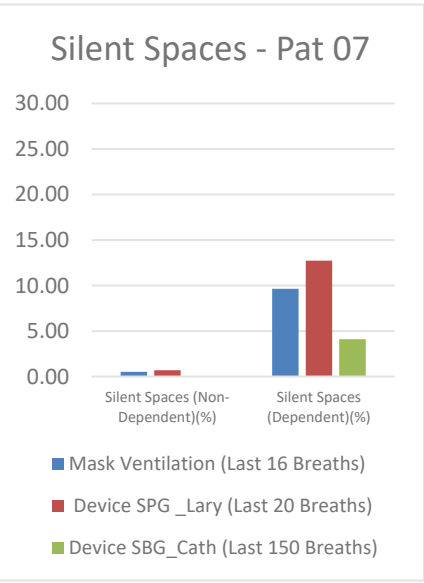

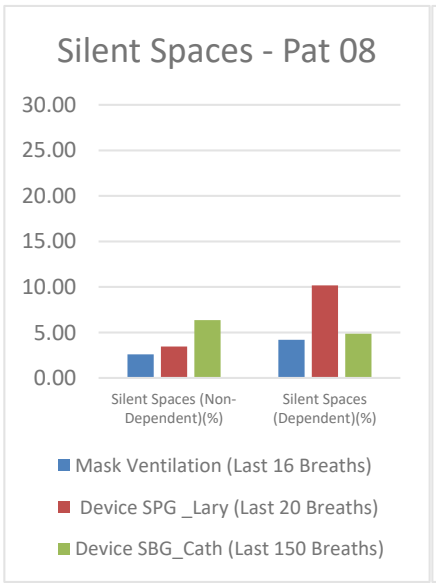

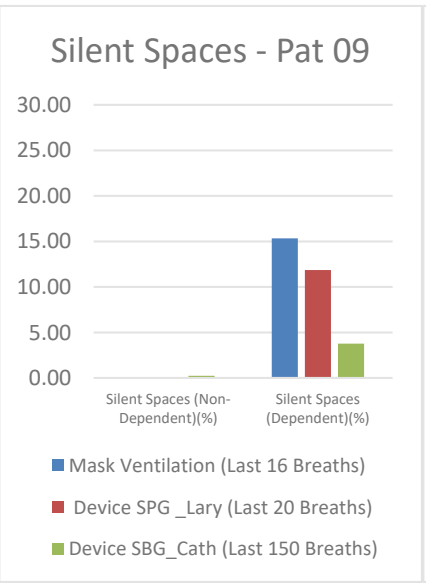

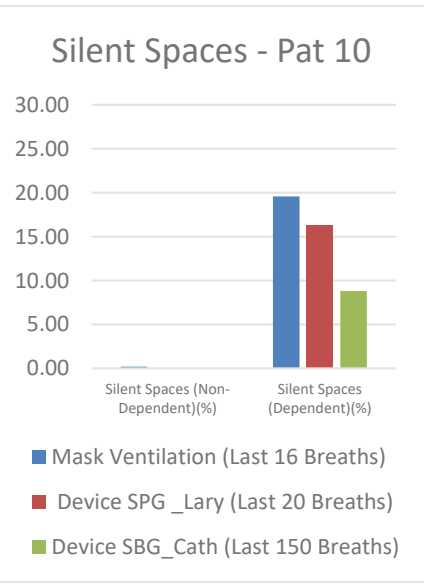

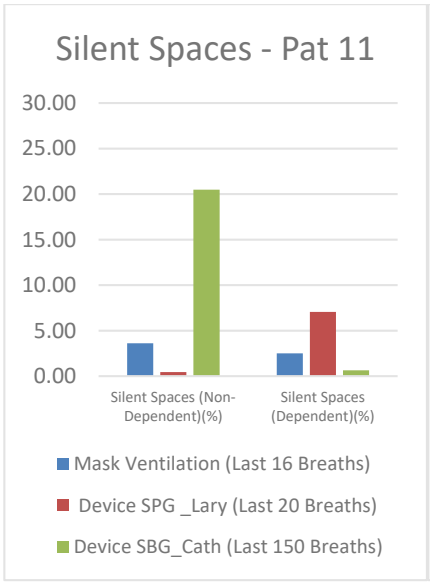

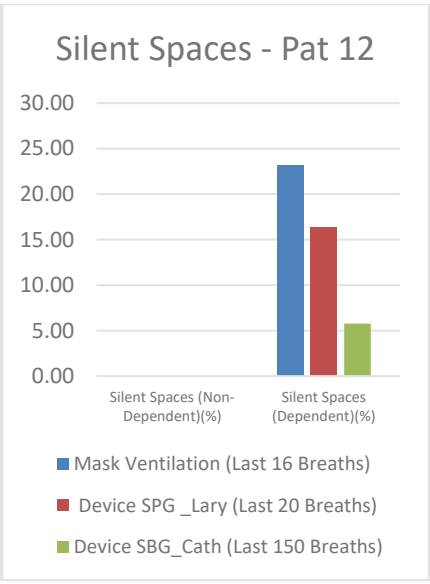

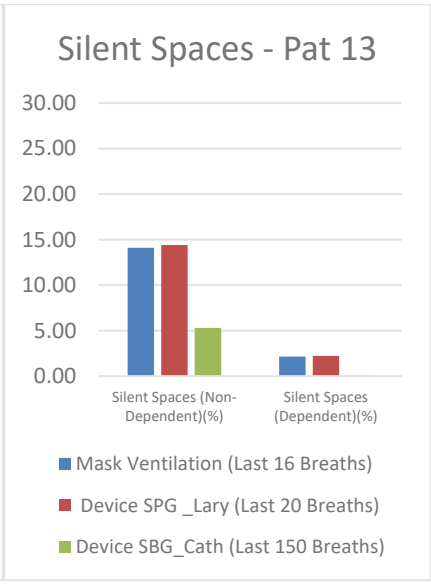

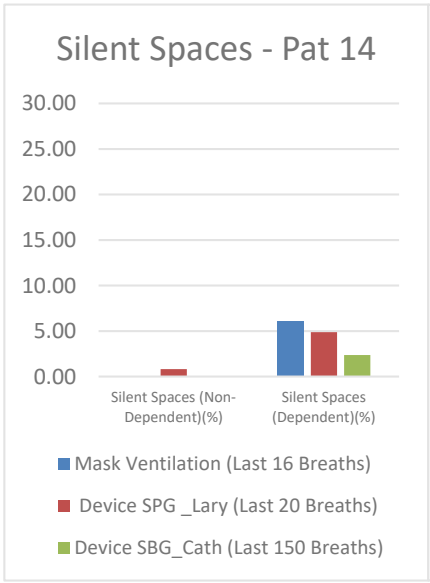

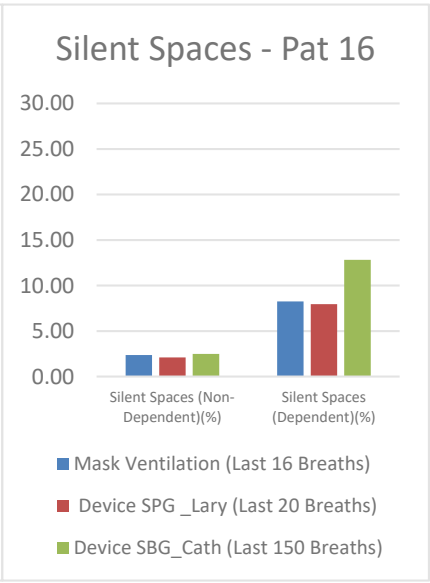

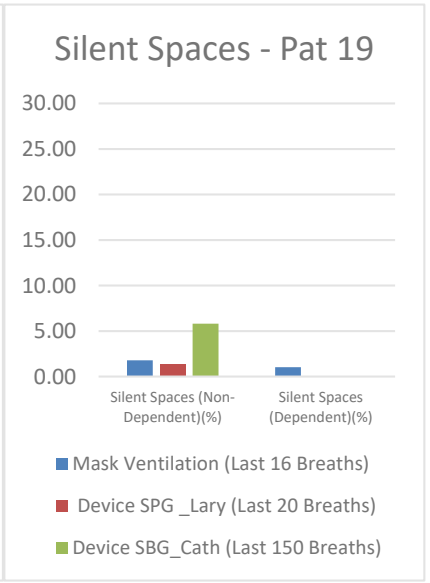

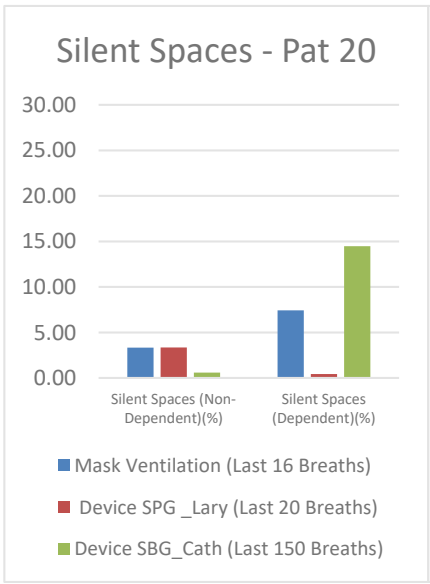

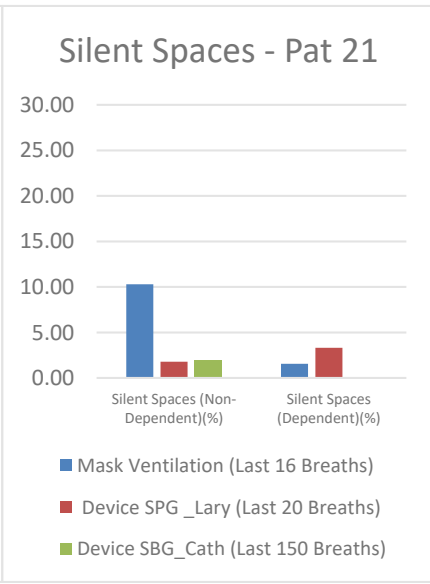

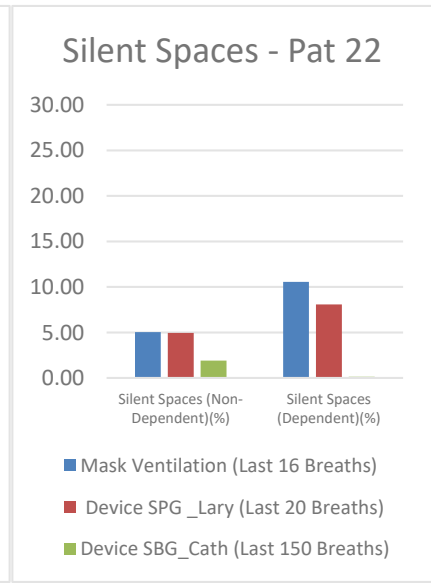

Fig 3.25 SS during the mask, jet laryngoscope and jet catheter for all patients

As previously mentioned, the gravity influences the ventilation distribution and may point to SS development [33]. The ANOVA test was performed for the SS between the NSS and DSS for each of the ventilation modes, Table 3.8. *P*-value < .05 between the NSS and DSS for mask ventilation and jet laryngoscope modes. In jet catheter mode, *P*-value > .05 between the NSS and DSS. The ANOVA test revealed that there is a significant difference between the average DSS and NSS of mask and jet laryngoscope ventilation, Fig 3.26 (A). There is no statistically significant difference between the DSS and NSS during the jet catheter ventilation, Fig 3.26 (B).

During the mask and jet laryngoscope, the developed DSS magnitude is greater than the NSS magnitude. This proves the hypothesis that in the supine position, the dorsal regions (dependent region)

develop more SS than the ventral regions (non-dependent region) which are significant during mask and supraglottic JV.

SUMMARY DSS-NSS Mask Ventilation

Groups	*Count*	*Sum*	*Average*	*Variance*
DSS-Mask	23	199.37	8.67	52.74
NSS-Mask	23	75.37	3.28	10.99

ANOVA DSS-NSS Mask Ventilation

Source of Variation	*SoS*	*df*	*MS*	*F*	*P-value*	*F crit*
Between Groups	334.23	1	334.2341	10.4904	0.002286074	4.0617
Within Groups	1401.88	44	31.8608			
Total	1736.11	45				

SUMMARY DSS-NSS Laryngoscope Ventilation

Groups	*Count*	*Sum*	*Average*	*Variance*
DSS-Laryngoscope	23	189.60	8.24	30.53
NSS-Laryngoscope	23	61.80	2.69	9.10

ANOVA DSS-NSS Laryngoscope Ventilation

Source of Variation	*SoS*	*df*	*MS*	*F*	*P-value*	*F crit*
Between Groups	355.08	1	355.0848	17.9167	0.000115458	4.0617
Within Groups	872.02	44	19.8186			
Total	1227.11	45				

SUMMARY DSS-NSS Catheter Ventilation

Groups	*Count*	*Sum*	*Average*	*Variance*
DSS-Catheter	23	140.02	6.09	42.93
NSS-Catheter	23	69.79	3.03	17.86

ANOVA DSS-NSS Catheter Ventilation

Source of Variation	*SoS*	*df*	*MS*	*F*	*P-value*	*F crit*
Between Groups	107.21	1	107.2115	3.5273	0.06700229	4.0617
Within Groups	1337.36	44	30.3946			
Total	1444.58	45				

Table 3.8: ANOVA test for NSS and DSS for each ventilation mode

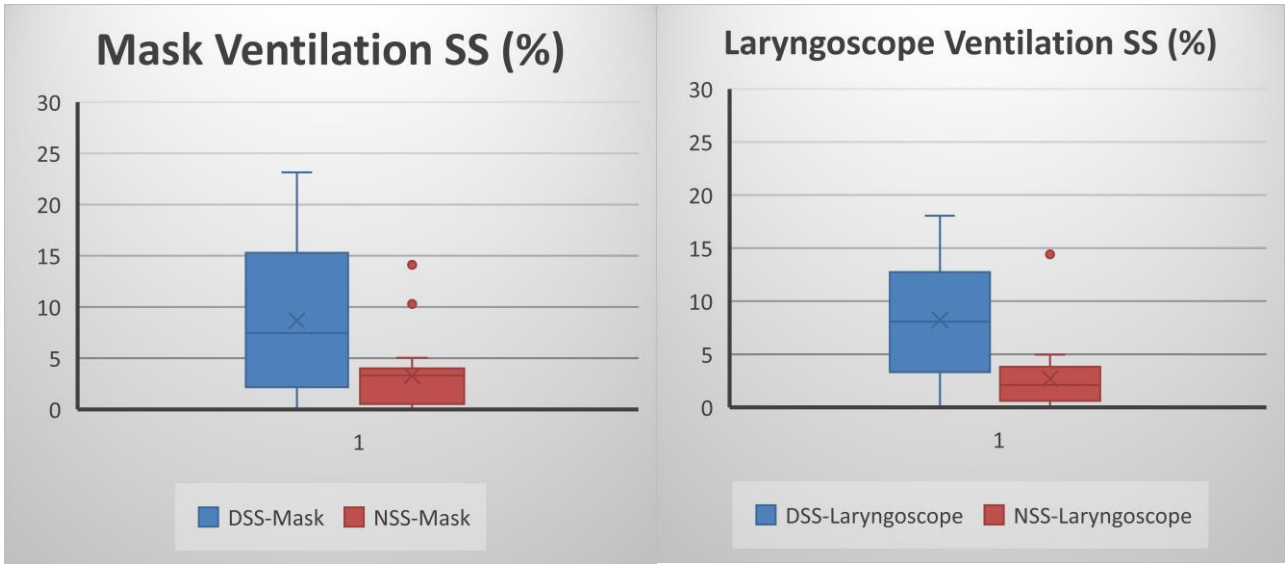

(A) Statistical significant difference between the average of DSS and NSS during mask and jet laryngoscope ventilation

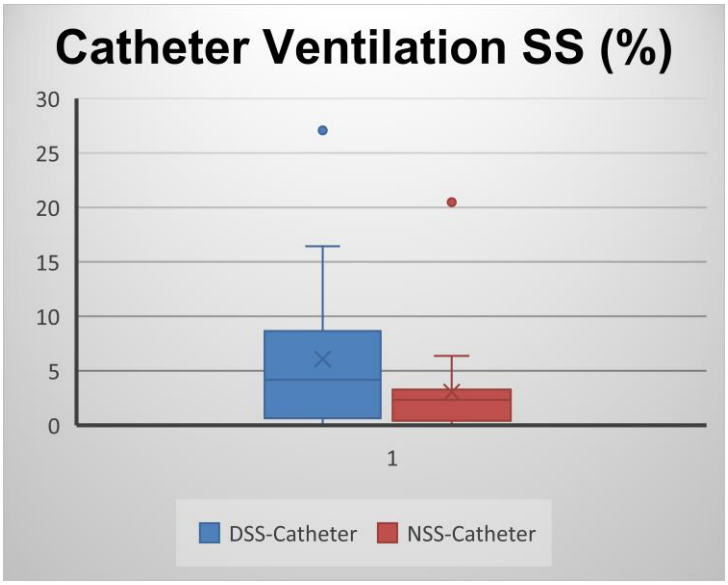

(B) Statistical significant difference between the average of DSS and NSS during mask and jet laryngoscope ventilation

Fig 3.26 Box and whisker analysis of the SS during the 3 modes of ventilation separately, the median is depicted by the line within the box, and the means by the x.

CoV can be used to assess the shifts in the ventrodorsal direction [34]. Center of Ventilation in Ventro-Dorsal direction (CoVvd) increases when the center of the ventilation distribution moves to the dorsal direction. The values of CoV lies between 0 and 100%. The 0% value indicates all image intensity located at the top for CoVvd whereas, for the 100% value, all intensity would be concentrated at the bottom. A CoV of 50% indicates a centered ventilation distribution. Optimal values of the CoV are highly dependent on the thorax anatomy of every patient. Statistically, there is no significant difference in the

mean value of the CoV between the 3 ventilation modes, Fig 3.27. The results for the ANOVA test for the CoV are shown in Table 3.9. where (*P*-value > .05).

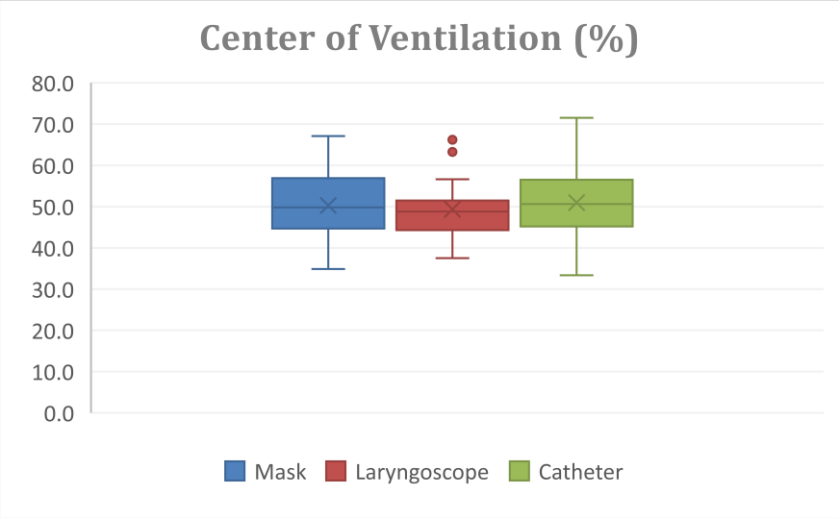

Fig 3.27 Box and whisker analysis of the CoV during the 3 modes of ventilation

SUMMARY CoV

Groups	*Count*	*Sum*	*Average*	*Variance*
Mask	23	1156.098	50.26511	66.35247
Laryngoscope	23	1134.726	49.33593	43.82635
Catheter	23	1171.952	50.95445	75.00391

ANOVA CoV

Source of Variation	*SoS*	*df*	*MS*	*F*	*P-value*	*F crit*
Between Groups	30.34573	2	15.17287	0.245804	0.782788	3.135918
Within Groups	4074.02	66	61.72758			
Total	4104.366	68				

Table 3.9: ANOVA test for the CoV

3.5 Effect of catheter position on ventilation distribution

Inhomogeneity in ventilation distribution across the lung is normal due to gravity, fluid accumulation and the developed SS. but, it is worth knowing that the position and direction of the jet catheter tip inside the trachea do affect the distribution of the ventilation between the left and the right lung. In Fig 3.28, we can see 3 different types of ventilation distribution between the right and the left lung in 3 different patients. Patient Nr.11 experienced more than 90% of the TV in the left lung, and vice versa in patient Nr.16. Patient Nr.08 experienced more or less semi-equal ventilation distribution between the right and left lung.

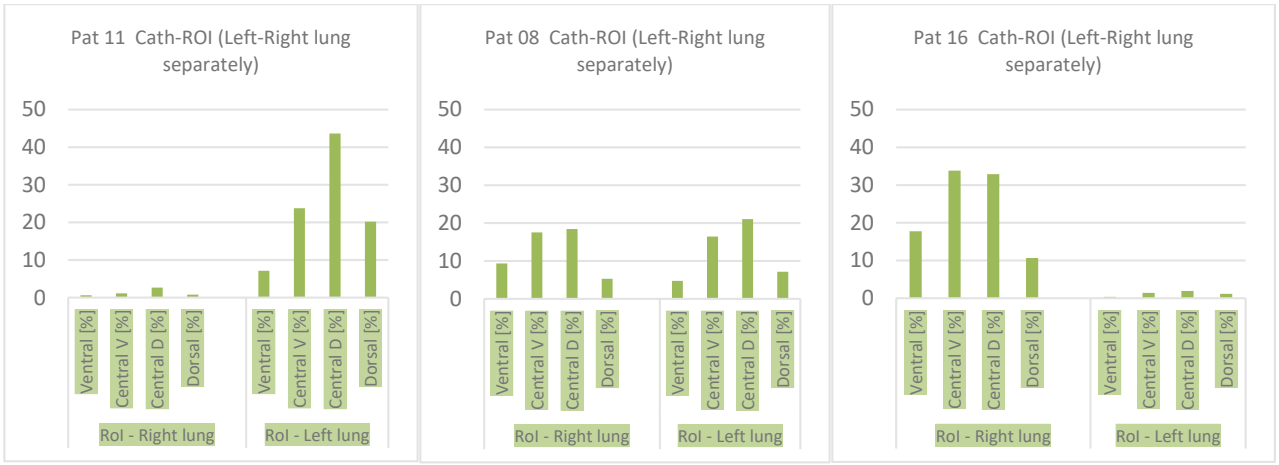

Fig 3.28 Three different types of ventilation distribution during the jet catheter ventilation between the right and the left lung in 3 different patients.it reveals that the catheter tip can affect the distribution of the air between the right and left lung

Another comparison between the 3 modes of ventilation in patient Nr.14 is illustrated in Fig 3.29. We can see a normal distribution of the ventilation between the right and the left lung in the mask and jet laryngoscope mode. In the jet catheter ventilation mode, the right lung receives much more TV than the left lung.

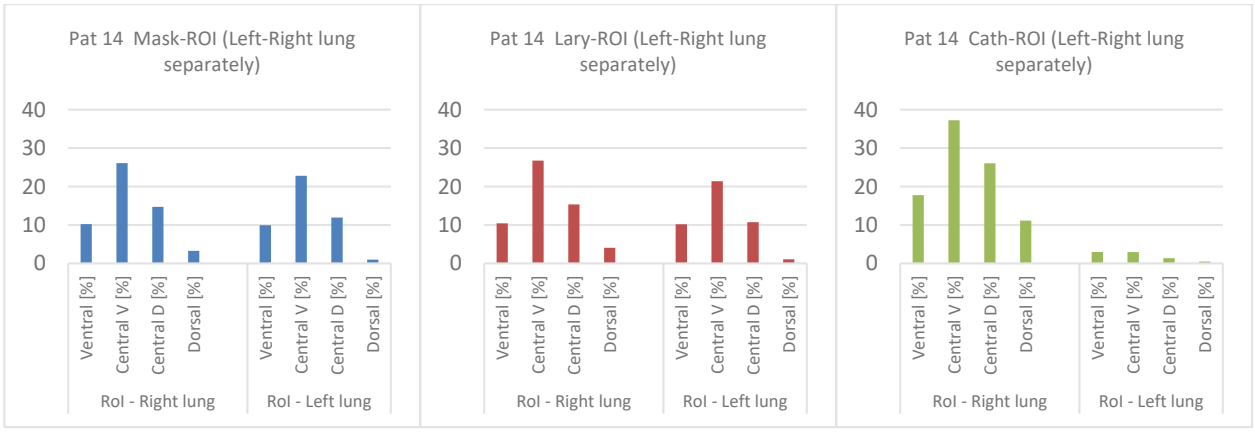

Fig 3.29 comparison between the right and the left lung ventilation distribution during the 3 modes of ventilation in patient Nr.14

3.6 Effect of driving pressure on ventilation distribution during jet laryngoscope ventilation

(Bialka et al, 2018) concluded that increasing the driving pressure, increases the overall TV, but this is based on over-inflation of the ventilated areas of the lung not on distributing the ventilation to the less ventilated areas [35]. This finding can be investigated in our study.

The base-line setting of the JV DP in patient Nr. 03 was 1.1 bar. During the SIHFJV, the CO2 accumulated inside the body and is required to be eliminated through 3 steps as follows:

1- Increasing the RR of the LF component from 12/min to 15/min

2- After ~1 min, Increase the RR of the LF component from 15/min to 18/min

3- After ~ 1 min, increase the DP from 1.1 bar to 1.6 bar.

This intervention sequence can be seen clearly in the EIT Plethysmogram during the SIHFJV in Fig 3.30. The impedance changes during the DP of 1.6 bar are greater than the impedance changes during the DP of 1.1 bar. This means that the TV increases by increasing the DP.

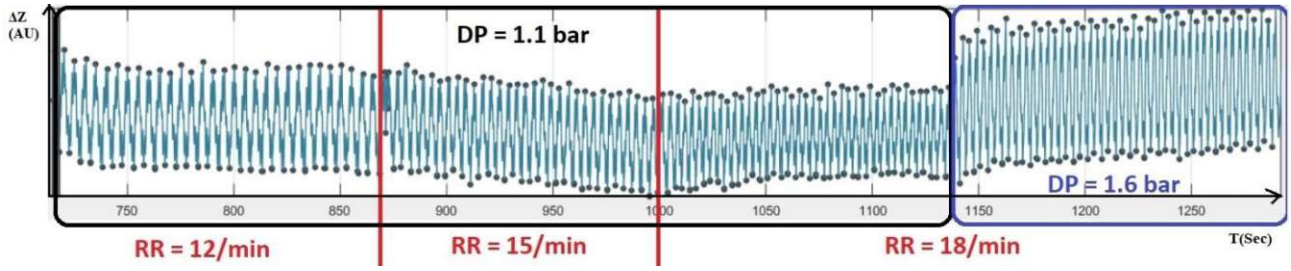

Fig 3.30 EIT Plethysmogram during SIHFJV of patient Nr.03. the Plethysmogram is divided into 3 regions through the two red lines to show the RR during each region. It is also divided into two regions inside the black and blue boxes to show the DP at each region [4].

To discuss the ventilation distribution through the lung ROIs, a bar chart describing the ventilation distribution during the SIHFJV for patient Nr.03 under 1.1 bar and 1.6 bar is plotted in Fig 3.31. We can see that there are no changes in the ventilation distribution in the lung between the 2 DP modes. There is only over-inflation of the ventilated areas of the lung and no changes in ventilation distribution in the areas with less ventilation during the high and low DP.

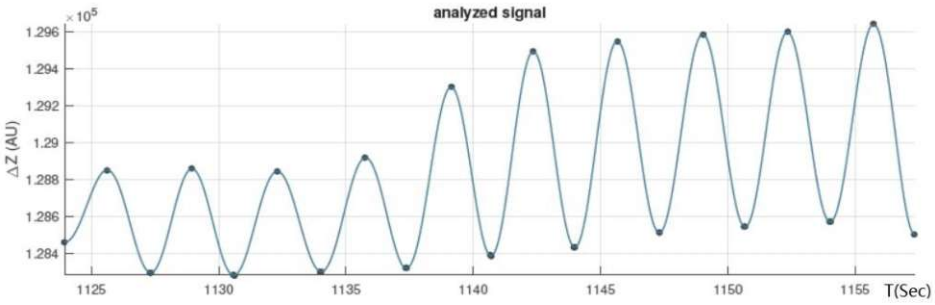

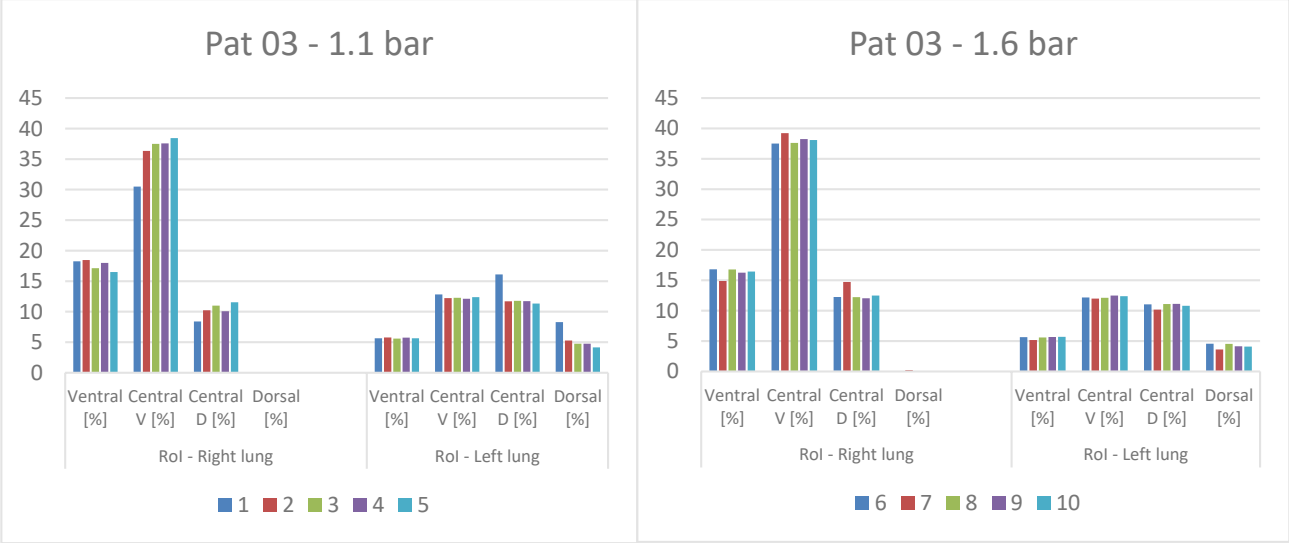

Fig 3.31 the upper figure is the Plethysmogram describing 5 breaths at 1.1 bar (first 5 breaths) and 5 breaths at 1.6 bars (last 5 breaths). At the bottom, a Bar Charts describing the ventilation distribution at each ROI in the right and left lung separately during DP of 1.1 bar and 1.6 bar under SIHFJV.

The tidal images in Fig 3.32 displays no change in the ventilation distribution during the 2 DP modes.

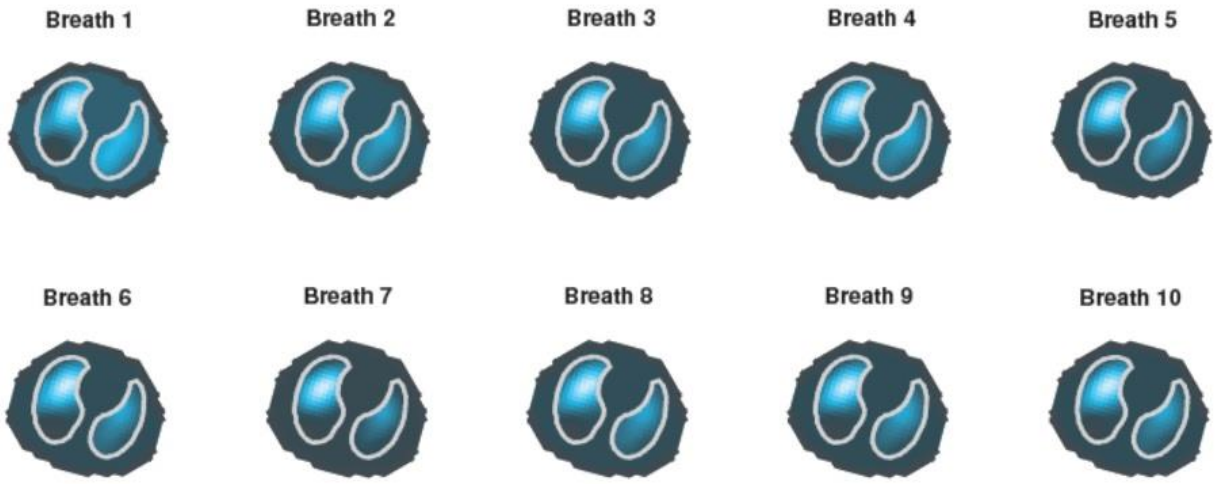

Fig 3.32 tidal images representing each breath separately. Breaths 1-5 are for the DP of 1.1 bars and breaths 6-10 are for the DP of 1.6 bar. brighter pixels are related to larger impedance change while black pixels represent no impedance change [4].

The silent spaces and CoV during the 2 DP modes are investigated in Fig 3.33. The DSS are ~9% and no NSS for the two groups of breaths. The magnitude and distribution of the silent spaces during the low and high DP are the same.

Fig 3.33 Silent Spaces (in pink) distribution and magnitude remain the same during low and high DP [4].

4 Discussion

The aim of the study was to evaluate the regional ventilation distribution of the lung in patients under anesthesia during Single HFJV and SIHFJV modes using EIT tool. The Single HFJV was provided for 5 minutes subglotticaly with a HF RR of 120/min via a 2-3 mm jet catheter. The SIHFJV was applied also for 5 minutes but supraglotticaly with a mix of 2 frequencies. This mix is a combination between LF JV with RR of 12/min and a HFJV with RR of 600/min. A mask ventilation mode with TV of 6mL/Kg preceded the JV modes for 2 minutes to be used as a reference of ventilation.

The most important finding of the study is, that SIHFJV induces more tidal volumes than the Single HFJV, but this was mostly based on over-inflation of the ventilated lung ROIs, not by shifting the ventilation to the low ventilation ROIs. There was no significant improvement in the ventilation distribution between the 2 JV modes. Also, there was no significant difference in the developed SS during both ventilation modes.

In the supine position and during general anesthesia, ventral ROIs of the lung are better ventilated than the dorsal ROIs and the lung strain is distributed heterogeneously across the lung ROIs leading to atelectasis and interrupting the CO2 elimination [36] [37].

In this study, the ventilation distribution in the lung ROIs and SS, and also the CoV position during SIHFJV and Single HFJV was compared by the EIT technique. Our hypothesis was that SIHFJV would improve the regional ventilation distribution in the dorsal regions and reduce the SS of the lung compared to the Single HFJV. The results indicate that ventilation in all ROIs of the lung increased during the SIHFJV mode compared to the Single HFJV mode. The EIT reflects no difference in the regional ventilation distribution of the lung, but the ventilation increase is based on over-inflation of the already ventilated areas of the lung and not the shift of ventilation to the less ventilated areas.

Increasing the DP of JV is always applied clinically to increase the TV to provide adequate SpO2 in the blood stream, which is reflected by this study especially during the SIHFJV mode. The TV increases by increasing the DP due to increased ventilation of the already ventilated lung ROIs without distributing the ventilation to the less ventilated areas. Increased TV causes a stretch to the lung tissue, which is worrisome. It might induce local inflammation which is known as ventilator-induced lung injury [38]. Therefore, whether SIHFJV or Single HFJV is applied, the anesthesiologists should be careful while handling the applied DP during JV modes and aim to keep it at minimum values to avoid ventilator-induced lung injury.

The findings of this study have some limitations. First, we didn't measure the TV during the JV, instead, a relative TV that depended on the TIV was considered during the analysis. Second, relatively slimmer patients (BMI < 30 kg/m2) were included in the study. Higher BMI affects the chest wall

compliance causing an increase in the chest pleural pressure. Third, we didn't assess whether atelectasis or pneumothorax was developed after the JV. Finally, increasing the TV by over-inflation of the already ventilated areas is worrisome. Increased TV causes a stretch to the lung tissues, and might develop a lung injury, known as ventilator-induced lung injury. Although of being of clinical interest, we didn't investigate the development of ventilator-induced lung injury.

5 Conclusion

EIT is a novel imaging technique that allows the possibility to continuously monitoring the lung activity and the regional ventilation distribution. The lung regional ventilation distribution during HFJV can be evaluated using the EIT in anesthetized patients undergoing surgeries in the airways. Ventilation was provided supraglotticaly via a jet laryngoscope during the SIHFJV and Subglotticaly via a jet catheter during the Single HFJV

This clinical study revealed that there is no significant change in the ventilation distribution in the lung ROIs between the supraglottic JV and the subglottic JV. There is no significant change in the developed silent spaces between the two JV modes as well. Furthermore, there is a significant change in the TV between the supraglottic and subglottic JV. Increased TV was achieved by supraglottic JV compared to the subglottic JV by over inflation of the already ventilated lung ROIs, instead of shifting the ventilation to the less ventilated lung ROIs.

Increasing the DP of the supraglottic JV, provides TV increase by over-inflation of the already ventilated ROI, but no change in the ventilation distribution. In Subglottic JV, the position of the Jet Catheter inside the trachea affects the ventilation distribution in the lung ROIs and also affects the ventilation distribution between the right and left lung.

HFJV is an effective mechanical ventilation technique that allows adequate lung ventilation distribution in patients under anesthesia. It allows the anesthesiologists to have uninterrupted airway in micro-laryngeal surgery, while surgeons are able to access the larynx and have good visibility. The regional lung ventilation and SS developed during the JV can be assessed by EIT to provide a real time monitoring of the lung functionality and allow fast response to any urgent clinical issues. A further studies comparing the JV modes on patients with higher BMI and significant airway stenosis are needed.

References

[1] Neural Academy. (2019, January 11). ANATOMY OF THE LUNGS [Video]. YouTube. https://www.youtube.com/watch?v=YNI0i6S3X14
[2] Chaudhry R, Bordoni B. Anatomy, Thorax, Lungs. [Updated 2021 Jul 31]. In: StatPearls [Internet]. Treasure Island (FL): StatPearls Publishing; 2022 Jan-. Available from: https://www.ncbi.nlm.nih.gov/books/NBK470197/
[3] User's Guide ibeX v1.1, SenTec AG
[4] SenTec AG. (2018). IbeX software (version 1.5) [PC software] https://tinyurl.com/mvt4s2ct
[5] Bryan A C, Milic-Emili J and Pengelly D 1966 Effect of gravity on the distribution of pulmonary ventilation J. Appl. Physiol. 21 778–84
[6] Eugenijus Kaniusas, Biomedical Signals and Sensors I. 1st rev. Berlin, Heidelberg: Springer; 2012. 15-17 p.
[7] Eugenijus Kaniusas, Biomedical Signals and Sensors I. 1st rev. Berlin, Heidelberg: Springer; 2012. 194-197 p.
[8] Kaniusas, E. (2018). Lecture 7: Biomedical Sensors and Signals [PDF slides]. Vienna University of Technology, Master of Biomedical Engineering
[9] Barber DC, Brown BH (1984) Applied potential tomography. J Phys E: Sei Instrum 17: 723–733
[10] Dreyfuss D, Soler P, Basset G, Saumon G. High inflation pressure pulmonary edema. Respective effects of high airway pressure, high tidal volume, and positive end-expiratory pressure. American Review of Respiratory Disease 1988;137:1159–1164.
[11] Aguiar Santos, S.; Robens, A.; Boehm, A.; Leonhardt, S.; Teichmann, D. System Description and First Application of an FPGA-Based Simultaneous Multi-Frequency Electrical Impedance Tomography. *Sensors* 2016, *16*, 1158. https://doi.org/10.3390/s16081158
[12]Sentec principle of operation, 2ST800-300 Rev. 000, 31 July 2020
[13] E. Teschner, I. Michael, and S. Leonhardt, "Electrical Impedance Tomography: The Realization of Regional Ventilation Monitoring (2nd Edition)", *Tech. rep. Draeger GmbH* , 2015.
[14]Sanders RD. Two ventilating attachments for bronchoscopes. Del Med J 1967; 39: 170
[15] Giunta F, Chiaranda M, Manani G, Giron GP. Clinical uses of high frequency jet ventilation in anaesthesia. Br J Anaesth 1989; 63: 102S–6S
[16] Klain M, Smith RB. Fluidic technology. A discussion and a description of a fluidic controlled ventilator for use with high flow oxygen techniques. Anaesthesia 1976; 31: 750 s
[17] Fritzsche K, Osmers A. Anesthetic management in laryngotracheal surgery. High-frequency jet ventilation as strategy for ventilation during general anesthesia. Hno. 2011;59:931–41. quiz 942-3
[18] Krishnan JA, Brower RG High-frequency ventilation for acute lung injury and ARDS Chest, 118 (3) (2000), pp. 795-807
[19] Abdelmalak, B., & Patel, A. (2020). Ear, Nose and Throat Surgery: Airway Management. In T. Cook & M. Kristensen (Eds.), Core Topics in Airway Management (pp. 223-242). Cambridge: Cambridge University Press. doi:10.1017/9781108303477.028
[20] TwinStream™, Fa. Reiner, Vienna, Austria
[21] Biro P, Spahn DR, Pfammatter T. High-frequency jet ventilation for minimizing breathing-related liver motion during percutaneous radiofrequency ablation of multiple hepatic tumours. Br J Anaesth 2009; 102: 650–3
[22] Biro P, Eyrich G, Rohling RG. The efficiency of CO2 elimination during high-frequency jet ventilation for laryngeal microsurgery. Anesth Analg 1998; 87: 180–4
[23] Aloy A Schachner M Cancura W Tubeless translaryngeal superimposed jet ventilation. Eur Arch Otorhinolaryngol. 1991; 248: 475-478
[24] Rezaie-Majd A, Bigenzahn W, Denk DM, Burian M, Kornfehl J, Grasl MCh, Ihra G, Aloy A. Superimposed high-frequency jet ventilation (SHFJV) for endoscopic laryngotracheal surgery in more than 1500 patients. Br J Anaesth. 2006 May;96(5):650-9. doi: 10.1093/bja/ael074. Epub 2006 Mar 30. PMID: 16574723.

[25] Metron QA-VT Adult Ventilator Tester, Michigan Instruments Inc., USA
[26] Biro P, Layer M, Wiedemann K, et al. Carbon dioxide elimination during jet ventilation for rigid bronchoscopy. Br J Anaesth 2000;84: 635–7
[27] SenTec AG, Ringstrasse 39, CH-4106 Therwil, Switzerland, www.sentec.ch
[28] Putensen C. et al. "Electrical Impedance Tomography for Cardio-Pulmonary Monitoring". J Clin Med. 2019; 8(8):1176.
[29] User's Guide for the LuMon™ System, 2ST200-110 Rev 006 │04 2021; 60 p.
[30] Frerichs I, Amato MBP, van Kaam AH, et alChest electrical impedance tomography examination, data analysis, terminology, clinical use and recommendations: consensus statement of the TRanslational EIT developmeNt stuDy groupThorax 2017;72:83-93.
[31]Grant CA, Pham T, Hough J, Riedel T, Stocker C, Schibler A. Measurement of ventilation and cardiac related impedance changes with electrical impedance tomography. Crit. Care. 2011; 15:R37. http://dx.doi.org/10.1186/cc9985
[32] Alan V. Oppenheim and Ronald W. Schafer. 2009. Discrete-Time Signal Processing (3rd. ed.). Prentice Hall Press, USA.
[33] Ukere A, März A, Wodack K H, Trepte C J, Haese A, Waldmann A D, Böhm S H and Reuter D A 2016 Perioperative assessment of regional ventilation during changing body positions and ventilation conditions by electrical impedance tomography ed T Asai Br. J. Anaesth. 117 228–35
[34] Frerichs I, Dargaville P A, Van Genderingen H, Morel D R and Rimensberger P C 2006 Lung volume recruitment after surfactant administration modifies spatial distribution of ventilation Am. J. Respir. Crit. Care Med. 174 772–9
[35] Bialka, S., Copik, M., Rybczyk, K. et al. Assessment of changes of regional ventilation distribution in the lung tissue depending on the driving pressure applied during high frequency jet ventilation. BMC Anesthesiol 18, 101 (2018). https://doi.org/10.1186/s12871-018-0552-2
[36] Paula LF, Wellman TJ, Winkler T, Spieth PM, Guldner A, Venegas JG, Gama de Abreu M, Carvalho AR, Vidal Melo MF. Regional tidal lung strain in mechanically ventilated normal lungs. J Appl Physiol (1985). 2016;121:1335–47.
[37] Duggan M, Kavanagh BP. Pulmonary atelectasis: a pathogenic perioperative entity. Anesthesiology. 2005;102:838–54.
[38] Sutherasan Y, Vargas M, Pelosi P. Protective mechanical ventilation in the non-injured lung: review and meta-analysis. Crit Care. 2014;18:211.